Task 38
Solar Air-Conditioning
and Refrigeration

Description of simulation tools used in solar cooling

New developments in simulation tools and models and their validation

Solid desiccant cooling

Absorption chiller

A technical report of subtask C
Deliverable C2-A

Date: Novembre 9, 2009

By

Paul Bourdoukan[1]

Contributions by

Edo Wiemken[2], Paul Kohlenbach[3], Etienne Wurtz[4], Harald Moser[5], Alexander Morgenstern[6], Antoine Dalibard[7], Felix Ziegler[8], Constanze Bongs[9]

[1] LOCIE FRE CNRS 3220, Institut National de l'Energie Solaire (INES),
Tel: +33 (0)4 79444545
Fax: +33 (0)4 79 253690
Email: Paul.Bourdoukan@univ-savoie.fr

[2] Fraunhofer Institute for Solar Energy Systems ISE, Freiburg, Germany
Tel: +49 761 4588 5412
Fax: +49 761 4588 9000
Email: edo.wiemken@ise.fraunhofer.de

[3] Solem Consulting
Postfach 2127, 71370 Weinstadt, Germany
Tel:+49 (0)174/ 41 30 92 1
Fax:+49 (0)7151/ 60 48 62 5
Email: info@solem-consulting.com

[4] LOCIE FRE CNRS 3220, Institut National de l'Energie Solaire (INES),
Tel: + 33 (0) 4 79444554
Fax:+ 33 (0) 4 79253690
Email: Etienne.wurtz@univ-savoie.fr

[5] Graz University of Technology, Institute of Thermal Engineering, Austria
Tel: +43 316 873 7304
Fax:+43 316 873 7305
Email: harald.moser@tugraz.at

[6] Fraunhofer Institute for Solar Energy Systems ISE, Freiburg, Germany
Tel: +49 761 4588 5107
Fax:+49 761 4588 9000
Email: alexander.morgenstern@ise.fraunhofer.de

[7] ZAFH.NET (Stuttgart University of Applied Sciences)
Tel: +49 (0)711/ 89 26-29 81
Fax: +49 (0)711/ 89 26-26 98
Email: antoine.dalibard@hft-stuttgart.de

[8] Technische Universität Berlin, Institute for Energy Engineering
Tel: 314-25624
Fax: 314-22253
Email: felix.ziegler@tu-berlin.de

[6] Fraunhofer Institute for Solar Energy Systems ISE, Freiburg, Germany
Tel: +49 761 4588 5487
Fax:+49 761 4588 9000
Email: constanze.bongs@ise.fraunhofer.de

Content

Introduction

Numerical simulation offers the possibility to study virtually physical systems and to test rapidly the proposed solutions. Simulation is then the most adapted method to understand the behaviour of a system in order to optimize it. The enhancement and the development of a technology are essentially based on the capacity to simulate accurately its behaviour in order to optimize it. This reality applies to solar cooling technologies.

In this report simulation tools used in the solar cooling domains are described. Then the recent development in the components and system models and validation are presented.

In part 1 of the report the simulation tools applicable in the domain of solar cooling are presented and the main advantages of each tool are highlighted.

Part 2 concerns the recent developments in modelling solid desiccant cooling technologies and the vacuum tube solar collectors with an experimental validation of an implementation in the SPARK simulation environment. Part 3 presents a recent transient model of the Li/Br absorption chiller with an experimental validation.

Each part has its reference section and conclusion.

This report and the authors don't pretend to include all the simulation tools used in solar cooling or all the recent models related to solid desiccant cooling and absorption chiller. The simulation tools described in this report are those identified and used by the participants of the IEA Task 38.

Chapter I: Description of simulation software, applicable for solar cooling

In this chapter a brief description of some simulation tools applicable in solar cooling is given. These tools are the most commonly used by IEA Task 38 participants. The range goes from predefined simple configuration software to low level equation solver. Some of the tools are developed by research groups and are dedicated for internal use and other are commercially available software. The simulation tools highlighted here are SPARK, EnergyPlus, EES, EasyCool, TRNSYS and INSEL.

SPARK

Paul Bourdoukan and Etienne Wurtz,
LOCIE FRE CNRS 3220, Institut National de l'Energie Solaire

SPARK is a general simulation environment that supports the definition of simulation models and solution of these models via a robust and efficient differential/algebraic equation solver. In SPARK, the modeller describes the set of equations defining a model as equation-based objects. At the lowest level, an atomic object characterizes one equation and its variables. Then, macroscopic objects can be created as an assembly of various atomic or macroscopic objects. The entire model is built by connecting the different necessary objects. If one class of objects needs to be reused, it can be instantiated as many times as required, without any additional effort.
At this stage, it is necessary to observe that the model is input/output free. The particular problem to be solved is then described by imposing the adequate input data (boundary and initial conditions) and by specifying the variables to be solved. So in this environment it is not necessary to order the equations or to express them as assignments statements (algorithms) in opposition to conventional modular environments such as Matlab/Simulink or TRNSYS.
SPARK uses a mathematical graph of the model to decompose it as strong components to be solved independently. Within each component, SPARK finds the appropriate function call sequence to get the solution. If no direct sequence is possible, as evidence by a cyclic problem graph, a small "cut set" is determined so as to minimize the number of variables involved in the Newton-like iterative numerical solution process. As a result, this decreases the size of the Jacobian matrix involved in the Newton iteration within the component. Consequently, the way SPARK handles the solution of coupled nonlinear equations makes it a fast solver for building energy simulation problems.
Since the "cut sets" of variables have been identified, the problem specification file is converted into a C++ program which is then compiled, linked and executed to solve the problem for given boundary and initial conditions.

SPARK is free and has a detailed reference manual. Using SPARK requires a 3 to 5 months learning period to be able to create models. A support service is available and provided by the simulation research group (SRG) of the Lawrence Berkeley National Laboratory (LBNL)

SPARK has it's own HVAC library based on some simple models. However various doctoral researches in the domain of building physics and HVAC systems were accomplished using SPARK as a simulation environment [1], [2], [3], [4], [5] and [6]. This allowed the creation of models library for the building envelope [1], [2] and [3], and a library for the systems [4], [5] and [6]. Recently works [4], [5] were developed on solar desiccant cooling beside an on going PhD thesis on absorption chillers powered by solar collectors. However all these models are dedicated for internal use but can be distributed by their developers.

Important links

http://gundog.lbl.gov/VS/spark.html (download)
http://simulationresearch.lbl.gov/dirpubs/spkall.html (reference manual)

References

[1]. Musy, M. « Génération automatique de modèles zonaux pour l'étude du comportement thermo-aéraulique des bâtiments ». PhD thesis, Université de La Rochelle, France. (1999).

[2]. Mora, L. « Prédiction des performances thermo-aérauliques des bâtiments par association de modèles de différents niveaux de finesse au sein d'un environnement ». PhD thesis, Université La Rochelle, France (2003).

[3]. Cordeiro Mendonça, K. **«** Modélisation thermo-hydro-aéraulique des locaux climatisés selon l'approche zonale (prise en compte des phénomènes de sorption d'humidité) ». PhD thesis, Université La Rochelle, France (2004).

[4]. Maalouf, C. « Étude du potentiel de rafraîchissement d'un système évaporatif àdésorption avec régénération solaire ». PhD thesis, Université de La Rochelle, France (2006)

[5]. Bourdoukan. P. « Etude numérique et expérimentale destinée à l'exploitation des techniques de rafraîchissement par dessiccation avec régénération par énergie solaire ». Ph.D thesis*,* Université La Rochelle, (2008) (Available in English)

[6]. Tittelin, P. « Environnements de simulation adaptés à l'étude du comportement énergétique des bâtiments basse consommation ». PhD thesis, Université de Savoie, France (2008)

EnergyPlus

Paul Bourdoukan and Etienne Wurtz
LOCIE FRE CNRS 3220, Institut National de l'Energie Solaire

EnergyPlus has its roots in both the BLAST and DOE–2 programs. BLAST (Building Loads Analysis and System Thermodynamics) and DOE–2 were both developed and released in the late 1970s and early 1980s as energy and load simulation tools. Their intended audience is a design engineer or architect that wishes to size appropriate HVAC equipment, develop retrofit studies for life cycling cost analyses, optimize energy performance, etc. Born out of concerns driven by the energy crisis of the early 1970s and recognition that building energy consumption is a major component of the American energy usage statistics, the two programs attempted to solve the same problem from two slightly different perspectives. Both programs had their merits and shortcomings, their supporters and detractors, and solid user bases both nationally and internationally.
Like its parent programs, EnergyPlus is an energy analysis and thermal load simulation program. Based on a user's description of a building from the perspective of the building's physical make-up, associated mechanical systems, etc., EnergyPlus will calculate the heating and cooling loads necessary to maintain thermal control setpoints, conditions throughout an secondary HVAC system and coil loads, and the energy consumption of primary plant equipment as well as many other simulation details that are necessary to verify that the simulation is performing as the actual building would. Many of the simulation characteristics have been inherited from the legacy programs of BLAST and DOE–2. Below is list of some of the features of the first release of EnergyPlus. While this list is not exhaustive, it is intended to give the reader and idea of the rigor and applicability of EnergyPlus to various simulation situations.

- **Integrated, simultaneous solution** where the building response and the primary and secondary systems are tightly coupled (iteration performed when necessary)
- **Sub-hourly, user-definable time steps** for the interaction between the thermal zones and the environment; variable time steps for interactions between the thermal zones and the HVAC systems (automatically varied to ensure solution stability)
- **ASCII text based weather, input, and output files** that include hourly or sub-hourly environmental conditions, and standard and user definable reports, respectively
- **Heat balance based solution** technique for building thermal loads that allows for simultaneous calculation of radiant and convective effects at both in the interior and exterior surface during each time step
- **Transient heat conduction** through building elements such as walls, roofs, floors, etc.using conduction transfer functions
- **Improved ground heat transfer modeling** through links to three-dimensional finite difference ground models and simplified analytical techniques
- **Combined heat and mass transfer** model that accounts for moisture adsorption/desorption either as a layer-by-layer integration into the conduction transfer functions or as an effective moisture penetration depth model (EMPD)
- **Thermal comfort models** based on activity, inside dry bulb, humidity, etc.
- **Anisotropic sky model** for improved calculation of diffuse solar on tilted surfaces
- **Advanced fenestration calculations** including controllable window blinds, electrochromic glazings, layer-by-layer heat balances that allow proper assignment of solar energy absorbed by window panes, and a performance library for numerous commercially available windows
- **Daylighting controls** including interior illuminance calculations, glare simulation and control, luminaire controls, and the effect of reduced artificial lighting on heating and cooling

- **Loop based configurable HVAC systems** (conventional and radiant) that allow users to model typical systems and slightly modified systems without recompiling the program source code
- **Atmospheric pollution calculations** that predict CO2, SOx, NOx, CO, particulate matter, and hydrocarbon production for both on site and remote energy conversion
- **Links to other popular simulation environments/components** such as WINDOW5, DElight and SPARK to allow more detailed analysis of building components More details on each of these features can be found in the various parts of the EnergyPlus documentation library.

No program is able to handle every simulation situation. However, it is the intent of EnergyPlus to handle as many building and HVAC design options either directly or indirectly through links to other programs in order to calculate thermal loads and/or energy consumption on for a design day or an extended period of time (up to, including, and beyond a year). While the first version of the program contains mainly features that are directly linked to the thermal aspects of buildings, future versions of the program will attempt to address other issues that are important to the built environment: water, electrical systems, etc.

References:

http://www.energyplus.gov/pdfs/gettingstarted.pdf
http://www.eere.energy.gov/buildings/energyplus/cfm/reg_form.cfm (Link for download)

EES

Harald Moser, Graz TU

Graz University of Technology, Institute of Thermal Engineering, Austria

EES is an acronym for Engineering Equation Solver. The basic function provided by EES is the numerical solution of a set of algebraic equations. EES can also be used to solve differential and integral equations, do optimization, provide uncertainty analyses and linear and non-linear regression, convert units and check unit consistency and generate publication-quality plots.

There are two major differences between EES and other equation-solving programs:

1. EES allows equations to be entered in any order with unknown variables placed anywhere in the equations; EES automatically reorders the equations for efficient solution.
2. EES provides many built-in mathematical and thermophysical property functions useful for engineering calculations. For example, the steam tables are implemented such that any thermodynamic property can be obtained from a built-in function call in terms of any two other properties. Similar capability is provided for most refrigerants, ammonia, methane, carbon dioxide and other fluids. Air tables are built-in, as are psychrometric functions and JANAF data for many common gases. Transport properties are also provided for all substances.

The available built-in thermophysical property functions are listed below in alphabetical order. Additional fluid property data can be added by the user.

EES built-in thermophysical property functions

ACENTRICFACTOR	CONDUCTIVITY	CP
CV	DENSITY	DEWPOINT
DIPOLE	ENTHALPY	ENTHALPY_FUSION
ENTROPY	FUGACITY	HUMRAT (humidity ratio)
INTENERGY	ISIDEALGAS	MOLARMASS
PRANDTL	PRESSURE	P_CRIT
P_SAT	QUALITY	RELHUM
SOUNDSPEED	SPECHEAT	SURFACETENSION
TEMPERATURE	T_CRIT	T_SAT
T_TRIPLE	VISCOSITY	WETBULB
VOLUME	V_CRIT	VOLEXPCOEF

The built-in thermophysical property data for the fluids listed below are provided by EES.

Fluids with EES built-in thermophysical properties

Ideal Gas		**Real Fluid**		
Air	Air_ha*	Methanol*	R11	R404A
AirH2O	Ammonia*	n-Butane*	R12	R407C
CH4	Argon*	n-Dodecane*	R13	R410A
C2H2	Carbondioxide*	n-Heptane*	R14	R500
C2H4	Carbonmonoxide	n-Hexane*	R22*	R502
C2H6	Cyclohexane*	n-Octane*	R23*	R507A
C2H5OH	Deuterium*	n-Pentane*	R32*	R508B
C3H8	Ethane*	Neon*	R114	R600*
C4H10	Ethanol*	Nitrogen*	R116*	R600a
C5H12	Ethylene*	Oxygen*	R123*	R717*
C6H14	Fluorine*	Propane*	R124*	R718*
C8H18	Helium*	Propylene*	R125*	R744*
CO	Hydrogen*	Steam*	R134a*	RC318*
CO2	HydrogenSulfide	Steam_IAPWS*	R141b*	
H2	Ice*	Steam_NBS*	R143a*	
H2O	Isobutane*	SulfurHexafluorid	R152a*	
N2	Isopentane*	Toluene*	R227ea	
NO	Krypton*	Water*	R290*	
NO2	Methane*	Xenon*		
O2				
SO2				

* These fluids are implemented using a high accuracy equation of state.

Further more the thermodynamic properties of mixtures of lithium bromide / water and ammonia / water are implemented as an externally compiled EES routine.

EES allows the user to enter his or her own functional relationships in three ways. First, a facility for entering and interpolating tabular data is provided so that tabular data can be directly used in the solution of the equation set. Second, the EES language supports user-written functions, procedures, modules and subprograms. Third, compiled functions and procedures, written in a high-level language such as Pascal, C, or FORTRAN, can be dynamically-linked with EES.

EES is particularly useful for design problems in which the effects of one or more parameters need to be determined. The program provides this capability with its Parametric Table, which is similar to a spreadsheet. The user identifies the variables which are independent by entering their values in the table cells. EES will calculate the values of the dependent variables in the table. Plotting capability is provided to display the relationship between any two variables in the table.

EES offers the advantages of a simple set of intuitive commands which a novice can quickly learn to use for solving complex problems. The large data bank of thermodynamic and transport properties built into EES is helpful in solving problems in thermodynamics, fluid mechanics, and heat transfer.

TRNSYS

Alexander Morgenstern

Fraunhofer Institute for Solar Energy Systems ISE, Freiburg, Germany

TRNSYS is a commercially available energy simulation tool designed for the transient simulation of thermal systems and multizone buildings.

The software is generally used by engineers and researchers for the validation of new energy concepts for simple applications like solar domestic hot water systems as well as complex systems for testing of control strategies like buildings with solar heating and cooling equipment (e.g. thermally activated slabs, capillary tube systems and chilled ceilings) with consideration of the occupant behavior. An extensive standard component library and a large number of AddOns like geothermal and heat pump libraries or air flow models allows the use for a wide field of application. The open, modular structure of TRNSYS afford the extension and the design of models in dependence of the user requirements. This provides a basis for the coupled simulation of the building and the active system.

TRNSYS offer dynamic building simulation with an arbitrary number of thermal zones, different walls and windows, also buffer zones like double facades, furthermore the consideration of convective and radiative internal loads, the influence of shading devices as well as natural and mechanical ventilation and interzonal air change. A special building editor is available to configure the building type of TRNSYS.

The support for the integration of control strategies for shading, ventilation, heating and air-conditioning as well as the import of weather data is implemented in the software. Time steps can be defined by user.

All common programming languages (C++, PASCAL, FORTRAN, …) can be used by developers to add custom component models.

TRNSYS allows e.g. simulations for the following applications:

- Solar systems (solar hot water, solar combi systems and electric systems with PV)
- Low energy buildings and HVAC systems
- Renewable energy systems
- Cogeneration and fuel cells

More information: http://sel.me.wisc.edu/trnsys/ ; www.trnsys.de

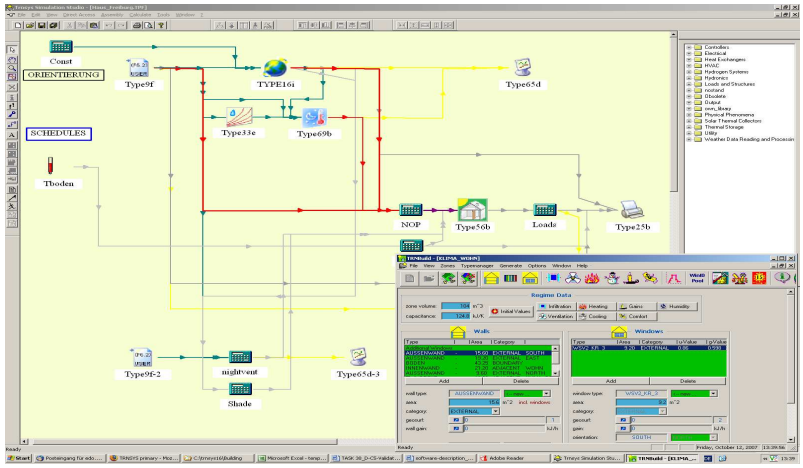

Example: graphical display of a building load simulation with TRNSYS. The building configuration editor is shown in the front.

EASYCOOL

Edo Wiemken,
Fraunhofer Institute for Solar Energy Systems ISE, Freiburg, Germany

The simulation tool was developed in the frame of the project Solar Air-Conditioning in Europe (SACE), funded by the European Commission. It was originally designed to perform easy to programme applications and fast simulation runs for energetic and economic performance studies in SACE and in IEA Task 25.

EasyCool provides 11 pre-defined system configurations for solar thermally driven cooling applications, of which 4 configurations are foreseen for reference calculatios (non-solar, conventional system solutions). The program reads annual time series with hourly building load data and meteorological data of the respective site (these data set has to be prepared in advance) and calculates annual energetic and econonomic performance data as well as environmental figures such as CO_2 savings. With each simulation run, a range of system size (collector area and hot water storage size) is varied.

In input boxes, the most relevant average performance coefficients, power consumptions (pums, fans, ..) collector coeffictients and component costs are to be defined. A special economic input box requires cost data for installation, planning, maintenance, interest rate, fuel, water and electricity costs, etc.

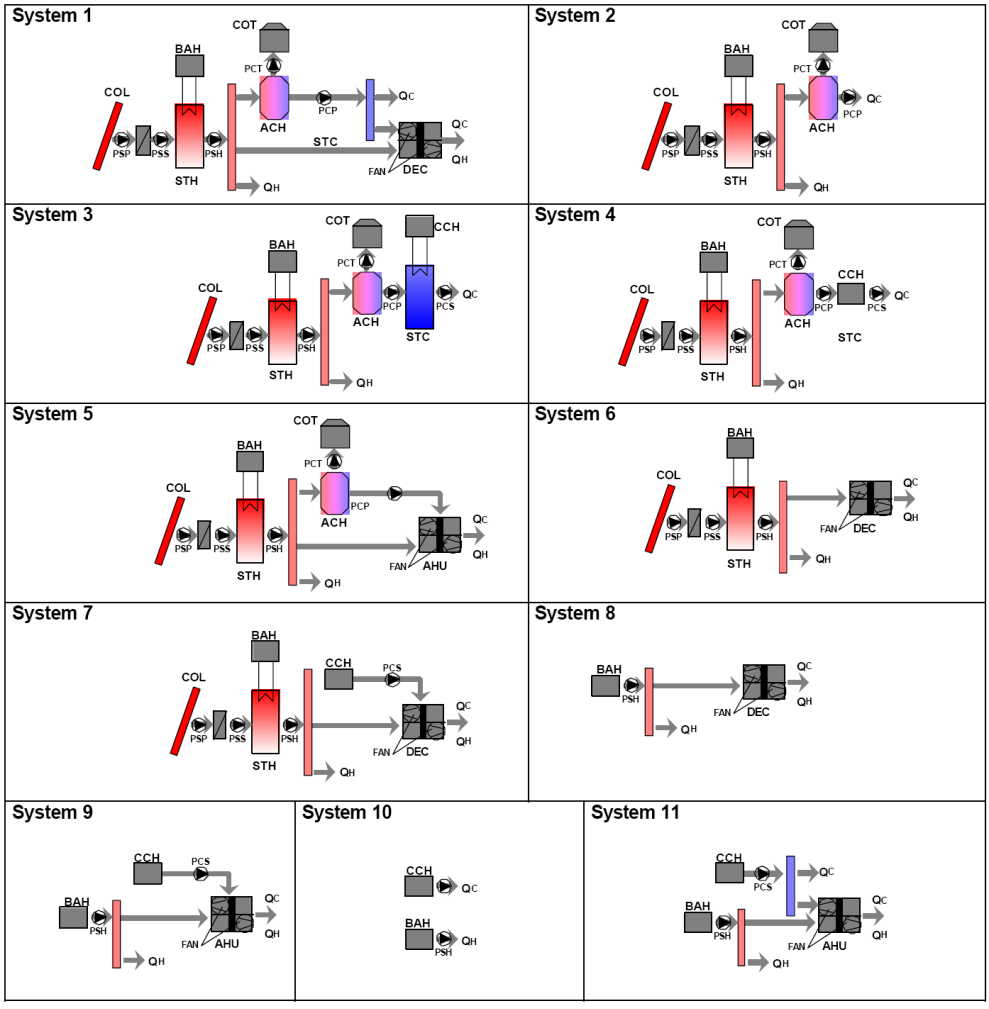

Pre-defined system configurations, accessible in EasyCool. System configurations 8 to 11 are for reference system calculations.

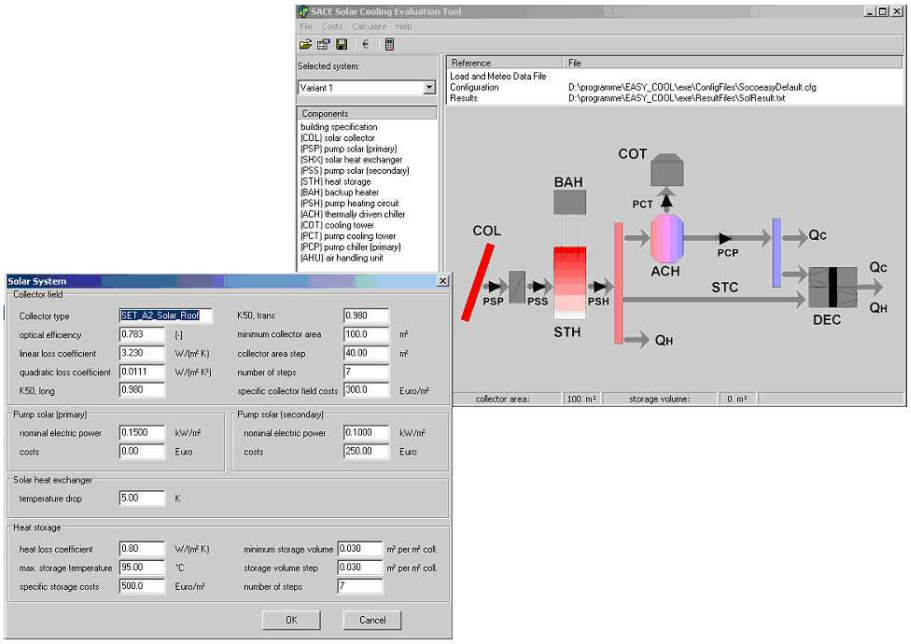

One of the pre-defined system configurations is selected and the input box for the solar thermal collector description is opened.

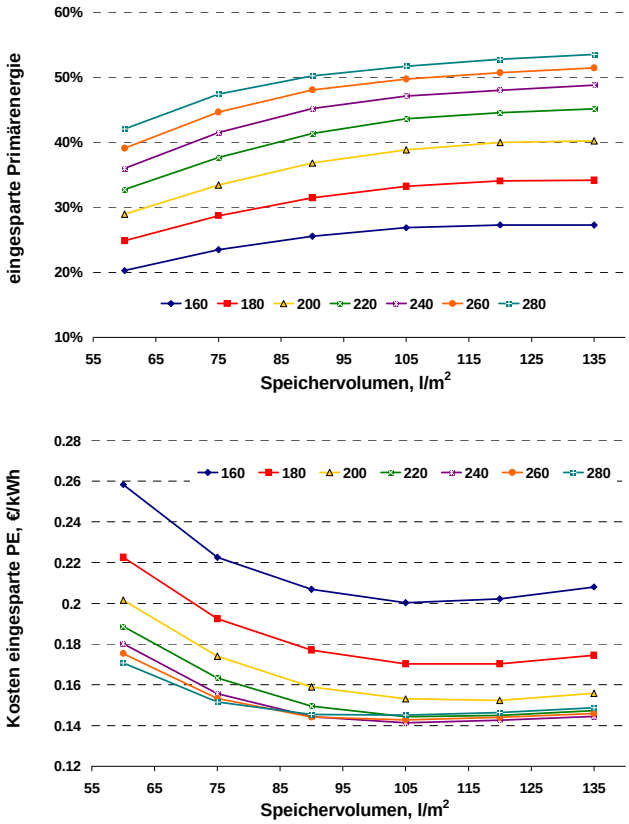

Example of simulation results: For a defined system configuration and load data file, the savings in primary energy consumption (compared to a reference system calculation) and specific cost per saved kWh of primary energy are displayed as a function of the system size (storage volume is shown at the x.-axis, the collector area is represented by the different curves)

EasyCool is used internally by Fraunhofer ISE and currently not disseminated for public use.

INSEL

Antoine Dalibard
ZAFH.NET (Stuttgart University of Applied Sciences)

The acronym INSEL stands for INtegrated Simulation Environment Language. This graphical programming language has been developed at the Faculty of Physics of Oldenburg University (Germany) in the early 1990's and was originally designed for the modelling of renewable electrical energy systems. Today INSEL covers the whole range of renewable energy systems, including building simulation and communication technologies. The software can be adapted by the user for completely own software developments and offers a transparent software solution from the planning phase to automation and simulation based control of any energy plants.

Basic idea of INSEL

The graphical programming language INSEL is based on the principle of "structured programming" on blocks diagrams. It consists of connecting blocks in order to obtain block diagrams that express a solution for a certain simulation task.

Application areas of INSEL

The main application areas of the program INSEL are:

- Energy meteorology
- Photovoltaic systems
- Solar thermal systems
- Solar thermal power plants
- Building simulation (under development)
- Building automation (under development)
- Facility management (under development)

Main uses of INSEL

INSEL is a block diagram simulator that can be used by researchers, planers, designers, operators and investors for:

- Design of complex energy systems
- Visualisation and Internet monitoring
- Monitoring and control of energy plants
- Highly precise yield prognoses and economic calculations of energy systems.

Structure of the program

The different layers of INSEL are:

Graphical Interface : HP-VEE panel view	
Graphical simulation model (file .vee)	**Text simulation model (file .ins)**
Data bases (weather, components,…)	
INSEL compiler: inselEngine.dll	
Execution: inselDi.dll	
Interfaces: call of the conventions, header	
Blocks implementation	
INSEL block concept	

Additional Information:

- *INSEL main window*:

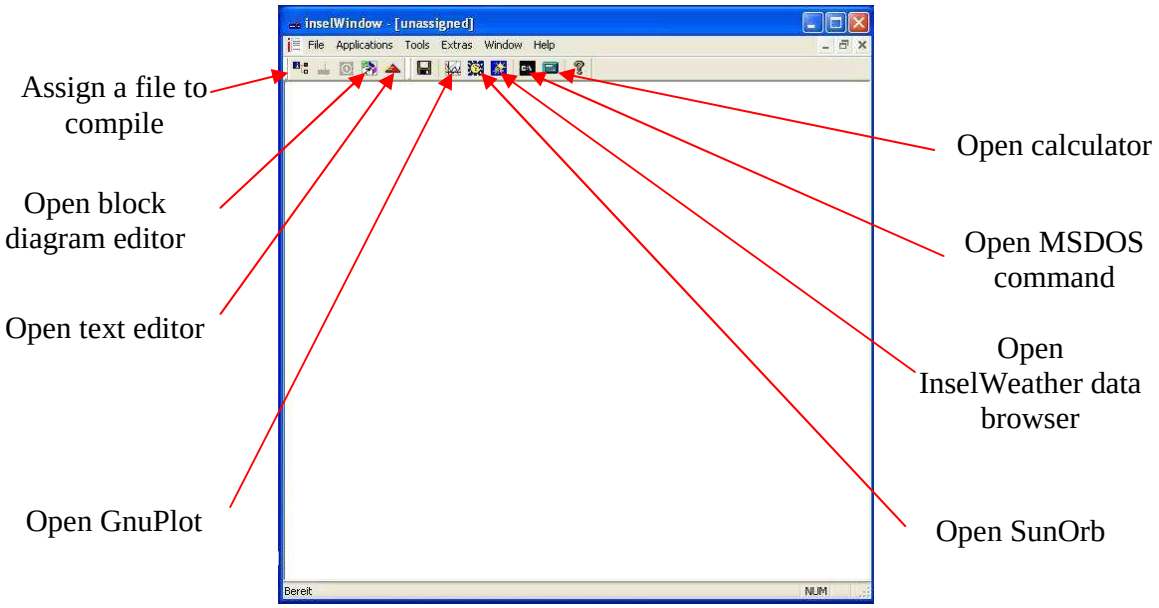

- *Graphical Interface*: HP-VEE is used as graphical interface

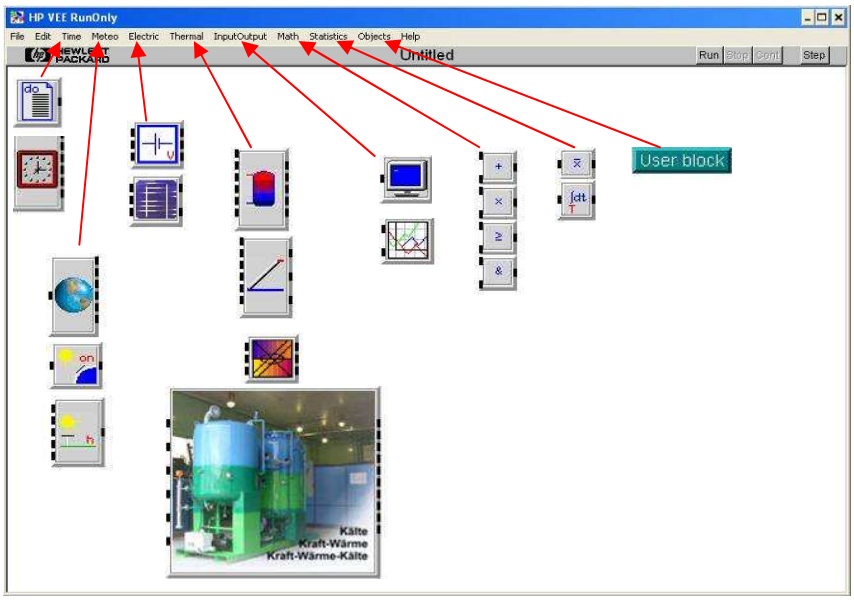

- *Source code of the models:* not available

- *Modularity*: since INSEL is a programming language, it is entirely modular. It is possible to define any energetic systems.
- *Time steps increment*: any time steps can be defined from less than 1sec to several years.
- *Components library extension*: It is possible to write source code in Fortran and C++ and to create new components in order to extend the components library by linking the code to a dynamic link library DLL.
- *Meteorological databases used*: INSEL database (2000 locations worldwide), European solar radiation Atlas, Meteonorm, S@tel light plus any other source available.

Components library

The main components of INSEL related to solar thermal application and solar cooling in particular are:

- *Collectors:* dynamic models of air and liquids collectors
- *Storage tanks:* fully mixed and stratified models
- *Heat exchangers:* simple models (parallel, counter and cross flows), cross flow heat exchanger with condensing and icing, earth heat exchanger (under development).
- *Desiccant wheel*
- *Absorption chillers:* models for Phönix (10 kW) and EAW (from 15 to 200 kW) chillers.
- *Adsorption chillers:* dynamic model under development.
- *Cooling towers*: open-wet model

A specific application for solar cooling: INSEL Cool

An application for solar cooling (INSEL Cool) has been implemented into INSEL in order to help planners during the pre-design phase of a solar cooling plant. Users have the possibility to perform simulation of solar cooling installing by selecting in a list the main components of the installation (cooling machines, solar collectors, cooling towers, storage tanks, heat exchangers), the location of the installation and the cooling load profile. It is also possible to define new components and new locations by introducing himself the required parameters and external cooling load files can be used for simulation. The analysis of the results can be done (either with hourly or monthly values) directly from the application as can be seen in the figure below.

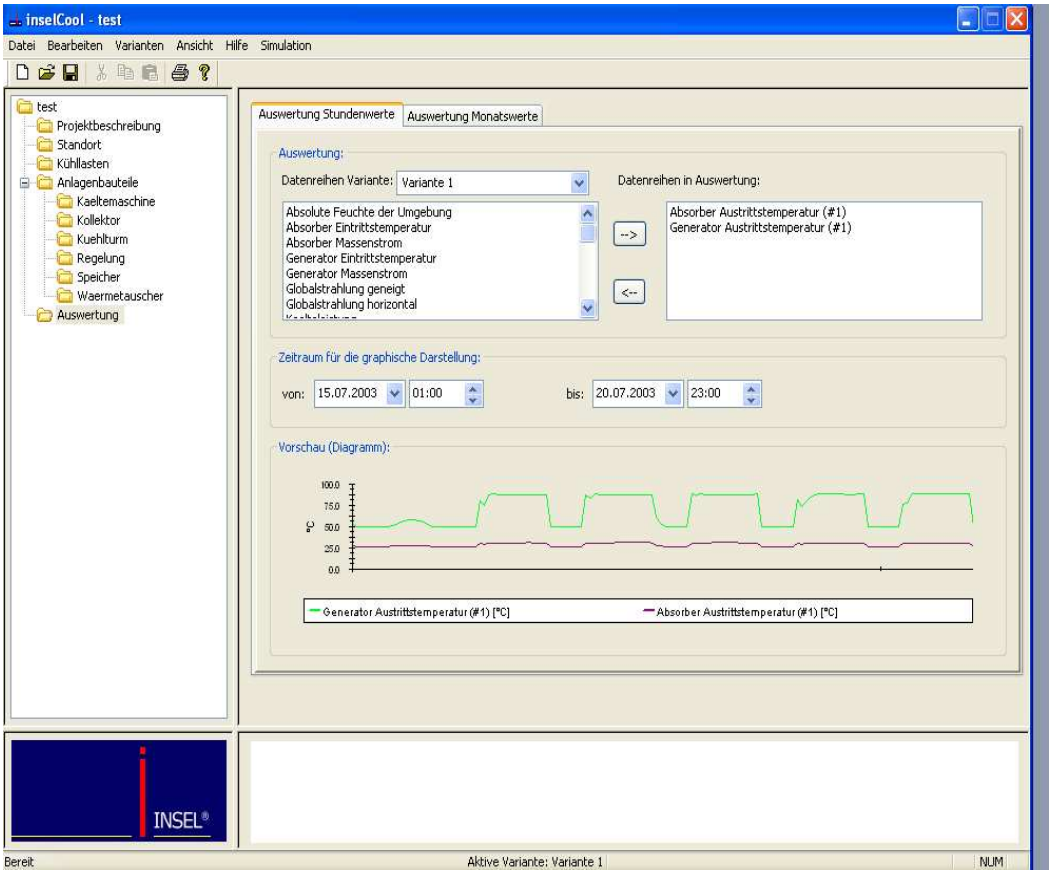

Reference projects

INSEL has been used in several solar cooling projects, some examples are given below:

- 55 kW solar desiccant cooling system with 244 m² ventilated PV-Façade, 330 m² ventilated PV-Roof sheds and 155 m² of solar air collectors in the Library of Mátaro (Spain).
- 100 kW solar desiccant cooling system with 100 ² of solar air collectors and additional thermal energy delivered by a heat recovery system of the production process, installed in an production hall in Althengstett (Germany)
- 15 kW solar absorption cooling system with 37 m² flat plate and 29 m² vacuum tube collectors, 2 m³ hot and 1 m³ cold storage tank, installed in an office building of the SolarNext AG (Germany)
- Simulation based analysis of different control options for a 1.218 m² solar collector field which supplies the heating system of an office building in winter and three MYCOM adsorption chillers with a nominal cooling capacity of 353 kW, FESTO AG & C0. KG in Esslingen
- Performance and economic analysis of a 140 kW absorption cooling system for a production hall with 2.500 m² conditioned space of the ft-fertigungstechnik GmbH in Viernheim, Germany

Download

A demonstration version of INSEL and a detailed tutorial can be downloaded from the following website: www.insel.eu

Chapter II: New developments in simulations tools and models

A solar desiccant cooling installation model in SPARK, A transient detailed model of the desiccant wheel.

Paul Bourdoukan
LOCIE FRE CNRS 3220, Institut National de l'Energie Solaire (INES),

Etienne Wurtz
LOCIE FRE CNRS 3220, Institut National de l'Energie Solaire (INES),

The present chapter presents a modelling approach of a solid desiccant air handling unit powered by vacuum tube solar collectors. It is divided into 3 sections.

In section (1) the model of the installation is described by separately considering each component (i.e. sensible heat regenerator, desiccant wheel, evaporative coolers, solar collectors, storage tank).

In the section (2) an experimental validation of the presented model is performed under different operating conditions on a component level and on a system level.

Section (3) is dedicated for a transient model of the desiccant wheel. Unlike conventional models that give a mean temperature and a mean humidity ratio at the outlet of the wheel this detailed transient model gives the temperature and humidity profile at the outlet of the wheel. The model is then validated experimentally.

The presented models with the experimental validation are a summary of different research work [1], [2], [3], [4] and [5] published recently and highlighted in the reference section.

1. Modelling of the solar desiccant cooling installation

A model implementation of a desiccant cooling installation powered by vacuum tube solar collectors in SPARK is described in this section. The Desiccant wheel, the sensible regenerator and the evaporative cooler are selected from bibliography. **However a new developed model of the vacuum heat pipe solar collectors is presented.**

The aim of this implementation is to predict accurately the supply conditions of a desiccant air handling for different operating conditions and to predict the real potential of solar energy in this process.

Nomenclature

Symbols

c_{pa} heat capacity of air [J.kg^{-1}.K^{-1}]

c_{pv} heat capacity of water vapor [J.kg^{-1}.K^{-1}]

c_{pm} heat capacity of the regenerator matrix [J.kg^{-1}.K^{-1}]

C_{min} min capacitance rate of the regenerator inlet fluids [J.s^{-1}.K^{-1}]

C_r parameter used in the correlation of the regenerator [-]

e thickness [m]

F_i potential characteristic [-]

G solar global radiation [W. m^{-2}]

h heat transfer coefficient [W.K^{-1}m^{-2}]

h_a enthalpy of moist air [J.Kg^{-1}]

h_{fg} latent heat of vaporization [J.kg]

H enthalpy of the sensible or desiccant regenerator matrix [J.Kg^{-1}]

J_t lumped heat transfer coefficient [s^{-1}]

J_m lumped mass transfer coefficient [s^{-1}]

K heat loss constant [W.K^{-1}m^{-2}]

L width of the desiccant wheel [m]

L_v latent heat of vaporization of the heat pipe fluid [J.kg^{-1}]

Le Lewis number [-]

m_a air mass flow rate [Kg.s^{-1}]

M mass [kg]

M_d mass of the desiccant matrix [Kg]

M_m mass of the aluminium matrix [Kg]

N angular speed of the wheel [rd.s^{-1}]

Na number of nodes in the angular direction of the desiccant wheel [-]

Np number of nodes in the width direction of the desiccant wheel [-]

NTU number of transfer unit [-]

S area [m^2]

t time [s]

T_a air temperature [K]

T_{eq} equilibrium temperature [K]

T_i air temperature in the section i (i=1;9) [K]

T_m matrix temperature [K]

u fluid velocity ($m.s^{-1}$)

V volume (m^3)

w_a humidity ratio of moist air. [$Kg.Kg^{-1}_{dryair}$]

W_d water content of desiccant [$Kg.Kg^{-1}_{desiccant}$]

x variable [arbitrary]

z coordinate in the fluid flow direction [m]

Greek letters

ε emissivity [dimensionless]

γ_i parameter used in the reduction of desiccant wheel equations [-]

$\Delta\lambda$ parameter in the desiccant enthalpy [-]

μ ratio of matrix mass over air mass [-]

η_{cf} efficiency of the counter flow heat exchanger [-]

$\tau\alpha$ transmission-absorptance coefficient

σ Stefan Boltzmann constant [$W.K^{-4}m^{-2}$]

ρ density [$kg.m^{-3}$]

λ conductivity [$W.K^{-1}m^{-1}$]

τ_{ro} half period of rotation of the desiccant wheel [s]

θ cylindrical coordinate or angular position [rd]

Subscripts

a air

b buffer

c condenser

d desiccant

eq equilibrium

f fluid

g glass

i inlet

H heat pipe

m matrix (sensible regenator)

p plate absorber

o outlet

reg regeneration

sat saturation

Desiccant cooling principle

A desiccant cooling installation operating under the conventional configuration (100% air-change rate), with corresponding changes in the air properties in the psychometric chart, is shown in Figure 1.

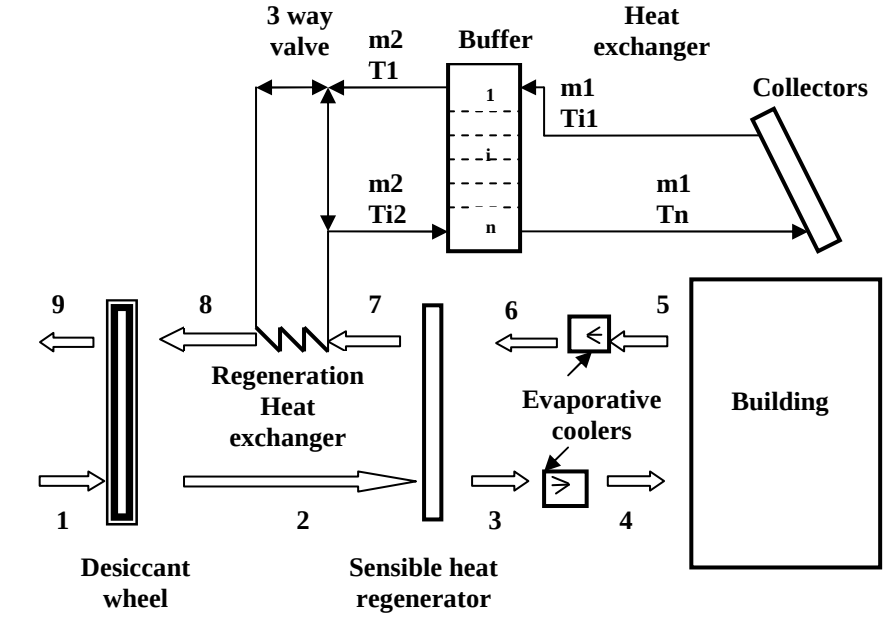

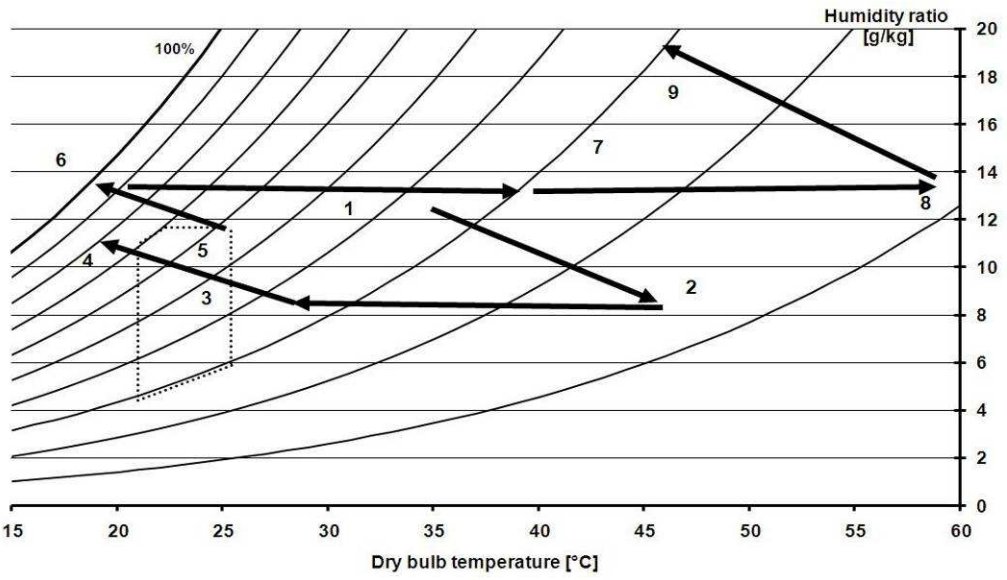

Figure 1: Desiccant cooling system with corresponding evolution of air properties in the psychometric chart

With reference to Figure 1, the conventional cycle operates as follows: outside air (1) is dehumidified in a desiccant wheel (2); it is then cooled in the sensible regenerator (3) by the return cooled air before undergoing another cooling stage by evaporation (4) and being introduced into the building. The operating sequence for the return air (5) is as follows: it is cooled to its saturation temperature by evaporative cooling (6) and then it cools the fresh air in the rotary heat exchanger (7). It is then heated in the regeneration heat exchanger by solar energy (8), it regenerates the desiccant wheel (9) by removing the humidity and exits the installation.

Modelling of the components

Sensible regenerator

A sensible regenerator is a porous matrix which passes periodically between a hot and a cold stream. The cellular matrix of the regenerator stores heat from the hot gas stream and releases it to the cold gas stream.

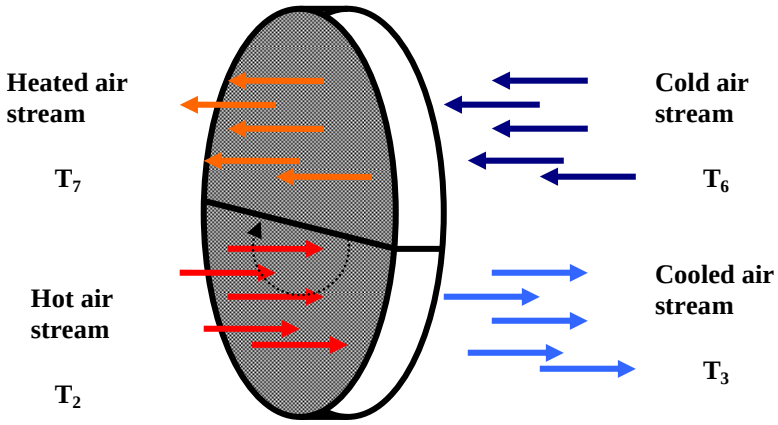

Figure 2: Sensible heat regenerator principle

For modelling purposes, the following assumptions are made:

- Heat transfer between air and the regenerator matrix is considered using a lumped transfer coefficient or a number of transfer units *(NTU)*
- The channels where the fluid flows are identical and parallel
- No leakage occurs between the air streams

The heat conservation and transfer governing equations, after Kays and London [6] and Maclaine-cross and Banks [7], are:

$$\frac{\partial Ta}{\partial t} + u\frac{\partial Ta}{\partial z} + \mu\frac{c_{pm}}{c_{pa} + w_a c_{pv}}\frac{\partial Tm}{\partial t} = 0 \quad (1)$$

$$\mu\frac{c_{pm}}{c_{pa} + w_a c_{pv}}\frac{\partial Tm}{\partial t} + J_t(T_{a,m} - T_a) = 0 \quad (2)$$

Kays and London [6] proposed the following correlation for regenerator efficiency (RE):

$$RE = \eta_{cf}\left(1 - \frac{1}{9\left(C_r^*\right)^{1.93}}\right) \quad (3)$$

Where:

$$C_r^* = \frac{M_m.c_{pm}.N}{C_{\min}} \quad (4)$$

$$\eta_{cf} = \frac{NTU_{cf}}{1 + NTU_{cf}} \quad (5)$$

is the efficiency of the counter-flow heat exchanger for balanced flow.

The outlet temperature (T_3) of the sensible regenerator can thus be calculated using:

$$RE = \frac{T_2 - T_3}{T_2 - T_6} \quad (6)$$

Desiccant wheel

The wheel is divided into two sectors the first is for dehumidification of moist air while the second is for the regeneration. It is a rotating porous matrix impregnated with a desiccant material that alternates periodically between a process air stream and a hot air stream. In contact with the dry desiccant, process air is dehumidified and heated by the heat of adsorption. The saturated desiccant then enters into contact with the hot air stream and is regenerated to again dehumidify the process air, perpetuating the dehumidification-regeneration cycle.

The wheel is driven by a small electrical motor, with a rotation speed that varies between 7 and 20 rph

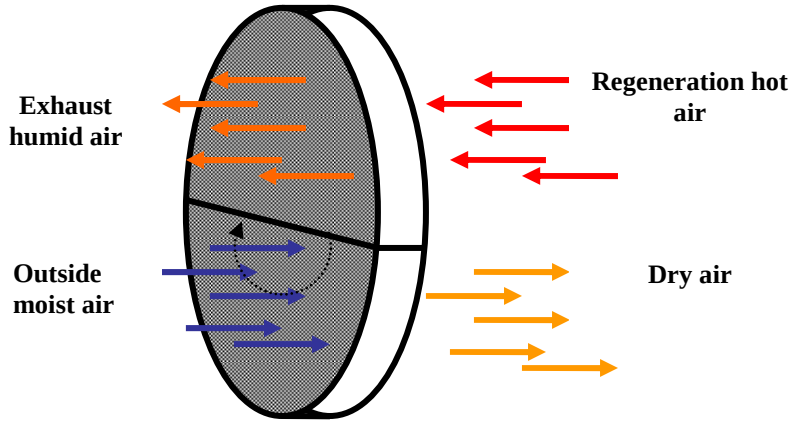

Figure 3: Desiccant wheel

The desiccant wheel model used below is that proposed first by Banks [8] and also by Maclaine-cross and Banks [7]. The following assumptions are made [3]:

- The state properties of the air streams are spatially uniform at the desiccant wheel inlet
- The interstices of the porous medium are straight and parallel
- There is no leakage or carry-over of streams
- The interstitial air velocity and pressure are constant
- Heat and mass transfer between the air and the porous desiccant matrix is considered using lumped transfer coefficients
- Diffusion and dispersion in the fluid flow direction are neglected
- No radial variation of the fluid or matrix states
- The sorption isotherm does not represent a hysteresis
- Air reaches equilibrium with the porous medium

Heat and mass conservation equations:

$$\frac{\partial h_a}{\partial t} + u\frac{\partial h_a}{\partial z} + \mu\frac{\partial H_d}{\partial t} = 0 \qquad (7)$$

$$\frac{\partial w_a}{\partial t} + u\frac{\partial w_a}{\partial z} + \mu\frac{\partial W_d}{\partial t} = 0 \qquad (8)$$

Heat and mass transfer equations:

$$\mu\frac{\partial H_d}{\partial t} + J_m\left(Le(T_{a,eq} - T_a)\frac{\partial h_a}{\partial T_a}\bigg|_w\right) + (w_{a,eq} - w_a)\frac{\partial h_a}{\partial w_a}\bigg|_T = 0 \qquad (9)$$

$$\mu\frac{\partial W_d}{\partial t} + J_m(w_{a,eq} - w_a) = 0 \qquad (10)$$

Equations (7), (8), (9) and (10) are coupled, hyperbolic and non-linear. With the assumption of the Lewis number *(Le),* equal unity and the desiccant matrix in equilibrium with air means that ($T_d = T_{eq}$ and $w_{eq} = w_a$). Banks [8] used matrix algebra and demonstrated that these equations (7 to 10) can be reduced by applying the potential function *Fi(T,w)* to the following system:

$$\gamma_i \mu \frac{\partial F_{i,eq}}{\partial t} + u \frac{\partial F_{i,a}}{\partial t} + \frac{\partial F_{i,a}}{\partial z} = 0 \quad \text{i=1;2} \tag{11}$$

$$\gamma_i \mu \frac{\partial F_{i,d}}{\partial t} + J_m (F_{i,eq} - F_{i,a}) = 0 \quad \text{i=1;2} \tag{12}$$

These equations are similar to those for the sensible regenerator (Equations 1 and 2), with the potential function F_i replacing the temperature and the parameters γ_i replacing the specific heat ratio, and they can be solved using analogy with heat transfer alone as suggested by Maclaine-cross and Banks [7] and Close and Banks [9]. There are many expressions for the potential functions of moist air-silica gel; we chose those proposed by Jurinak [10] and Stabat [11].

$$F_1 = h \tag{13}$$

$$F_2 = \frac{(273.15 + T)^{1.5}}{6360} + 1.1 w^{0.8} \tag{14}$$

The solution sequence for the desiccant wheel is then:

$$C_j^i = \dot{m}_a^j$$

$$C_{ri}^* = \frac{M_d N}{\dot{m}_{a\,\min}} \gamma_j^{i(moy)}$$

$$C_i^* = \frac{C_{\min}^i}{C_{\max}^i}$$

$$NUT_0 = \frac{1}{C_{\min}} \left(\frac{1}{(h_m A)_s} + \frac{1}{(h_m A)_r} \right)^{-1}$$

$$\varepsilon_i = \varepsilon_{cc} \left(NUT_0^m, C_i \right) \left[1 - \frac{1}{9 (C_{ri}^*)^{1.93}} \right] \text{ or } \varepsilon_i = C_{ri}^* \ (C_{ri}^* \le 0.4) \text{ for very low rotation speed}$$

For the desiccant wheel the efficiency is written with the potential functions instead of temperatures for the sensible regenerator:
(With $F_{i,k}$ where the subscript *i* indicates the potential and the subscript *k* indicates the position relatively to figure 1)

$$\varepsilon_1 = \frac{C_n^1}{C_{\min}^1} \frac{F_{1,2} - F_{1,1}}{F_{1,8} - F_{1,1}}$$

$$\varepsilon_2 = \frac{C_n^2}{C_{\min}^2} \frac{F_{2,2} - F_{2,1}}{F_{2,8} - F_{2,1}}$$

To calculate the outlet conditions of the regeneration stream the conservation equations are applied to the potential functions:

$$C_n^1\left(F_{1,2} - F_{1,1}\right) = C_r^1\left(F_{1,9} - F_{1,8}\right)$$

$$C_n^2\left(F_{2,2} - F_{2,1}\right) = C_r^2\left(F_{2,9} - F_{2,8}\right)$$

Having the potential functions calculated the temperature and humidity ratio at both outlet of the wheel can thus be calculated

Evaporative coolers

The humidification process occurs at a constant wet-bulb temperature. During the process, the energy needed for droplet evaporation is taken from the air which yields its temperature decrease and humidity increase. The enthalpy of the moist air at the evaporative cooler inlet is the sum of the enthalpy of the dry air and that of the water vapor. At the evaporator cooler outlet; the enthalpy of the dry air decreases due to the temperature decrease while that of water vapor increases due to the increased water vapor mass but the total enthalpy of moist air is approximately constant, with a slight increase due to the addition of the enthalpy of liquid water droplets.

$$h(T,w)_{a,inlet} = h(T,w)_{a,outlet} \quad (15)$$

The validity of this assumption can be verified on the psychometric chart where the lines of constant wet-bulb temperature are parallel to the constant enthalpy lines, especially when the temperature and humidity ratio are, respectively, between 19 and 25℃ and 7 and 15g/Kg, which is in the application domain of desiccant evaporative cooling.

Heat pipe vacuum tube solar collectors

In an evacuated heat pipe collector (figure 4), a sealed copper pipe containing a vaporizable fluid is bonded to a copper fin plate absorber located inside a glass tube. A small copper condenser is attached from one side to the top of the heat pipe and from the other side to the storage working fluid. The heat pipe is an evaporating-condensing device. As the sun shines on the absorber, the pipe is heated and some of the liquid inside evaporates. The vapour rises toward the condenser at the top of the heat pipe and condenses on being cooled by the storage water circulating in the manifold. The liquid then returns to the heat pipe. The vacuum tube ensures minimization of the heat losses of the collector.

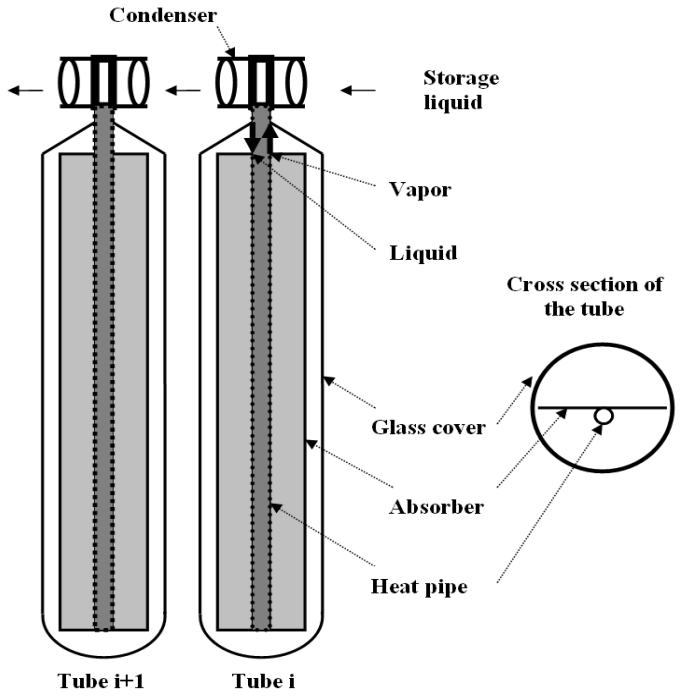

Figure 4: Heat pipe vacuum tube collectors

A model for the HPVT is proposed below, separately considering each component [12] and [13] of the tube, i.e. the glass cover, the absorber, the heat pipe fluid, the condenser and the storage fluid. The following assumptions are made regarding the model:

- The properties of the materials are independent of the temperature.
- The temperature gradient along the absorber and the condenser is negligible.
- Due to the sufficient quantity of fluid in the heat pipe (more than 90% of the heat pipe volume), the vapour is not superheated
- The liquid returning from the condenser to the heat pipe is saturated.
- The glass cover is clean and completely transparent to solar radiation.
- The part of radiation reflected by the absorber leaves the tube.
- Due to the vacuum, convection does not occur inside the tube.
- Conduction in the storage fluid direction (z) is considered to be negligible.

The glass cover exchanges heat by convection with the outside air and by radiation with the sky and the absorber. The absorber receives solar radiation and heats the fluid inside the tube. The vapour rising from the heat pipe enters the condenser and releases energy to the circulating storage fluid, then exits the condenser as a saturated liquid. The heat pipe liquid is heated to saturation before the evaporation process begins.

The governing equations for each component (characterized by heat capacity *C* and temperature *T*):

Glass cover:

$$M_g C_g \frac{dT_g}{dt} = \varepsilon_g \sigma S_g (T_{sky}^4 - T_g^4) + \varepsilon_p \sigma S_p (T_p^4 - T_g^4) + S_g h_g (T_a - T_g) \quad (16)$$

Absorber:

$$M_p C_p \frac{dT_p}{dt} = \varepsilon_p \sigma S_p (T_g^4 - T_p^4) + G \tau \alpha S_p + S_H h_H (T_{sat} - T_p) \quad (17)$$

Vapour flow rate:

$$m_v L = S_H h_H (T_p - T_{sat}) \quad (18)$$

Condenser:

$$M_c C_c (\frac{dT_c}{dt}) = m_v L_v + S_c h_c (T_f - T_c) \quad (19)$$

Storage fluid:

$$m_1 C_f (\frac{\partial T_f}{\partial t} + u \frac{\partial T_f}{\partial z}) = S_c h_c (T_c - T_f) \quad (20)$$

Storage tank

In order to take into account thermal stratification in the storage tank, it is divided into *n* nodes [14]. The following equations apply to the first node, the last node (*n=12*) and the *ith* current node:

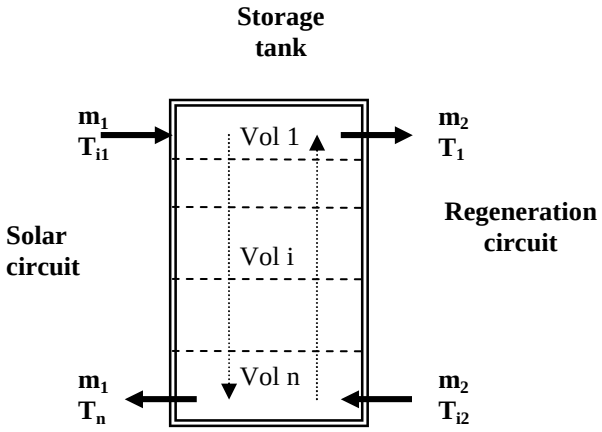

Figure5: Storage tank divided to n nodes

$$\rho_1 V_1 C_f \frac{dT_1}{dt} = m_1 C_f (T_{i1} - T_1) + \frac{\lambda S_i}{e_{12}}(T_2 - T_1) + m_2 C_f (T_2 - T_1) + S_1 K_1 (T_a - T_1) \quad (21)$$

$$\rho_n V_n C_f \frac{dT_n}{dt} = m_1 C_f (T_{n-1} - T_n) + \frac{\lambda S_i}{e_{n-1,n}}(T_{n-1} - T_n) + m_2 C_f (T_{i2} - T_n) + S_n K_n (T_a - T_n) \quad (22)$$

$$\rho_i V_i C_f \frac{dT_i}{dt} = m_1 C_f (T_{i-1} - T_i) + \frac{\lambda S_i}{e_i}(T_{i-1} - T_i) + m_2 C_f (T_{i+1} - T_i) + S_i K_i (T_a - T_i) - \frac{\lambda S_i}{e_i}(T_i - T_{i+1}) \quad (23)$$

These sets of equations describing the above-presented models are introduced into SPARK [15] - a general simulation environment that supports the definition of simulation models, providing the solution of these models via a robust and efficient differential/algebraic equation solver [16]. In SPARK, the modeler describes the set of equations defining a model as an equation-based object. At the lowest level, an atomic object characterizes, in SPARK language, a single equation and its variables. Macroscopic objects can then be created as an assembly of various atomic or macroscopic objects. The entire model is built by connecting the various required objects. One should note that the model is input/output-free. The particular problem to be solved is then described by imposing the adequate input data (boundary and initial conditions) and by specifying the variables to be solved. So in this environment it is not necessary to order the equations or to express them as assignment statements (algorithms), unlike conventional modular environments.

In next section the above presented model is experimentally validated.

2. Experimental validation

The experimental desiccant installation at La Rochelle [1] was used to validate the model presented above. The desiccant air handling unit consists of silica gel desiccant wheel, an aluminum sensible regenerator, two rotating humidifiers, high performance ventilators, a regeneration heat exchanger (water to air) and an electrical backup used for experimental purpose. The air handling unit is powered by 40 m^2 of heat pipe vacuum tube collectors and storage tank of 2350 liters.

Psychrometers are used to measure the moist air properties at each section of the air handling unit (position 1 to 9). Each psychrometer consists of 2 Pt100 sensors: the first delivers the dry bulb temperature and the second the wet bulb temperature. The local atmospheric pressure is measured too thus the humidity ratio and relative humidity can be accurately measured. The temperature of hydraulic system is measured by the means of Pt100 sensors integrated to the pipes by means of thermo wells. All the Pt100 sensors were tuned on a temperature range going from 0° to 100℃ . The water flow rates are measured using ultrasonic sensor. The air flow rates were measured using the gas tracer method.In the difficulty to tune a pyranometer the solar global radiation is measured using two different pyranometers.

Figure 1 shows a general scheme of the experimental installation. In order to test different outside operating conditions (to test the models under different conditions) an outside conditions simulator was coupled to the desiccant air handling unit. The outside conditions simulator consists of a pre-heater, a humidifier and a heater, this permits the test at high temperatures and high humidity ratio.

The cooling load on the installation was controlled using load simulator that consists of heater and replaces the building load. This permitted to control the return conditions during the tests.

For the model validation different operating were considered for all the components.

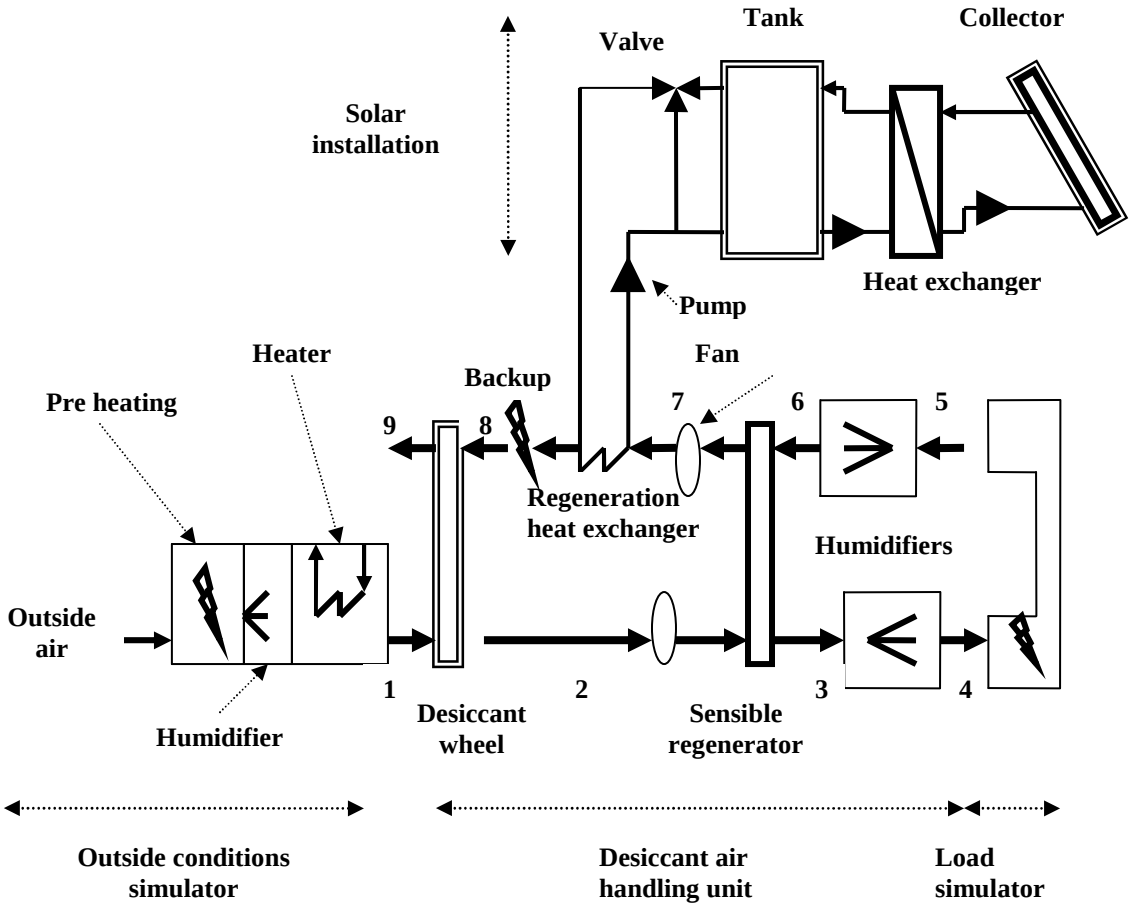

Figure 6: Experimental solar desiccant cooling installation of La Rochelle

Experimental validation of components' model

The sensible regenerator

The outlet temperature of the sensible regenerator depends on the temperature at both inlets of the regenerator. Various temperature differences between the inlets of the regenerator (position 2 and 6) were considered. Figure 7 below plots the experimental efficiency of the regenerator as well as the outlet temperature deviation of the model relative to the measurements.

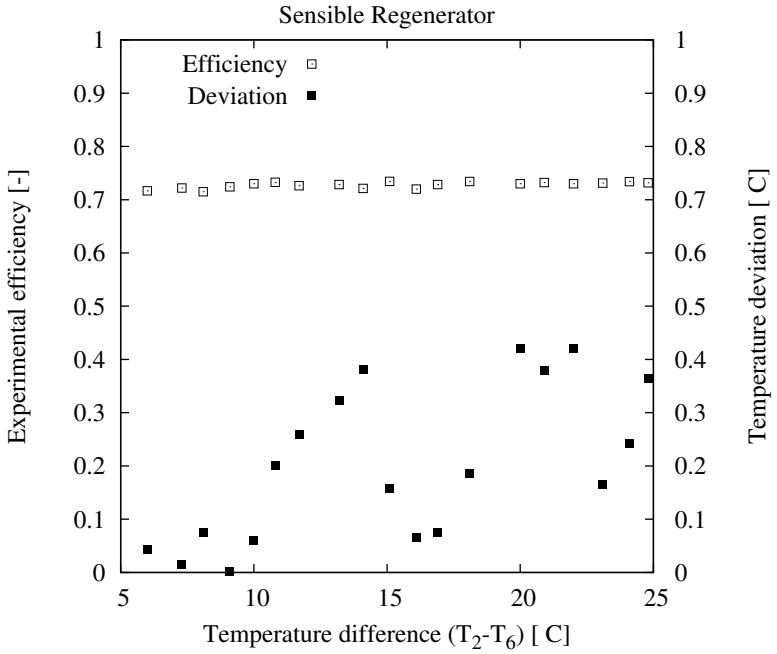

Figure 7: experimental efficiency of the sensible regenerator and deviation of the model prediction of the outlet temperature with respect to measurements

Figure 7 shows that the measured efficiency of the sensible regenerator is nearly constant and equal to 0.7 in all cases; it also shows that the error in predicting the outlet temperature (position 3 in Figure 1) of the regenerator using the model presented above is low, never exceeding 0.5℃. It should be noted that this deviation is in the domain of the accuracy of the measurements. This accuracy can be predicted, as the efficiency is constant, independent of the operating temperature.

The desiccant wheel

For the desiccant wheel model, different inlet conditions (position 1 with reference to Figure 1) were considered with the temperature varying from 25℃ to 38℃ and the humidity ratio from 10 to 15g/kg, and for different regeneration temperatures (60℃, 65℃, 70℃ and 80℃). Figure 8 plots temperature error against humidity ratio error for the most significant points.

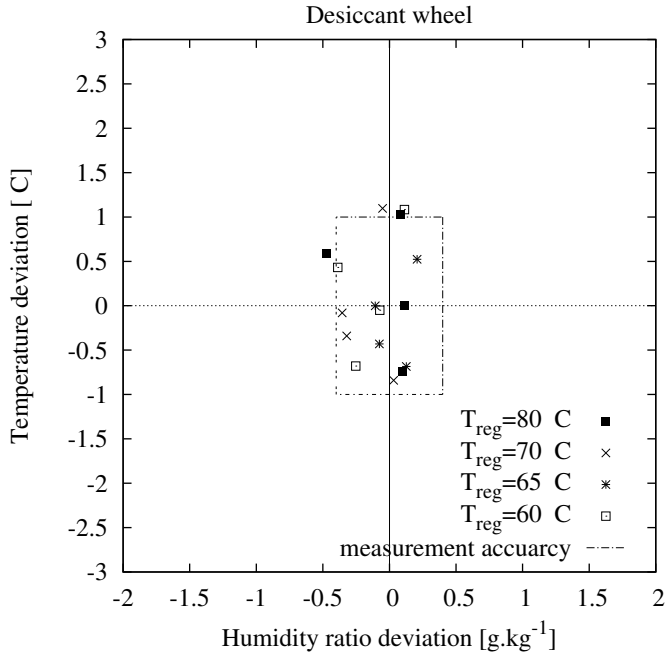

Figure 8: Deviation of the outlet temperature and outlet humidity ratio in comparison with measured results for different operating conditions

The maximum error in predicting the temperature at the outlet of the desiccant wheel is 1℃ (a relative error of 2.5%). This error occurs for different regeneration temperatures and for the same inlet temperature of the wheel, 38℃, whic h is not in the application domain of desiccant cooling. For the humidity ratio, the maximum error is 0.5 g/kg but it should be noted that the accuracy of humidity ratio measurement in the air handling unit is 0.4 g/kg (this accuracy can be tested by comparing the humidity ratio at points 2, 3 and 4 of Figure 1 with the supply humidifier switched off; in this case the points must have the same humidity ratio), so the error is in the validity domain of the measurements.

This accuracy of the model is obtained when the model is dynamically parameterized in function of the operating regeneration temperature; if this is not the case, the deviation will be more significant when the operating regeneration temperature is much higher than that of rating conditions used to parameterize the model [1].

The evaporative cooler

For the evaporative cooler model, Figure 9 demonstrates that the enthalpy is constant across the evaporative cooler and that the constant enthalpy model can thus accurately predict the outlet temperature of the evaporative cooler.

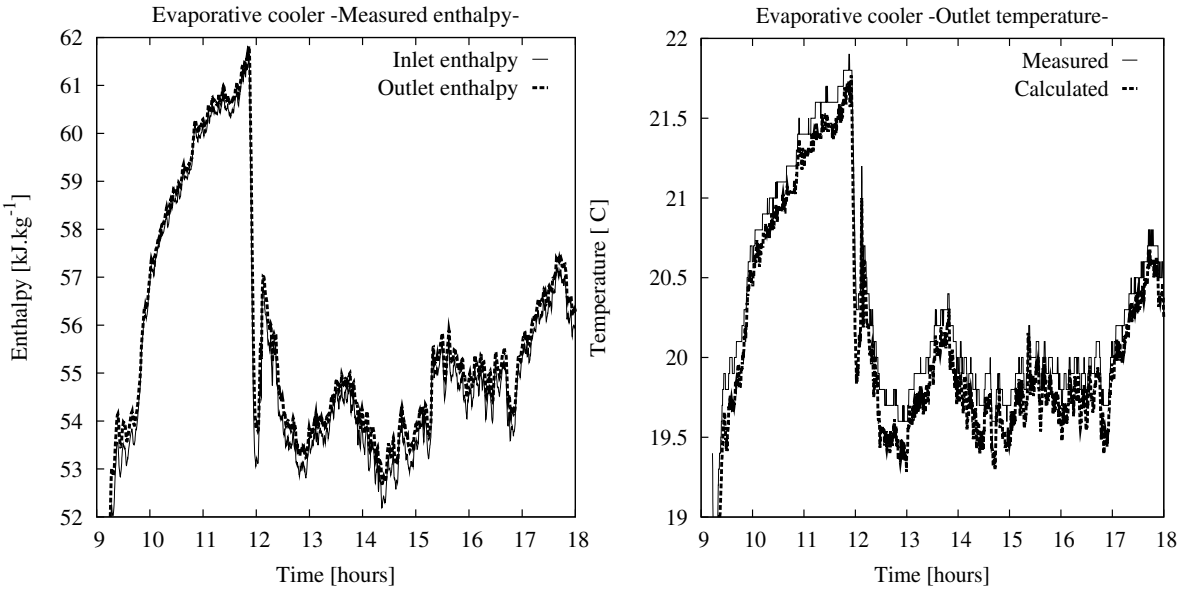

Figure 9: Measured inlet and outlet enthalpy of the evaporative cooler (left) and comparison between the measured and calculated outlet temperature of the evaporative cooler

Solar Collectors

Three different recorded days were used to validate the collector model. The first day is representative of typical summer conditions and the collectors are under storage load only, the second day is of atypical solar radiation with the same storage load and the third day represents a typical desiccant cooling load conditions e.g. storage in the morning and regeneration in the afternoon.

Once the solar radiation in the collectors' plane, the outside temperature, and the inlet temperature were recorded, the computed and measured collector outlet temperatures were compared.

Day 1:

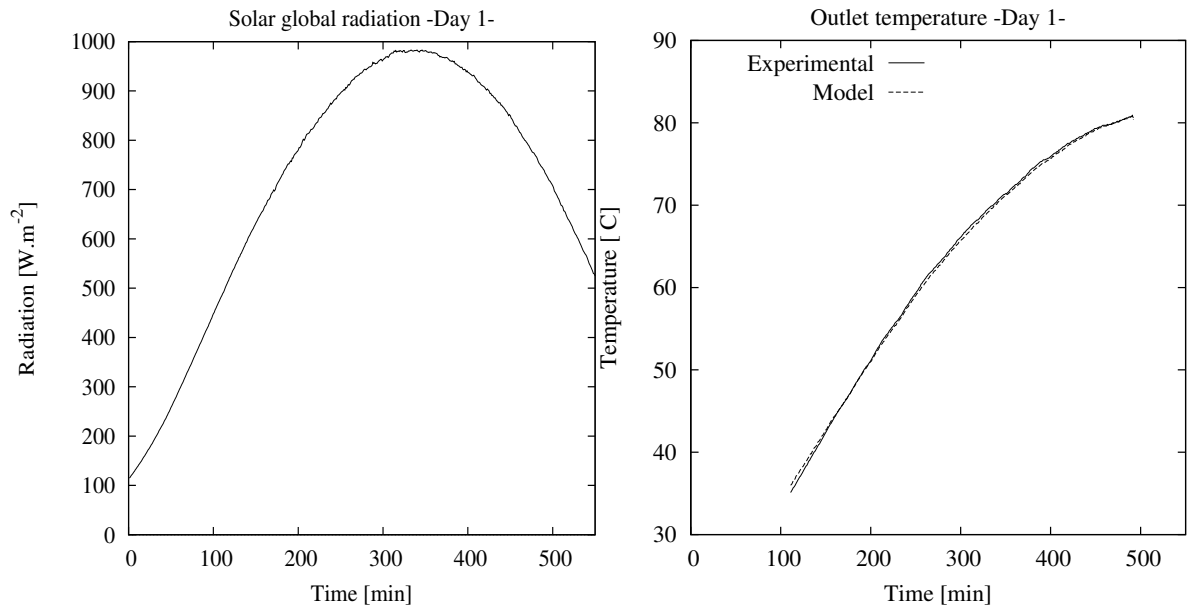

Figure 10: comparison of the predicted outlet temperature of the collectors with the measured one for perfect radiation conditions and a storage load

Comparison between the computed and the measured temperatures for the typical summer day conditions shows the model's high performance in predicting collector outlet temperature with a negligible error. This accuracy is due to the fact that each component is taken into consideration by the model and the calculations are performed in each vacuum tube simultaneously (400 tubes).

While collector outlet temperature can thus be predicted accurately in normal radiation conditions, it is very important to study the performance of the model for atypical conditions.

Day 2:

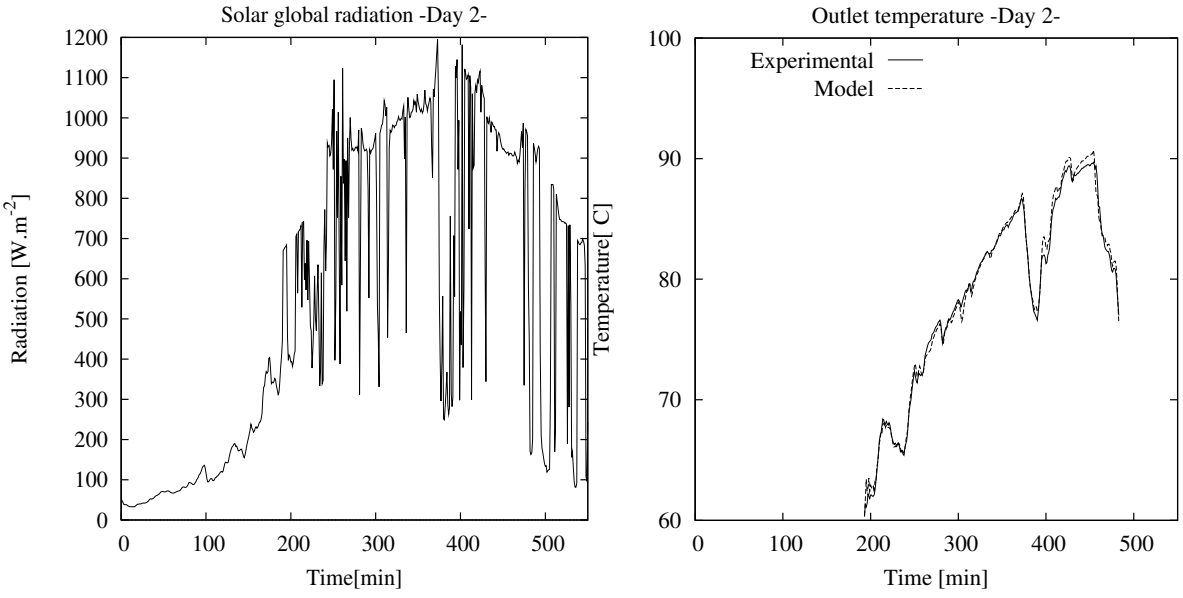

Figure 11: comparison of the predicted outlet temperature of the collectors with the measured one for fluctuating radiation conditions and a storage load

By comparing the calculated and the measured outlet temperatures for the atypical conditions day, when the overall solar radiation fluctuated constantly, it can be seen that the model very accurately predicts the outlet temperature for the whole day, whatever the amplitude of the solar radiation fluctuations and the maximum error is always below 2℃ but the model does not show any time delay with respect to the measurments.
In these first two cases, the model correctly predicts the collector outlet temperature under different radiation conditions but for storage load. The next step in the validation procedure is to study the model's response to a desiccant cooling load, i.e. storage in the morning, with regeneration in the afternoon.

Day 3:

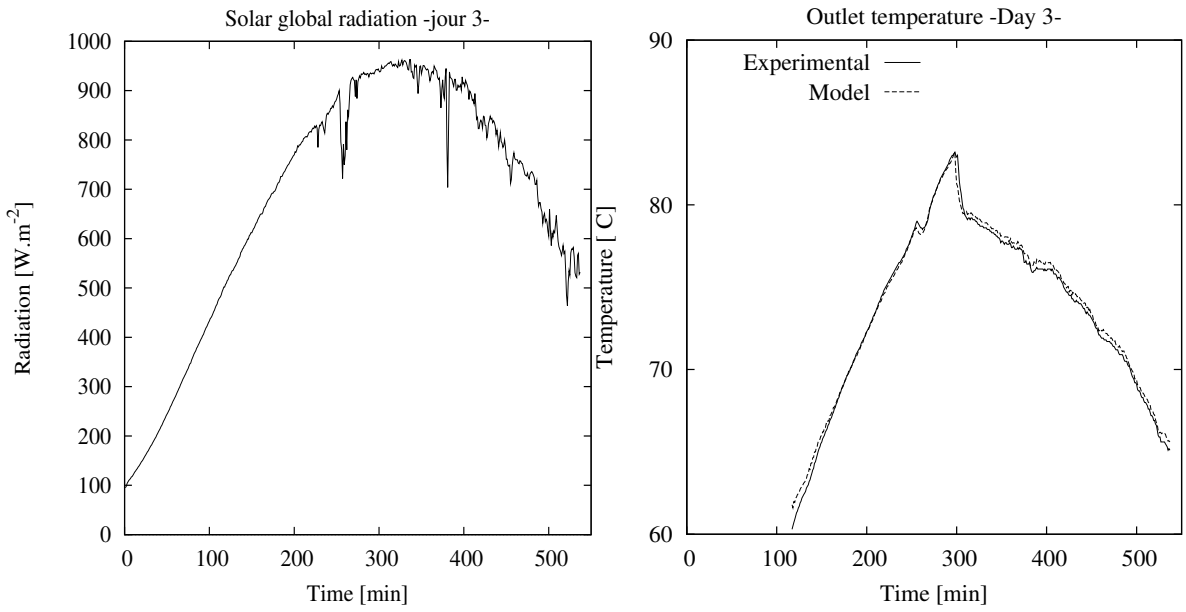

Figure 12: comparison of the predicted outlet temperature of the collectors with the measured one for good radiation conditions and a desiccant load (storage in the morning and regeneration starts in the middle of the day)

Under typical desiccant cooling load there is remarkable agreement between the predicted and the measured outlet temperatures, for both storage and regeneration periods even for a sever transition period at t=300 min.

These three typical days show the capacity of the model to predict the outlet temperature of the collectors with a negligible error.

Storage Tank

Two different scenarios are considered for the validation of the storage tank model. In the first only storage is considered (m_1>0 and m_2=0 in reference to Figure 5) while for the second it concerns desiccant cooling application with storage in the morning and regeneration in the afternoon (m_1>0 and m_2>0). The flow rates m_1 and m_2 are measured as well as the inlet temperature of the storage tank. The predicted and measured temperatures at the top and the bottom of the buffer are compared in the Figure 13 below.

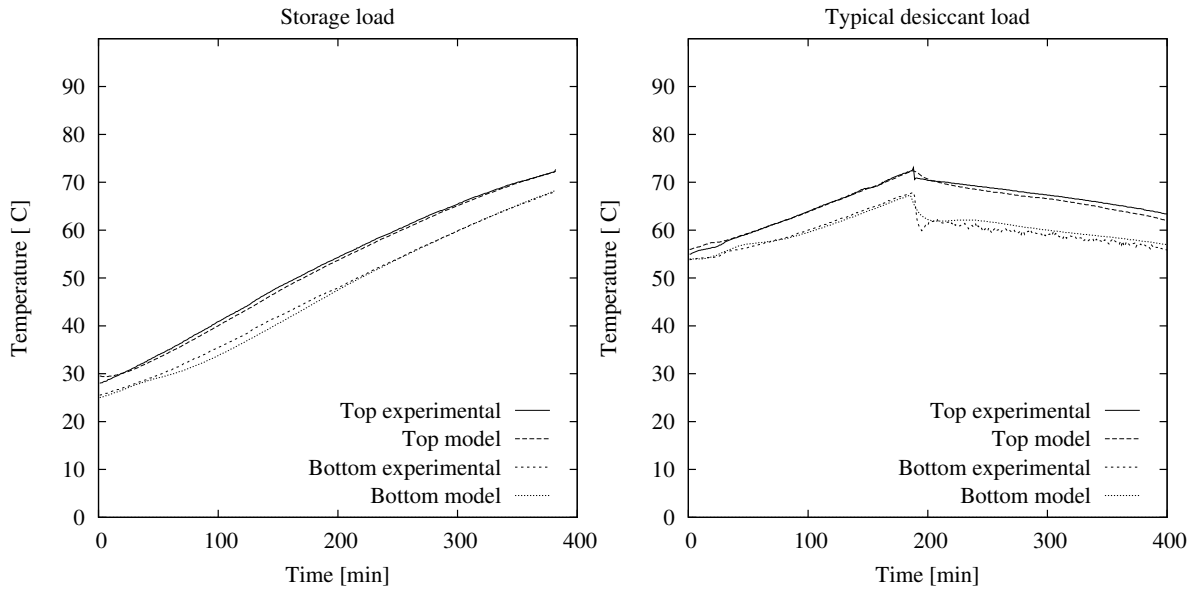

Figure 13: Comparison of the predicted temperature with measured one for the top and the bottom of the storage tank under a storage load (left) and a desiccant load (right)

In both scenarios the model can accurately predict the temperature at the top and the bottom of the buffer. In the first case the stratification remains fairly constant but increases when the storage and the regeneration are combined. This may at first, appear incoherent as more mixing occurs in the latter case. The fact that stratification is greater with the regeneration is that the regeneration load was applied by water loss and the return water was cold and significantly below the tank temperature which amplified the stratification. Even with this extreme case the model was capable to predict accurately the temperature at the top and the bottom of the buffer.

Now if the model has shown an acceptable accuracy when considered solely, we have to be sure that this accuracy will not be lost when coupling the components making the numerical simulation useless. In the next section the error propagation will be analysed and the impact on the supply temperature is examined.

Error propagation

For the solar installation the maximum error in the temperature prediction was that of the tank with a maximum error of 1℃ which yields an er ror in the prediction of the regeneration temperature. Or the experimental results showed that 1℃ difference in the regeneration temperature does not have any practical impact on the performance of the desiccant wheel and thus on the supply conditions.

For the air handling unit the evaporative cooler model and the sensible regenerator models has shown negligible errors. In reversal the desiccant wheel model has shown simultaneous error in temperature and humidity. Let us consider an error α in the prediction of the outlet temperature T_2 of the desiccant wheel.

The temperature T_3 at the outlet of the sensible regenerator in function the inlet temperature T_2 and T_6 of the regenerator and its efficiency η:

$$T_3 = T_2(1-\eta) + \eta T_6 \tag{24}$$

With the error α in the prediction of the temperature T_2 the temperature T_3 is now:

$$T_3^{'} = T_3 + \alpha(1-\eta) \tag{25}$$

This means that an error α in the prediction of the T_2 will yield an error $(1-\alpha)$ in the prediction of T_3. Now considering an error β in the prediction of the humidity ratio at the outlet of the wheel, this will yield an error at the outlet temperature of the evaporator cooler in the order of:

$$\Delta T = \frac{h_{fg}\beta}{c_{pa}} \tag{26}$$

h_{fg} is the latent heat of vaporization of water.

With a maximum deviation of 2℃ and 0.4 g/kg in the temperature and humidity prediction at the outlet of the desiccant wheel and appropriately combining the impact of the errors we have a maximum error of 1.3℃ in the prediction of the supply temperature. This is the maximum error in the supply temperature that can be committed by the model.

Finlay we will compare the overall model prediction for the air handling unit coupled with the solar installation for day under typical desiccant operations.

Overall performance of the model

A day under desiccant operation is selected to validate the overall model. The response of the model will be compared with the measured performance for the most important components and especially for the supply conditions. Figure 14 below shows the outside conditions.

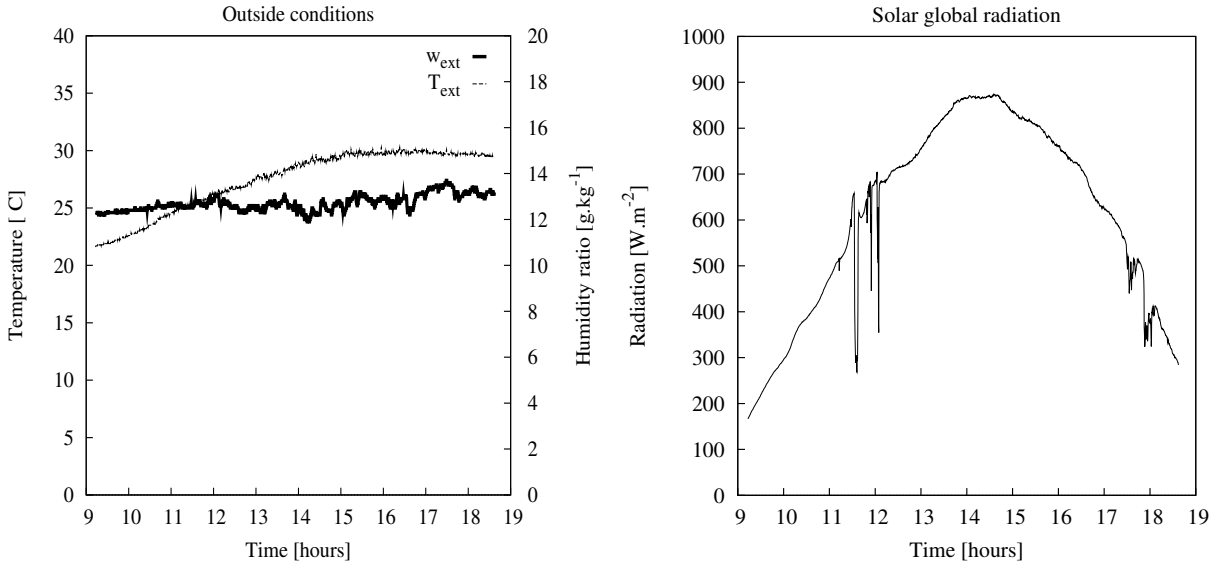

Figure 14: Outside temperature and humidity ratio (left) and solar global radiation for the considered day

The outlet temperature of the collectors, the temperature at the bottom and the top the storage tank as well as the regeneration temperature are shown on the figures below. We notice that the error is below 1℃ in all the cases .

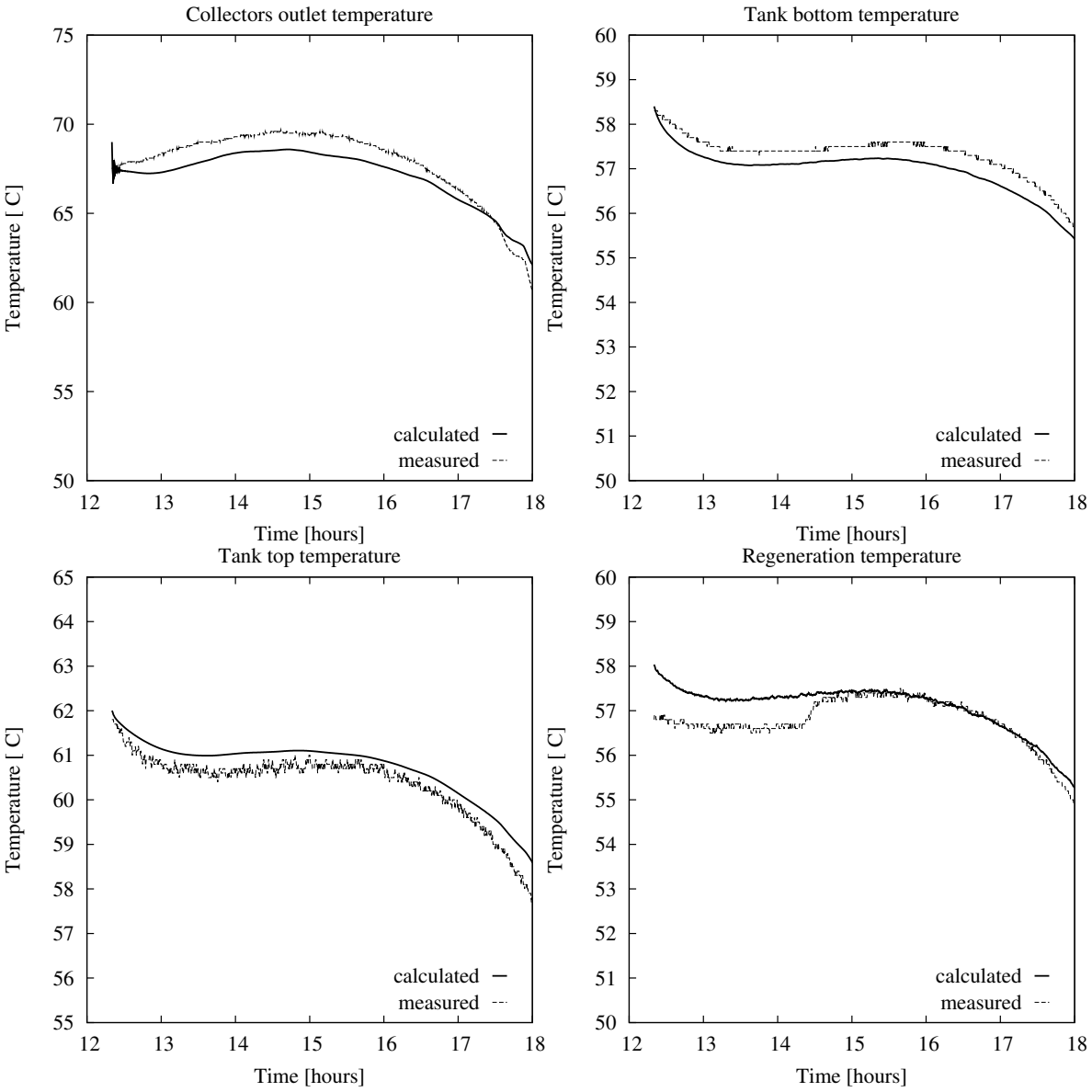

Figure 15: Comparison of the predicted temperature with the measured one for the collectors outlet, storage top, storage bottom, and regeneration air

Figure 16 compares the measured outlet conditions of the desiccant wheel to those predicted by the model. The profiles of the temperature and humidity ratio are very well predicted by the model during the whole day. For the measured temperature we noticed some peaks et we can count 7 peaks per hour and for each peak in the temperature corresponds a minimum in the outlet humidity of the wheel. Or the angular speed of the wheel is 7 rounds per hour this mean for each revolution of the wheel corresponds a peak. The reason behind this behaviour is a probable anomaly in the desiccant wheel with a sector having more desiccant and yields more dehumidification this mean an increase in the outlet temperature of the wheel. It is evident that the desiccant does not take into account this anomaly.

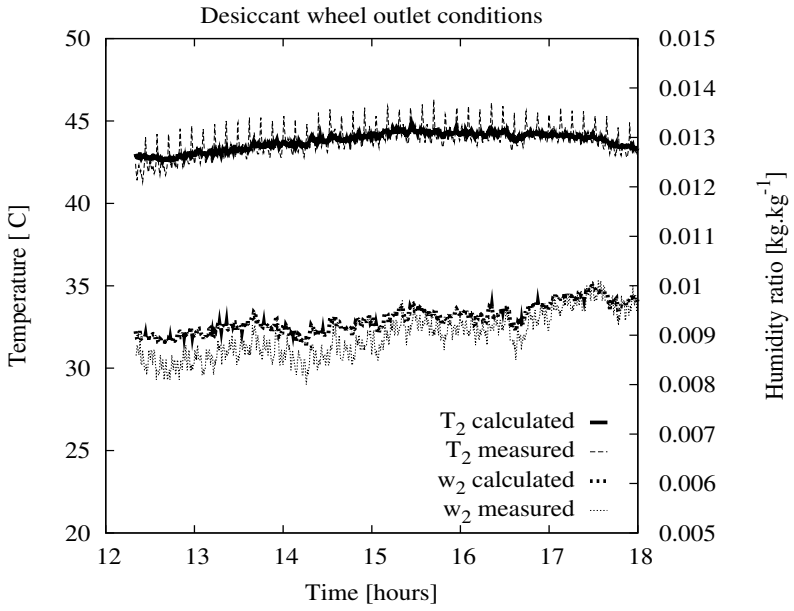

Figure 16: Comparison of the outlet temperature and outlet humidity ratio of the desiccant wheel for the considered day

For the supply temperature, figure 17 shows that the maximum committed error is below 0.5 ℃ and appears during the increase of the humidific ation rate.

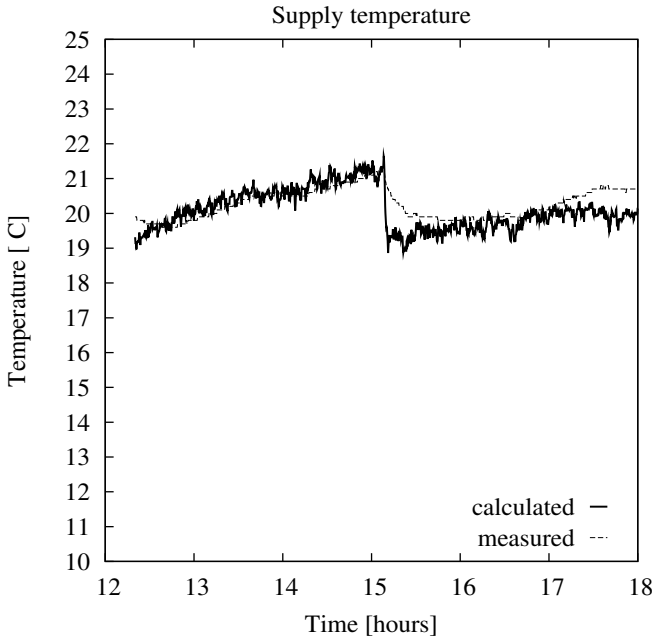

Figure 17: Comparison of the predicted and measured supply temperature of the installation (position 4 on the figure 1) for the considered day

All these results proofs that the model of the installation can predict accurately the supply conditions of the solar desiccant installation.

In the next section a transient model of the desiccant wheel is presented.

3. Transient model of the desiccant wheel and experimental validation

Conventional models of the desiccant wheel predict a mean temperature and a mean humidity ratio at the outlet of the desiccant wheel. In reality and due to the low rotation speed of the desiccant wheel, the temperature and humidity distribution at the outlet is not uniform. The model presented in this section is a two dimensional model that gives the temperature and humidity evolution across the wheel and at its outlets.

Model description

The desiccant wheel scheme is given in the figure below

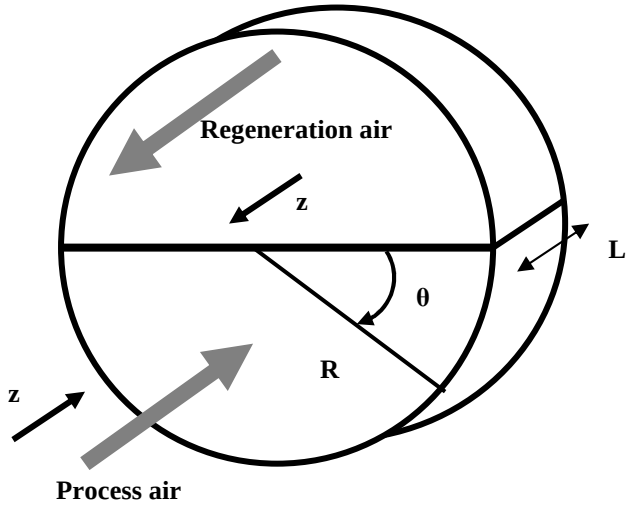

Figure 18: Schematic of the desiccant wheel

In the model development the following assumption are taken:

- The state properties of the air streams are spatially uniform at the desiccant wheel inlet
- The interstices of the porous medium are straight and parallel
- There is no leakage or carry-over of streams
- The interstitial air velocity and pressure are constant
- Heat and mass transfer between the air and the porous desiccant matrix is considered using lumped transfer coefficients
- Diffusion and dispersion in the fluid flow direction are neglected
- No radial variation of the fluid or matrix states

A basic element in the angular and width direction of the desiccant wheel is considered and can be presented as follows:

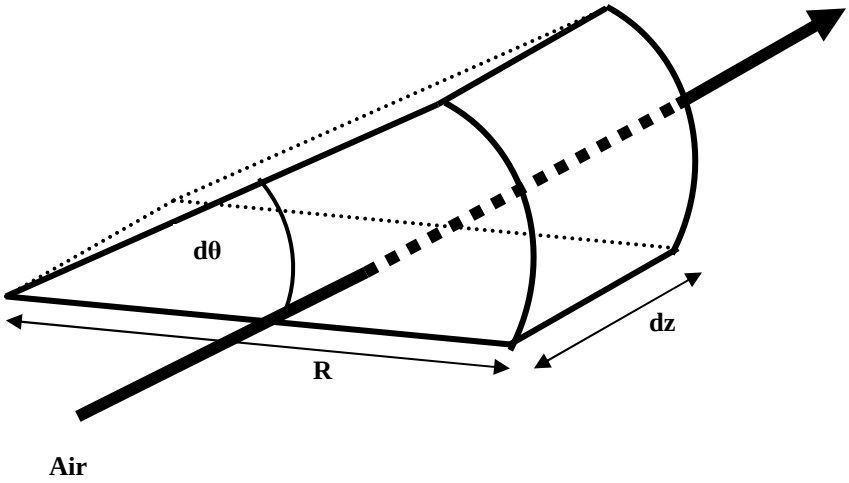

Figure 19: Basic element of the desiccant wheel

Fundamental equations of heat and mass transfer for the basic element

Mass conservation equation

$$M_d \frac{\partial W}{\partial t} + m_a \left(\frac{\partial w_a}{\partial t} + u \frac{\partial w_a}{\partial z} \right) = 0 \quad (27)$$

Mass transfer equation

$$M_d \frac{\partial W}{\partial t} = h_m S \left(w_a - w_{eq} \right) \quad (28)$$

Heat conservation equation

$$M_d \frac{\partial H}{\partial t} + m_a \left(\frac{\partial h_a}{\partial t} + u \frac{\partial h_a}{\partial z} \right) = 0 \quad (29)$$

Heat transfer equation

$$M_d \frac{\partial H}{\partial t} = h_m S \left(w_a - w_{eq} \right) \left(h_{fg} + c_{pv} T_a \right) + h_t S \left(T_a - T_d \right) \quad (30)$$

Variable change

The time t is related to the angular position θ with the following equation

$$\frac{t}{\tau_{ro}} = \frac{\theta}{\pi} \text{ so } t = \frac{\tau_{ro}}{\pi} \theta ,$$

Where τ_{ro} is the rotation period of the process or regeneration and N is the angular speed of the wheel.

The partial derivative of a variable *x* with respect to time *t* can be thus written with respect to the angular position θ following: $\frac{\partial x}{\partial t} = \frac{\pi}{\tau_{ro}} \frac{\partial x}{\partial \theta}$

This yields the following system:

Mass conservation equation

$$M_d \frac{\pi}{\tau_{ro}} \frac{\partial W}{\partial \theta} + m_a \left(\frac{\pi}{\tau_{ro}} \frac{\partial w_a}{\partial \theta} + u \frac{\partial w_a}{\partial z} \right) = 0 \quad (31)$$

Mass transfer equation:

$$M_d \frac{\pi}{\tau_{ro}} \frac{\partial W}{\partial \theta} = h_m S \left(w_a - w_{eq} \right) \quad (32)$$

Heat conservation equation

$$M_d \frac{\pi}{\tau_{ro}} \frac{\partial H}{\partial \theta} + m_a \left(\frac{\pi}{\tau_{ro}} \frac{\partial h_a}{\partial \theta} + u \frac{\partial h_a}{\partial z} \right) = 0 \quad (33)$$

Heat transfer equation

$$M_d \frac{\pi}{\tau_{ro}} \frac{\partial H}{\partial \theta} = h_m S \left(w_a - w_{eq} \right) \left(h_{fg} + c_{pv} T_a \right) + h_t S \left(T_a - T_d \right) \quad (34)$$

The obtained equation system is coupled non linear hyperbolic, since the enthalpy of the moist air and of the desiccant depend on the water content and on the temperature.

In the bibliography the equations were solved by Macalaine-cross, [17] and Stabat, [11] by neglecting the terms $\frac{\partial w_a}{\partial \theta}$ and $\frac{\partial h_a}{\partial \theta}$ in front of transport term which yields a simplification of the equations and of the matrix to be solved. In this work we conserved these terms.

Transformation to a discrete problem and restriction to 2 dimensions

The wheel is divided into elementary domains following the figure below

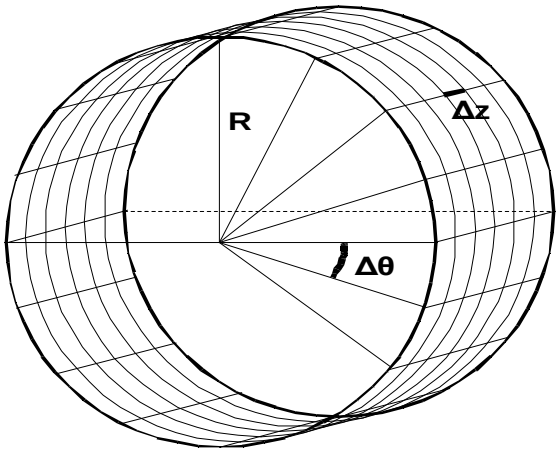

Figure 20 : discretisation of the desiccant wheel

Since in equations the radius R of the wheel does not appear since the variables are assumed to be constant in the radial direction the problem can thus be treated as two dimensional problem following z and θ.

The considered steps are then:

$$\Delta\theta = \frac{2\pi}{Na} \text{ and } \Delta z = \frac{L}{Np}$$

Where *Na* is the number of steps in the angular position θ direction and *Np* is the number of steps in the width z direction. The domain can be represented on Cartesian scale:

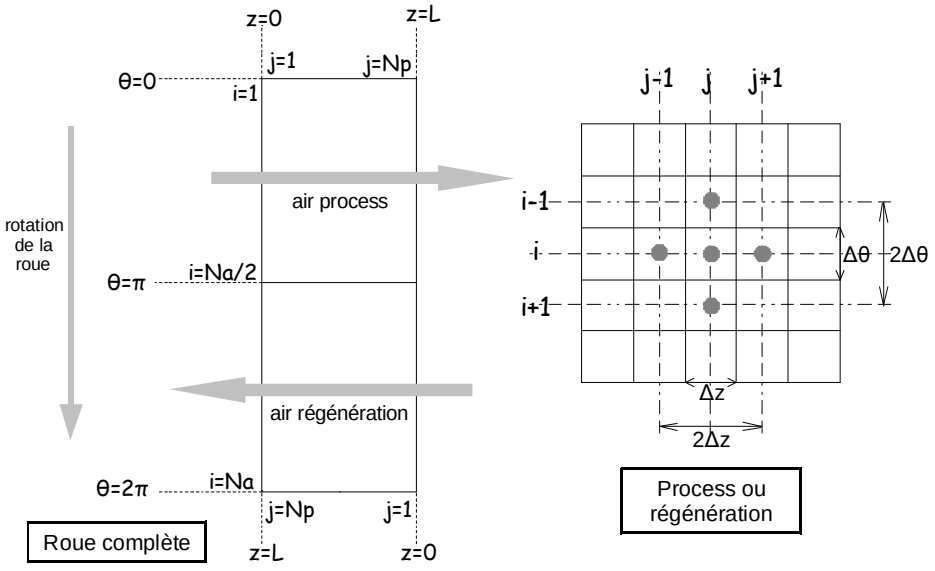

Figure 21: Cartesian representation of the grid

For each node in the center of the elementary domain is identified by the coordinate (i,j) where i corresponds to the angular position and j to the width position:

For the process:

$$0 < \theta < \pi \Leftrightarrow i = 1 \; to \; \frac{Na}{2} \quad \begin{cases} j = 1 & process \;\; inlet \quad (z = 0) \\ j = Np & process \;\; outlet \quad (z = L) \end{cases}$$

For the regeneration:

$$\pi < \theta < 2\pi \Leftrightarrow i = \frac{Na}{2} + 1 \; to \; Na \quad \begin{cases} j = 1 & regeneration \;\; inlet \quad (z = 0) \\ j = Np & regeneration \;\; outlet \quad (z = L) \end{cases}$$

Estimation of the partial derivatives

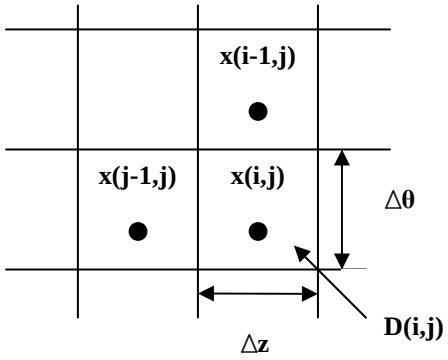

Figure 22: Current and neighbor nodes

The estimation of the partial derivatives is done using an upwind interpolation that permits expressing the frontiers values in function of the considered node and in function of the previous node.

The derivative with respect to θ:

$$\frac{\partial x}{\partial \theta} = \frac{\left(x_{i,j} - x_{i-1,j}\right)}{\Delta\theta}$$

The derivative with respect to z:

$$\frac{\partial x}{\partial z} = \frac{\left(x_{i,j} - x_{i,j-1}\right)}{\Delta z}$$

The moist air enthalpy is expressed by:

$$h_a = c_{pa}.T_a + w_a\left(h_{fg} + c_{pv}.T_a\right) \quad (35)$$

The desiccant enthalpy is expressed following Brandemuehl and Banks [18] and Stabat [11]

$$H = c_{pd}\,T_d + c_{pv}\,W\,T_d + \frac{h_{fg}\,\Delta\lambda}{k}e^{-kW} - 1 \quad (36)$$

Replacing the enthalpies and derivative by the above equations, for each node (i,j) we have finally:

Mass conservation equation

$$M_d'\left(W_{i,j} - W_{i-1,j}\right) + m_a'\left(w_{a\,i,j} - w_{a\,i-1,j}\right) + m_a * \left(w_{a\,i,j} - w_{a\,i,j-1}\right) = 0 \quad (37)$$

Mass transfer equation

$$M_d'\left(W_{i,j} - W_{i-1,j}\right) - h_m S' w_{a\,i,j} = -h_m S' w_{eq\,i,j} \quad (38)$$

Heat conservation equation

$$\begin{aligned}&\left(c_{m\,i,j}\,T_{d\,i,j}-c_{m\,i-1,j}\,T_{d\,i-1,j}\right)+\left(c_{a\,i,j}\,T_{a\,i,j}-c_{a\,i-1,j}\,T_{a\,i-1,j}\right)+m_a'\,h_{fg}\left(w_{a\,i,j}-w_{a\,i-1,j}\right)\\&+\left(c_a{}^*{}_{i,j}\,T_{a\,i,j}-c_a{}^*{}_{i,j-1}\,T_{a\,i,j-1}\right)+m_a{}^*\,h_{fg}\left(w_{a\,i,j}-w_{a\,i,j-1}\right)\\&=-M_d'\,h_{fg}\,\frac{\Delta\lambda}{k}\left(\exp(-kW_{i,j})-\exp(-kW_{i-1,j})\right)\end{aligned}\qquad(39)$$

Heat transfer equation

$$\begin{aligned}&\left(c_{m\,i,j}\,T_{d\,i,j}-c_{m\,i-1,j}\,T_{di-1,j}\right)-h'\,w_{a\,i,j}-h^*{}_{i,j}\,T_{a\,i,j}+h_c S'\,T_{d\,i,j}\\&=-M_d'\,h_{fg}\,\frac{\Delta\lambda}{k}\left(\exp(-kW_{i,j})-\exp(-kW_{i-1,j})\right)-h'\,w_{eq\,i,j}\end{aligned}\qquad(40)$$

With the following coefficients [19]

$$M_d'=\frac{\pi\,M_d\,\Delta z}{\tau_{ro}}\qquad m_a'=\frac{\pi\,m_a\,\Delta z}{\tau_{ro}}\qquad m_a^*=m_a\,u\;\Delta\theta$$

$$S'=S\,\Delta\theta\,\Delta z\qquad h'=h_m\,S'\,h_{fg}$$

$$c_{m\,i,j}=M_d'\left(c_{pd}+c_{pv}\,W_{i,j}\right)\qquad c_{a\,i,j}=m_a'\left(c_{pa}+c_{pv}\,w_{a\,i,j}\right)$$

$$c_a{}^*{}_{i,j}=m_a{}^*\left(c_{pa}+c_{pv}\,w_{a\,i,j}\right)\qquad h^*{}_{i,j}=h_m\,S'\,c_{pv}\left(w_{a\,i,j}-w_{eq\,i,j}\right)+h_c\,S'$$

For the details of the boundary conditions of the model please check the French version of [1].

Model performance

The above presented model of the desiccant was implemented in SPARK. The figure below shows the evolution of the air and the desiccant properties inside the wheel for an inlet temperature of 30℃, inlet humidity ratio of 12 g/k g, regeneration temperature of 60℃ and regeneration humidity ratio of 12 g/kg. The figures show the temperature and the humidity ratio distribution as a function of the angular position (0 to 180°) and as function of the width (0 to 0.2m) of the wheel for the process sector.

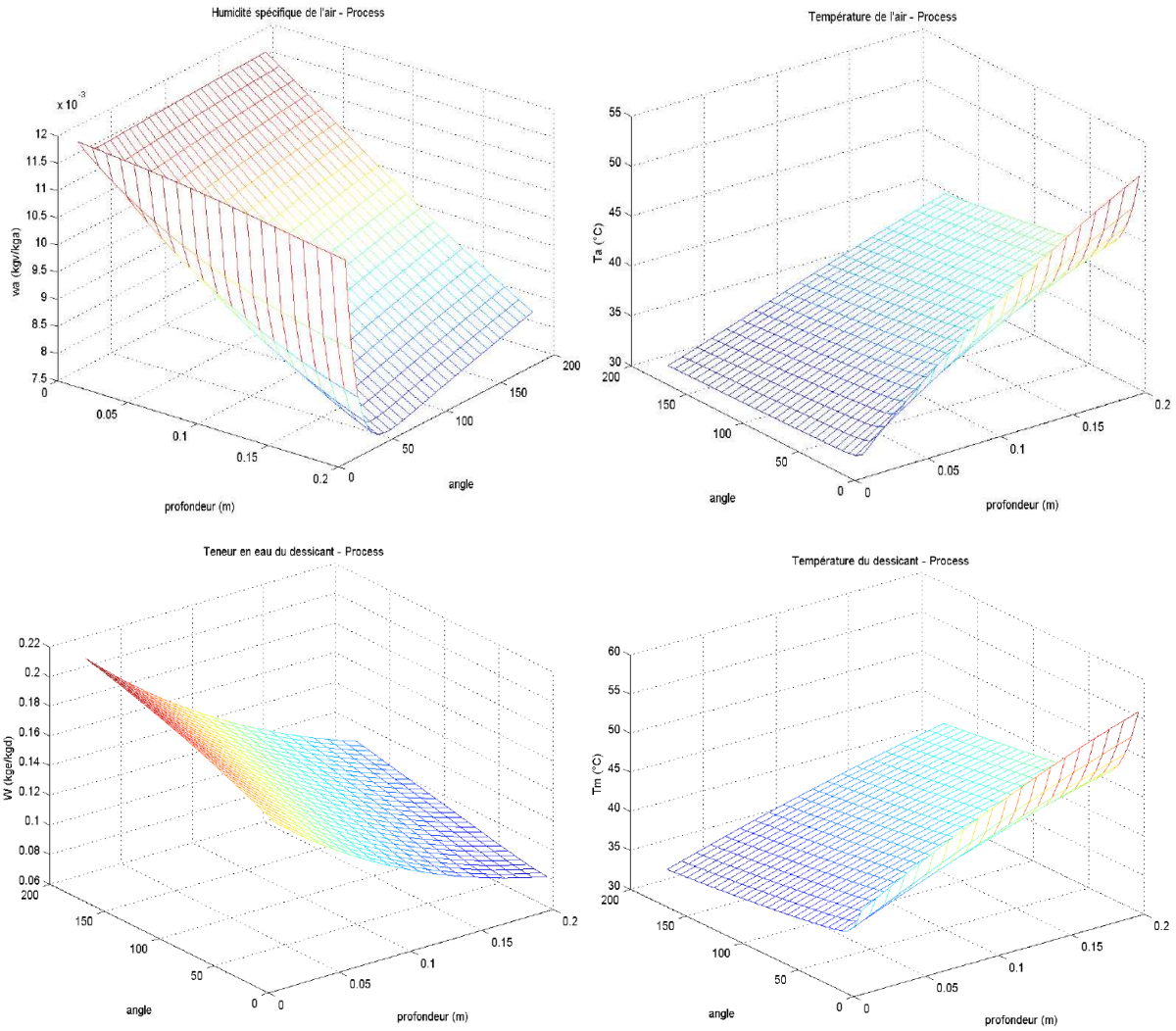

Figure 23: Evolution of air and desiccant properties for the process section in function of the wheel width and the angular position

We notice that for a given angular position the air humidity ratio decreases with the width of the wheel and yields a temperature increase. The dehumidification increase significantly in the first angular sector of the process (0-40°) and reaches its minimum and then increases slightly with the angular position. This behavior of the humidity is due to the fact that after the regeneration; the desiccant is dry and when reaching the process it starts to dehumidify and then starts to saturate. The other reason is the heat of adsorption that heats the desiccant which reduces its adsorption capacity.

While examining the air temperature and humidity ratio profiles we notice a certain angular delay of the dehumidification in comparison with the temperature increase. This can be explained that the desiccant coming from the regeneration is very hot and has a limited adsorption capacity. So in the process sector; outside air must first cool the desiccant and then dehumidification becomes effective.

The figures below show a similar behavior in the regeneration sector.

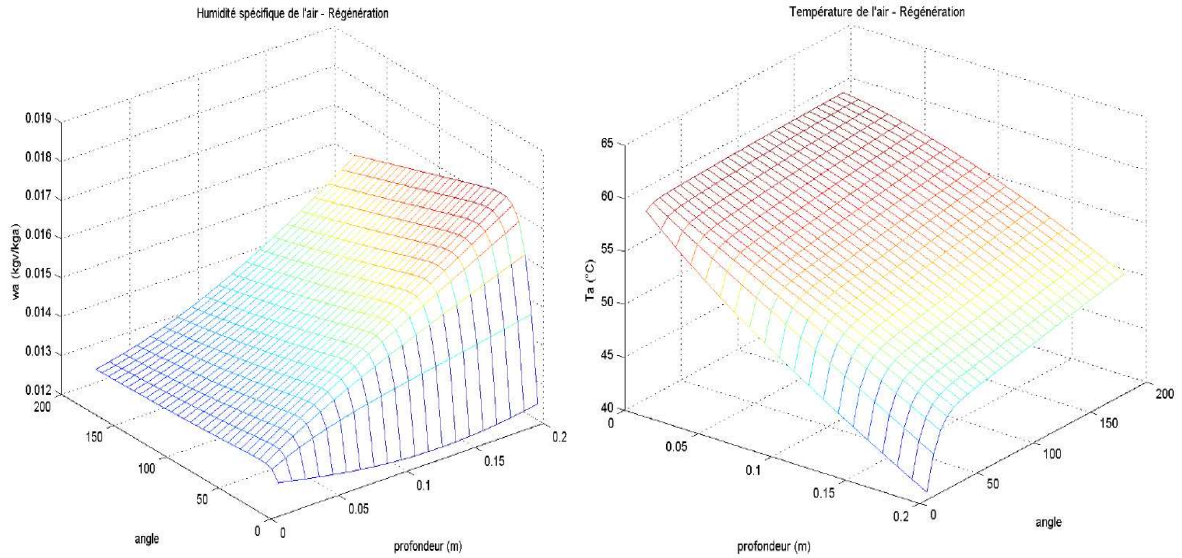

Figure 24: Evolution of the air properties in the regeneration section as a function of the width and angular position

Experimental validation

With the difficulty to measure the temperature and humidity inside the wheel for the detailed model only the temperature and humidity profiles as well as the mean temperature and humidity ratio at the outlet of the wheel will be validated.

In order to validate the temperature and humidity distribution at the outlet of the wheel, 3 psychrometers and 3 Pt100 temperature sensors (3 humidity measurments and 6 temperature measurements) are used in order to validate the profiles as shown in the below.

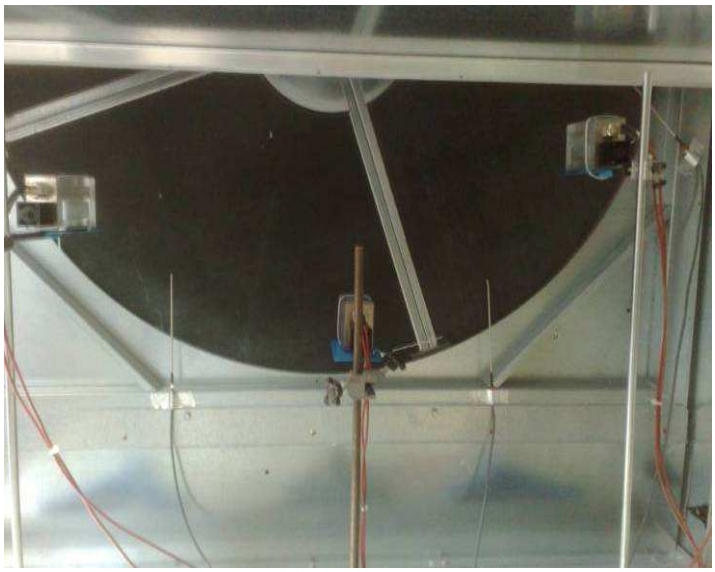

Figure 25: Psychrometers and temperature sensors distribution at the outlet of the desiccant wheel

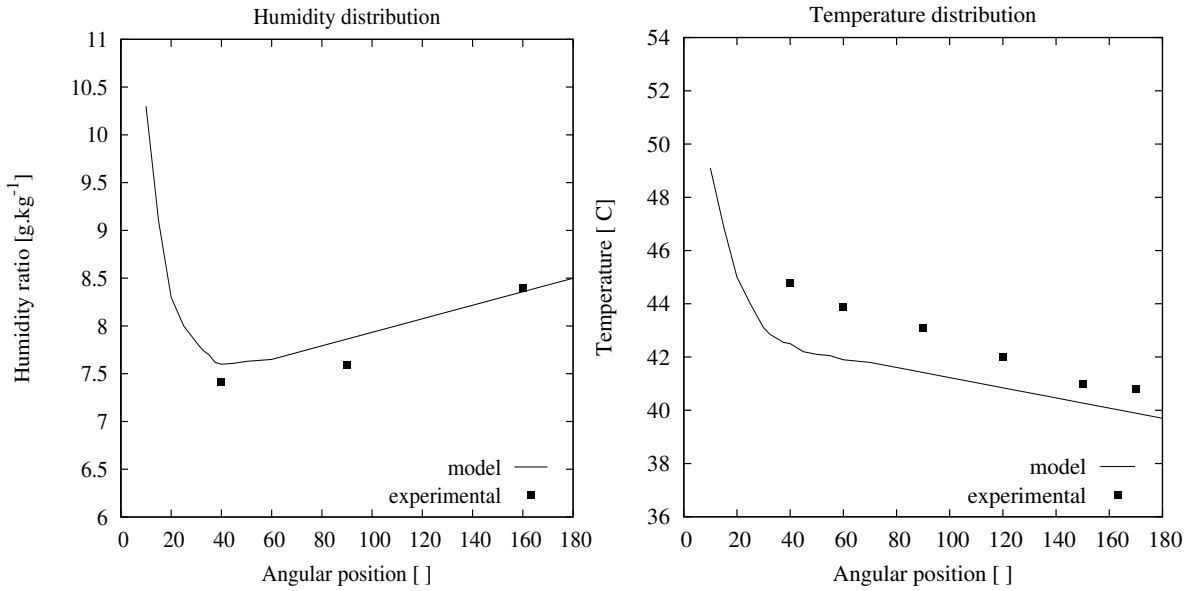

Figure 26: Comparison of the predicted and measured temperature and humidity distribution at the outlet of the desiccant wheel

The profiles obtained numerically are coherent with the measured profiles and we notice 0.3 g/kg error in the humidity ratio while an error of 2℃ in the temperature.

The outlet conditions of the desiccant wheel depend on the temperature and humidity at both inlets of the wheel. In order to validate the detailed and the simplified models of the wheel were considered. Different inlet conditions were considered: the inlet temperature of the process stream varies between 25 and 35℃ while the humidity ratio varies between 10 and 15 g/kg and the regeneration temperature was considered varying from 60 to 80℃.

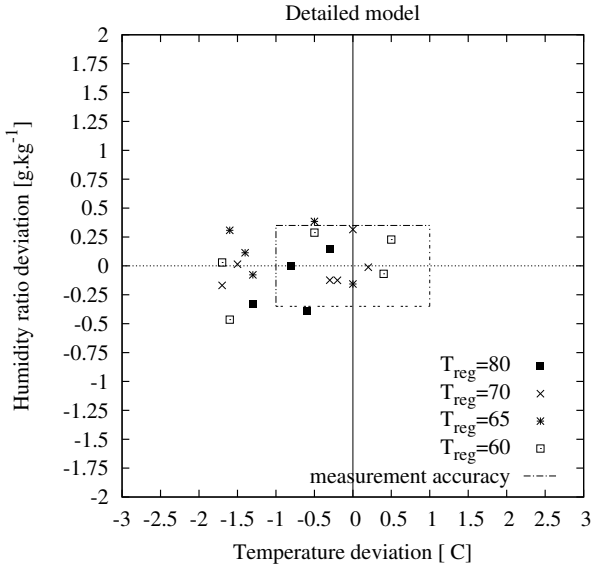

Figure 27: Comparison of the predicted and measured mean outlet temperature and humidity at the outlet of the desiccant wheel.

Figure 27 gives the temperature and humidity ratio deviations at the outlet of the desiccant wheel for the detailed. The maximum humidity ratio deviation of the detailed model is 0.4 g/kg and the maximum temperature deviation is 2℃. The uncertainty of the mean temperature at the outlet of the wheel is in the order of 1 to 1.5℃ (inhomogeneous outlet with 10℃ gradient) and the uncertainty of the humi dity ratio is 0.35 g/kg. The uncertainty of the humidity is evaluated by comparing the mean humidity at the outlet of the wheel (position 2) with the absolute humidity at points 3, 4 and 5 (with reference to figure 1) while turning off the supply humidifier. In these conditions the humidity must be constant. We notice that the humidity ratio deviations are in the domain of the validity of the measurements. The detailed model established of the physical description shows the same accuracy independently of the regeneration temperature.

Conclusion

In this chapter a model of the solar desiccant installation is developed and validated experimentally. First the components model considered solely showed acceptable accuracy and low errors under different operating conditions. Then the overall model of the air handling unit coupled with the solar installation gave satisfactory results for the considered day and predicts accurately the supply air conditions. For the developed solar collector model it showed a good accuracy in predicting the outlet temperature under transient operating conditions and permits a good estimation of the potential of the collectors in transient conditions. This model was used to elaborate control strategies and to optimize the operations of the installation in function of outside and load conditions.

The developed detailed transient model of the desiccant wheel showed a good accuracy in predicting the temperature and humidity distribution at the outlet of the wheel as well as the mean outlet temperature and mean outlet humidity ratio. This detailed model is not suited for seasonal simulation but it is very useful to elaborate control strategy and to study transient behaviour of the desiccant air handling unit. The model can be used to study different desiccant materials.

References

[1]. Bourdoukan, P. "Etude numérique et expérimentale destinée à l'exploitation des techniques de rafraîchissement par dessiccation avec régénération par énergie solaire." *Ph.D Thesis,* Université La Rochelle, (2008) (Available in English)

[2]. Bourdoukan, P., Wurtz, E., Joubert, P., and Sperandio, M.. "Potential of solar heat pipe vacuum collectors in the desiccant cooling process: modelling and experimental results." *Solar Energy* 2008; 82(12): 1209-1219.

[3]. Bourdoukan, P., Wurtz, E., Joubert, P., and Spérandio, M. "Overall cooling efficiency of a solar desiccant plant powered by direct flow vacuum tube collectors: simulation and experimental results" *Journal of Building Performance Simulation* 2008, 1(3):149-162

[4]. Bourdoukan, P., Wurtz, E., Joubert, P." Experimental investigation of a solar desiccant cooling installation Solar Energy 83 (2009) 2059–2073

[5]. Bourdoukan, P., Wurtz, E., Joubert, P "omparison between the conventional and recirculation modes in desiccant ooling cycles and deriving critical efficiencies of components" Energy an International Journal, 2009 1-11 In press Corrected Proof. doi:10.1016/j.energy.2009.06.021

[6]. Kays, W. M., and London, A. L. Compact Heat Exchangers, McGraw-Hill, New York. (1984)

[7]. Maclaine-cross, I. L., and Banks, P. J. "Coupled heat and mass transfer in regenerators- prediction using analogy with heat transfer." *Int. J. Heat Mass Transfer* 1972; 15: 1225-1242.

[8]. Banks, P. J. "Coupled equilibrium heat and single adsorbate transfer in field flow through a porous medium- 1. Characteristics potentials and specific capacity ratios." *Chemical Engineering Science* 1972; 27: 1143-1155.

[9]. Close, D. J., and Banks, P. J. "Coupled equilibrium heat and single adsorbate transfer in field flow through a porous medium-2. Prediction for a silica gel air drier using characteristic charts." *Chemical Engineering Science* 1972; 27: 1157-1168.

[10]. Jurinak, J. J. "Open cycle solid desiccant cooling - component models and system simulation," *Ph.D*, University of Wisconsin, Madison. (1982)

[11]. Stabat, P. "Modélisation de composants de systèmes de climatisation mettant en œuvre l'adsorption et l'évaporation d'eau," *Ph.D Thesis*, Ecole des Mines, Paris. (2003)

[12]. Kamminga, W.. "The approximate temperature within a flate plate solar collector under transient conditions." *Int. J. Heat Mass Transfer*, 28 (1985), 433-440.

[13]. Schnieders, J.. "Comparison of the energy yield predictions of stationary and dynamic solar collector models and the models' accuracy in the description of a vacuum tube collector." *Solar Energy*, 61(1997), 179-190.

[14]. Klein, S. A.. "A Design Procedure for Solar Heating Systems," PhD, University of Wisconsin-Madison (1976)

[15]. SPARK. "Simulation Problem Analysis and Research Kernel." LBNL, Berkeley, California. (2003)

[16]. Sowell, E. F., and Taghavi, K. "Generation of building energy system models." *ASHRAE Transactions* 1984, 106: 465-476.

[17]. Maclaine-cross, I. L. "A theory of combined heat and mass transfer in regenerator," *Ph.D*, Univeristy of Monach, Australie. (1974).

[18]. Brandemuehl, M. J., and Banks, P. J.. "Rotary heat exchangers with time varying or nonuniform inlet temperatures." *ASME Journal of Heat Transfer*, (1984) 106, 750-758.

[19]. Le Garrec, S. "Modélisation des transferts de masse et de chaleur dans une roue dessiccante," *Master*, ENTPE, Lyon. (2007).

Chapter III: New developments in simulation tools and models:

A dynamic simulation model for transient absorption chiller performance.

Paul Kohlenbach
Solem Consulting

Felix Ziegler
Technische Universität Berlin, Institute for Energy Engineering

This chapter presents the development of a dynamic model for single-effect LiBr/water absorption chillers and its experimental validation.
In section (A) the developed model is presented in detail and compared to experimental data. In section (B), general functionality of the model and a more detailed comparison with experimental data are presented. This part also presents a more detailed investigation of the model performance, including performance analysis, sensitivity checks. General model functionality is demonstrated.

1. A dynamic simulation model for transient absorption chiller performance. Part 1: the model

This section presents in detail the development of transient model for an absorption chiller. The model is based on external and internal steady-state enthalpy balances for each main component. Dynamic behaviour is implemented via mass storage terms in the absorber and generator, thermal heat storage terms in all vessels and a delay time in the solution cycle.For verification, the model has been compared to experimental data. The dynamic agreement between experiment and simulation is very good with dynamic deviations around 10s.

Nomenclature

Symbols

A	area, (m^2)
A	Duehring factor (deg C)
B	Duehring factor (-)
c	specific heat capacity ($kJkg^{-1}K^{-1}$)
c	number of simulation steps representing time constants for transport delay (-)
D	dew point temperature (deg C)
g	gravity constant (Nm^2kg^{-2})
h	height difference between generator outlet and absorber inlet (m)
h	enthalpy ($kJkg^{-1)}$
l	specific heat of solution ($kJkg^{-1}$)
$m, \dot{m}$	mass flow rate (kgs^{-1})
M	mass (kg)
p	pressure (Pa)
$Q, \dot{Q}$	heat flux (kW)
r	evaporation enthalpy ($kJkg^{-1}$)
R	gas constant for water vapour (Jkg^{-1})
T	temperature (deg C)
t	time (s)
UA	heat transfer coefficient (kWK^{-1})
x	Solution mass fraction ($kg_{Salt}kg_{Sol}^{-1}$)
X	mole ratio (-)
z	solution level in generator sump (m)

Greek letters

η	effectiveness (-)
ρ	density (kgm^{-3})
Δ	difference (-)
ϑ	temperature (deg C)

Subscripts

A	Absorber
C	Condenser
d	Duehring
E	Evaporator
ext	external
G	Generator
i	simulation time interval
in	inlet
int	internal
meas	measured
p	pump
p, pc	at constant pressure
s	strong
sim	simulated
sol	solution
st	storage
SHX	solution heat exchanger
sG	strong solution leaving the generator tube bundle
sA	strong solution leaving the generator sump and entering the absorber
t	tube
tb	tube bundle
out	outlet
v	vapour
w	water, weak
wA	weak solution leaving the absorber tube bundle
wG	weak solution leaving the absorber sump and entering the generator
X	general index for vessels (X=A, C, E, G)
*	time-delay of solution at generator and absorber inlet

Introduction

The dynamic model of an absorption chiller allows the simulation of its transient behaviour for changing input conditions or design parameters. This is important because absorption chillers usually have a high thermal mass, consisting of their internal heat exchangers, the absorbing solution and the externally supplied heat transfer media. The dynamics of an absorption chiller are therefore rather slow compared to similar capacity compression chillers. The time to achieve a new steady-state with all parameters after a change of input conditions is about 15 minutes for the chiller presented in this paper.

If the chiller is implemented in a complex heat supply/cooling demand system, e.g. a solar thermal or waste-heat driven system, the simulation of the chiller is usually being done using steady-state models. They simulate the chiller assuming constant operating conditions and allow the determination of internal and external cycle parameters, such as heat exchanger sizes, pump flow rates, temperatures and heat flows. However, steady-state models do not provide time-dependent information on the thermal behaviour of absorption chillers and are therefore not suitable for transient system simulations. In contrast, the model presented in this work allows the simulation of the dynamic chiller behaviour. It extends the range of applicable models for transient system simulations where the time constants of the chiller significantly influence the system performance.

Research on dynamic system behaviour was carried out for both LiBr/water and water/NH_3 heat pumps, chillers and components of such. Most complete are the recent papers by Bian et al. [1], and Jeong et al. [2]. Bian et. al. [1] have performed a transient simulation of an absorption chiller. They present a chiller model that can be run using variable time steps for the simulation. It includes a temperature change term of each heat exchanger per time step as well as a mass storage term in the generator, i.e. a part of the strong solution is being stored in the generator in each time step. The model has been verified with experimental data and shows good agreement in the transiency of the thermal behaviour, even if absolute values do not exactly match.

Jeong et. al. [2] present the dynamic simulation of a steam-driven LiBr/water absorption heat pump for the use of low-grade waste heat. The model assumes storage terms with thermal capacities and solution mass storage in the vessels. Solution and vapour mass flow rates are calculated in proportion to pressure differences between vessels. The heat transfer coefficients as well as the simulation time step are assumed to be constant. The model has been verified with good agreement using operational data for an absorption chiller.

The dynamic model presented here simulates the reaction of the absorption chiller on a change of external conditions. In contrast to the approach in the cited references above, a simpler model structure was chosen in order to learn more about the most important

interdependencies in a direct manner. For instance, emphasis is on the fact that the thermal storage terms respond partly to the temperatures of the external fluids and partly to the internal process streams and these effects are separated. In contrast to this, the steady state was incorporated very coarsely only, because time consuming iterations were to be avoided. The model has been developed for and verified on the 10kW absorption chiller manufactured by Phoenix SonnenWaerme AG [3].

Basic model

Figure 1 shows the single-effect LiBr/water absorption cycle with state points as assumed for the model.

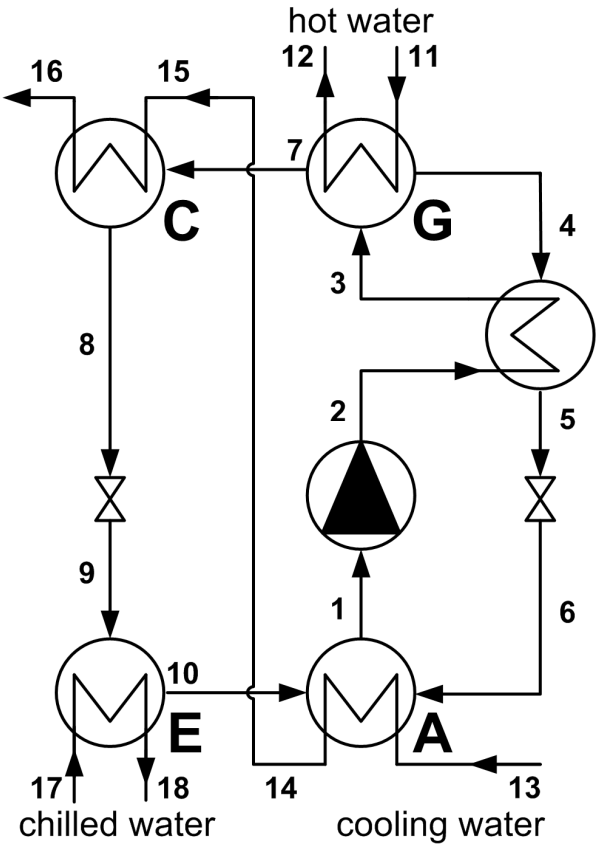

Figure 1. LiBr/water absorption cycle.

Shown are the four main components of an absorption chiller: generator (G), condenser (C), evaporator (E) and absorber (A). Also shown are solution heat exchanger, solution pump and the throttling valves between absorber/solution heat exchanger and condenser/evaporator. The internal state points characterize the thermodynamic properties of LiBr/water solution (points 1-6), water vapour (7, 10) and liquid water (8, 9). The external state points characterize the thermodynamic properties of hot water (11, 12), cooling water (13, 14, 15, 16) and chilled water (17, 18).

The input and output parameter of the model are given in the Appendix.

From Figure 1 the steady-state internal heat flows of the vessels are as follows.

Evaporator:
$$\dot{Q}_{E,\mathrm{int}} = \dot{m}_v \cdot \left(h_{10} - h_8\right) \quad (1)$$

Condenser:
$$\dot{Q}_{C,\mathrm{int}} = \dot{m}_v \cdot \left(h_7 - h_8\right) \quad (2)$$

Absorber:
$$\dot{Q}_{A,\mathrm{int}} = \dot{m}_v \cdot h_{10} - \dot{m}_{sol,w} \cdot h_1 + \left(\dot{m}_{sol,w} - \dot{m}_v\right) \cdot h_5 \quad (3)$$

Generator:
$$\dot{Q}_{G,\mathrm{int}} = \dot{m}_v \cdot h_7 + \left(\dot{m}_{sol,w} - \dot{m}_v\right) \cdot h_4 - \dot{m}_{sol,w} \cdot h_3 \quad (4)$$

In equations (1) to (4), $\dot{m}_{sol,w}$ is the mass flow of the diluted solution and $\dot{m}_v$ is the mass flow of the refrigerant water vapour which is of equal value at state points 7 and 10 in Figure 1. Equations (1) to (4) are based on the calculation of internal enthalpies for LiBr/water solution and refrigerant vapour which requires sound knowledge of these properties. For computational purposes this means that a property database of both LiBr/water and water vapour has to be implemented into the simulation model and usually requires time-consuming iterations.

The main aim of the model presented is to account for the dynamics. Therefore, no detailed steady-state simulation with all state points was performed but a simpler approach was taken which considers the most important physical properties only. This may be refined later on but is not intended to be the focus of this work. This kind of refinement will not change the basic findings of this report. So, to keep the model fast, equations (1) to (4) can be simplified using the latent heat of evaporation and sorption, *r* and *l*, as shown in equations (6) to (9). This approach has been proposed by Ziegler [4] to avoid a detailed enthalpy calculation for each state point. Please note that the latent heat is taken at condenser pressure. The dependency of latent heat on temperature is treated according to Plank's rule [4].

Moreover, not all internal temperatures in Figure 1 are being calculated in the model. Instead, each vessel is being modelled using external and internal mean temperatures of the respective fluids (heat carrier and working fluid) as well as a mean vessel temperature. External mean heat carrier temperatures $\overline{\vartheta}_X$ are being calculated using the arithmetic mean temperature of inlet and outlet temperature. Internal mean temperatures $\overline{T}_X$ are assumed to be the mean of the equilibrium temperatures of strong and weak solution and of the

condensing or evaporating refrigerant. Mean vessel temperatures T_X are the arithmetic mean temperature of the external and internal mean temperatures.

The boiling temperature of saturated LiBr/water solution can be calculated using the Duehring relation, as described by Feuerecker [5]. In the model, this temperature is by definition the mean of the equilibrium temperatures of strong (or weak) solution, $\overline{T}_x$.

$$\overline{T}_x = A_d(X) + B_d(X) \cdot D \qquad (5)$$

with *X* being the mole fraction and D being the dew point temperature of the water vapour. A_d and B_d are the Duehring coefficients which depend on the solution concentration but are constant with regard to the dew point [5]. Some simplifying assumptions have been made for the model. These are:

(a) There is no heat loss to or gain from the ambient.
(b) The pump work is neglected.
(c) The LiBr/water solution leaving generator and absorber tube bundle is saturated.
(d) The external inlet temperatures t_{11}, t_{13}, t_{17} are used as control parameters.
(e) The absorber cooling water outlet temperature equals the condenser inlet temperature (t_{14}=t_{15}).
(f) The solution heat exchanger has a constant effectiveness η_{SHX}.
(g) Water and LiBr/water solution have constant property data.
(h) The external and internal heat transfer coefficients (UA-values) are constant.
(i) Evaporation and solution enthalpy are constant.
(j) Constant pumping rate: The mass flow of weak solution from absorber to generator is constant (state points 1, 2 and 3).
(k) The generator pressure equals the condenser pressure; the absorber pressure equals the evaporator pressure.

Equations (1) to (4) do not account for dynamic effects. One way of accounting for a more precise dynamic calculation is the introduction of different vapour mass flows for state points 7 and 10. The vapour mass flow from generator to condenser, $\dot{m}_{v,G}$ (state point 7), and from evaporator to absorber, $\dot{m}_{v,A}$ (state point 10), are therefore used in equations (6) to (9) which describe the simplified internal enthalpy calculations.

$$\dot{Q}_{E,\mathrm{int}} = \dot{m}_{v,A} \cdot \left(r_{(pc)} - c_{p,v} \cdot \left(\overline{T}_C - \overline{T}_E \right) \right) \qquad (6)$$

$$\dot{Q}_{C,\mathrm{int}} = \dot{m}_{v,G} \cdot \left(r_{(pc)} + c_{p,v} \cdot \left(\overline{T}_G - \overline{T}_C \right) \right) \quad (7)$$

$$\dot{Q}_{G,\mathrm{int}} = \dot{m}_{v,G} \cdot \left(r_{(pc)} + l_{(pc)} + c_{p,w} \cdot \left(\overline{T}_G - \overline{T}_A \right) \right) + \dot{Q}_{SHX} \quad (8)$$

$$\dot{Q}_{A,\mathrm{int}} = \dot{m}_{v,A} \cdot \left(r_{(pc)} + l_{(pc)} - c_{p,v} \cdot \left(\overline{T}_G - \overline{T}_E \right) + c_{p,w} \cdot \left(\overline{T}_G - \overline{T}_A \right) \right) + \dot{Q}_{SHX} \quad (9)$$

The solution heat exchanger does not exchange the maximum possible heat between its two flows. The difference between actual and ideal heat transfer can be assumed as a parasitic heat flow which has to be added to the generator and has to be removed at the absorber. For a constant heat exchanger effectiveness η_{SHX} it can be calculated as

$$\dot{Q}_{SHX} = \left(1 - \eta_{SHX}\right) \cdot \dot{m}_{sol,sG} \cdot c_{p,sol,s} \cdot \left(\overline{T}_G - \overline{T}_A \right) \quad (10)$$

In equation (10), $\dot{m}_{sol,sG}$ is the mass flow rate of the strong solution from generator to absorber [4].

The dynamic performance of the absorption chiller is influenced by various time-dependent effects, caused by complex heat transfer phenomena in the internal and external heat exchangers. In order to keep the model simple, not all of the dynamic effects have been taken into account. Only the three effects with the estimated biggest influence on chiller performance have been chosen. These include a time delay in the solution transport between generator and absorber, mass storage in the vessel sumps, and thermal storage in the external and internal heat exchangers. These dynamic terms are the backbone of the model and will be discussed in detail.

Dynamic Modelling

Both generator and absorber vessel have been modelled as a serial connection of a tube bundle heat exchanger and a solution sump. The tube bundle is the active part; the sump is a storage and mixing device. Solution can accumulate in absorber and generator sump according to the actual load, however there is also some solution which is always stored on the tube bundle. This hold-up, usually, is small as compared to the amount of liquid in the sump because the film is less than half a millimetre thick. Moreover, the bundle should be wetted all the time with the consequence that the amount of liquid on the bundle will not change significantly. Therefore the amount of liquid on the bundle is neglected.

Due to the storage effect, we have to distinguish between the solution flow entering the vessel, the one leaving the bundle and entering the sump, and the one leaving the sump. Moreover, we have to consider different concentrations at the inlet of the bundle, at the exit

of the bundle dripping into the sump, and at the exit of the sump. Figure 2 shows the concentration and mass flow definitions, introducing time-discrete parameters (index *i*).

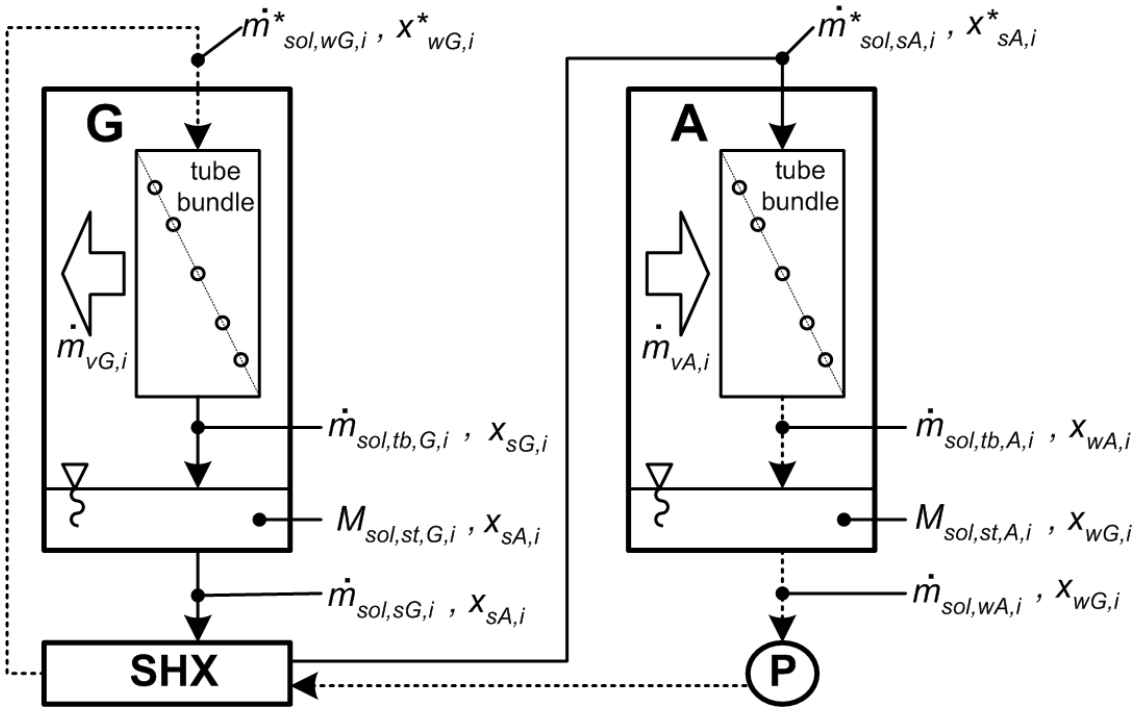

Figure 2. Definition of concentrations and mass flows in generator/absorber. Solid lines: strong solution, dotted lines: weak solution, white arrows: vapour.

Solution transport delay

A transport delay (c) is assumed to occur in both solution circuit legs. Referring to Figure 2, the inlet values of solution mass flow $\dot{m}^*_{sol,sA,i}$ and concentration $x^*_{sA,i}$ at the absorber at time interval *i* are assumed to equal the generator outlet values of time interval (i-c_1). The superscript * symbolizes the time-delayed arrival of the solution at absorber and generator inlet. By analogy, the inlet value of concentration $x^*_{wG,i}$ at the generator at time interval *i* is assumed to equal the outlet value of the absorber at time step (i-c_2). Constants c_1 and c_2 account for the time which the solution needs to flow from generator to absorber and vice versa. They are integers representing a number of simulation steps.

Absorber:

$$x^*_{sA,i} = x_{sA,i-c1} \qquad (11)$$

$$\dot{m}^*_{sol,sA,i} = \dot{m}_{sol,sG,i-c1} \qquad (12)$$

Generator:

$$x^*_{wG,i} = x_{wG,i-c2} \qquad (13)$$

$$\dot{m}^*_{sol,wG,i} = \dot{m}_{sol,wA,i-c2} = const. \qquad (14)$$

As stated in equation (14) above, the mass flow of weak solution is set constant. In equation (12) it is assumed that the mass flow entering the absorber tube bundle at time interval *i* equals the mass flow which has left the generator c_1 time intervals ago. Doing so, the physical incompressibility of the solution in the piping between generator and absorber is not modelled correctly. In reality, the mass flow entering the tube at time interval *i* should equal the mass flow leaving the tube at time interval *i*. The assumption, however, had to be made in order to achieve a correct salt balance in equation (22). The result is a hidden mass storage term in the solution tube. However, the amount of stored solution in the tube is only 0.6 % of the total amount of stored solution in the sumps [3]. The error introduced by this assumption is therefore negligible.

Mass balances

The vessel sumps (see Figure 2) are assumed to be fully mixed at each time interval. Thus vessel sump and solution leaving the vessel are assumed to have the same salt concentration, $x_{sA,i}$ and $x_{wG,i}$, respectively. The outlet of each tube bundle is assumed to exhibit the equilibrium concentration $x_{sG,i}$ and $x_{wA,i}$. The total solution mass stored in generator and absorber sump at time *i* is expressed by $M_{sol,st,G,i}$ and $M_{sol,st,A,i}$, respectively.

We know that the total mass (or salt mass, respectively) in the sump at time interval *i* equals the total mass (or salt mass) at time interval (*i-1)* plus the difference of ingoing and outgoing solution (or salt) flows at time interval *i*. The balances for the total solution contents in the sumps are given in equations (15) and (16). Δt is the time between two simulation intervals.

Generator:
$$\dot{m}_{sol,tb,G,i} - \dot{m}_{sol,sG,i} - \frac{M_{sol,st,G,i} - M_{sol,st,G,i-1}}{\Delta t} = 0 \qquad (15)$$

Absorber:
$$\dot{m}_{sol,tb,A,i} - \dot{m}_{sol,wA,i} - \frac{M_{sol,st,A,i} - M_{sol,st,A,i-1}}{\Delta t} = 0 \qquad (16)$$

The fraction term in equations (15 and 16) is the amount of solution which is added to the solution stored in either generator or absorber sump during the time Δt between consecutive simulation intervals *i* and (*i-1)*.

The salt flow balance, analogously, in both sumps can be written as:

Generator:
$$\dot{m}_{sol,tb,G,i} \cdot x_{sG,i} - \dot{m}_{sol,sG,i} \cdot x_{sA,i} - \frac{M_{sol,st,G,i} \cdot x_{sA,i} - M_{sol,st,G,i-1} \cdot x_{sA,i-1}}{\Delta t} = 0 \qquad (17)$$

Absorber:
$$\dot{m}_{sol,tb,A,i} \cdot x_{wA,i} - \dot{m}_{sol,wA,i} \cdot x_{wG,i} - \frac{M_{sol,st,A,i} \cdot x_{wG,i} - M_{sol,st,A,i-1} \cdot x_{wG,i-1}}{\Delta t} = 0 \qquad (18)$$

Proceeding from the sumps to the tube bundles, the mass flow balance yields

Generator: $$\dot{m}_{sol,wA,i-c2} - \dot{m}_{vG,i} - \dot{m}_{sol,tb,G,i} = 0 \quad (19)$$

Absorber: $$\dot{m}_{sol,sG,i-c1} + \dot{m}_{vA,i} - \dot{m}_{sol,tb,A,i} = 0 \quad (20)$$

The salt flow balances of the tube bundles read

Generator: $$\dot{m}_{sol,wA,i-c2} \cdot x_{wG,i-c2} - \dot{m}_{sol,tb,G,i} \cdot x_{sG,i} = 0 \quad (21)$$

Absorber: $$\dot{m}_{sol,sG,i-c1} \cdot x_{sA,i-c1} - \dot{m}_{sol,tb,A,i} \cdot x_{wA,i} = 0 \quad (22)$$

Pressure drop

The strong solution flow from generator to absorber is driven by gravity and a pressure difference. The pressure loss of the solution heat exchanger and its adjacent piping is assumed constant which is a good approximation as long as the flow variations are not too large; hence the mass flow of the strong solution depends only on the pressure difference between generator/absorber and the liquid solution column at heat exchanger inlet. This assumption, of course, can be refined in future works. During operation, the static pressure of the liquid column has to equal the dynamic pressure loss caused by flow restrictions through piping and solution heat exchanger. The mass flow of the strong solution can therefore be calculated as

$$\dot{m}_{sol,s,i} = A_t \cdot \sqrt{\frac{2 \cdot \rho_{sol,s} \cdot \left(p_{G,i} - p_{A,i} + \rho_{sol,s} \cdot g \cdot \left(h + z_i\right)\right)}{\varsigma}}, \quad (23)$$

where generator/condenser and evaporator/absorber pressure are calculated using the equation of Clausius-Clapeyron as shown in equation (24). There, the pressure and temperature values of solution interval *(i-1)* are being used to calculate the values of simulation interval *i*. This is a valid approximation as long as the time between two simulation intervals, Δt , is not too long.

$$\ln\left(\frac{p_{X,i}}{p_{X,i-1}}\right) = \frac{r_0}{R} \cdot \left(\frac{1}{\overline{T}_{X,i-1}} - \frac{1}{\overline{T}_{X,i}}\right) \quad (24)$$

Thermal storage

After a temperature change of one of the external flows entering a vessel, the temperatures of all components which are influenced either by the external heat carrier (external components such as the water headers) or by the refrigerant and sorbent (internal components such as the solution heat exchanger) change consecutively. This is, of course, connected with some heat being stored in all external and internal components which are involved in heat transfer mechanisms. The temperature change of these components is a complex three-dimensional heat transfer problem. One simplified approach to modelling it is the assumption that some components or parts of components follow internal temperatures and others follow external temperatures. To account for the accordingly different heat transfer rates the total thermal mass has been divided into an external and an internal part. The external part follows the mean external temperature $\overline{\vartheta}_X$, the internal part follows the mean internal temperature $\overline{T}_X$. Also, different heat transfer coefficients and exchange areas have been assumed for the internal and external parts. The external and internal components that have been incorporated for thermal storage are listed in Table 1.

Table 1. External and internal components involved in heat transfer.

Location	Component	Heat capacity [kJ/kgK]	Mass in E [kg]	Mass in C [kg]	Mass in G [kg]	Mass in A [kg]
external	Vessel wall (10% of total weight)	0.48	2.0	2.0	1.9	1.9
	External water header	0.48	7.6	7.3	9.8	10.6
	Water in external parts	4.19	8.5	7.4	12.6	11.9
	Heat exchanger tube bundles (50%)	0.38	5.7	5.1	8.9	8.0
internal	Heat exchanger tube bundles (50%)	0.38	5.7	5.1	8.9	8.0
	LiBr/water solution (50% each)	3.70	-	-	19.0	19.0
	Refrigerant water (50% each)	4.19	7.5	7.5	-	-
	Solution heat exchanger (50% each)	0.38	-	-	4.1	4.1
		0.48	-	-	5.0	5.0
	Solution pump (50% each)	0.48	10.0	10.0	9.5	9.5
	Vessel walls (50% of total weight)					

Figures 3 and 4 illustrate the assumptions for the heat transfer from the external heat carrier to the heat exchanger and further on to solution or refrigerant. For generator and absorber the tube bundle is divided into two virtual parts, one being at mean external temperature, $\overline{\vartheta}_X$, and one being at mean internal temperature, $\overline{T}_X$. The mean vessel temperature T_X is shown as a virtual crossover temperature between internal and external temperature levels.

Figure 3 shows the partition of the generator vessel into the external (right side) and internal (left side) part, Figure 4 shows the same partition for the absorber.

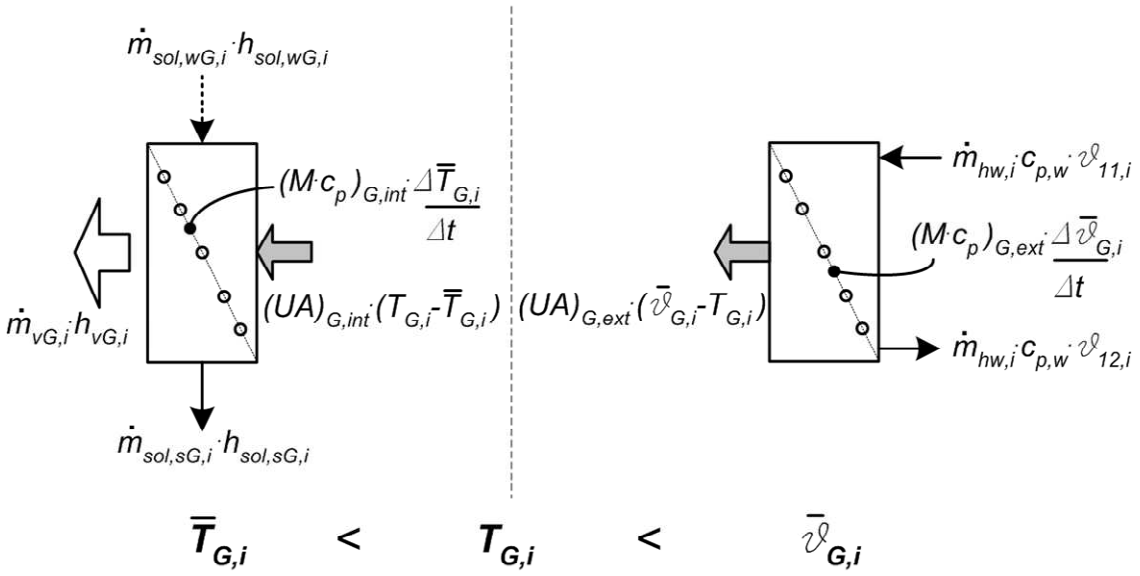

Figure 3. Enthalpy balance for generator vessel. Grey arrows: heat flow, white arrow: vapour flow, black arrows: fluid flow. Left side: internal, right side: external

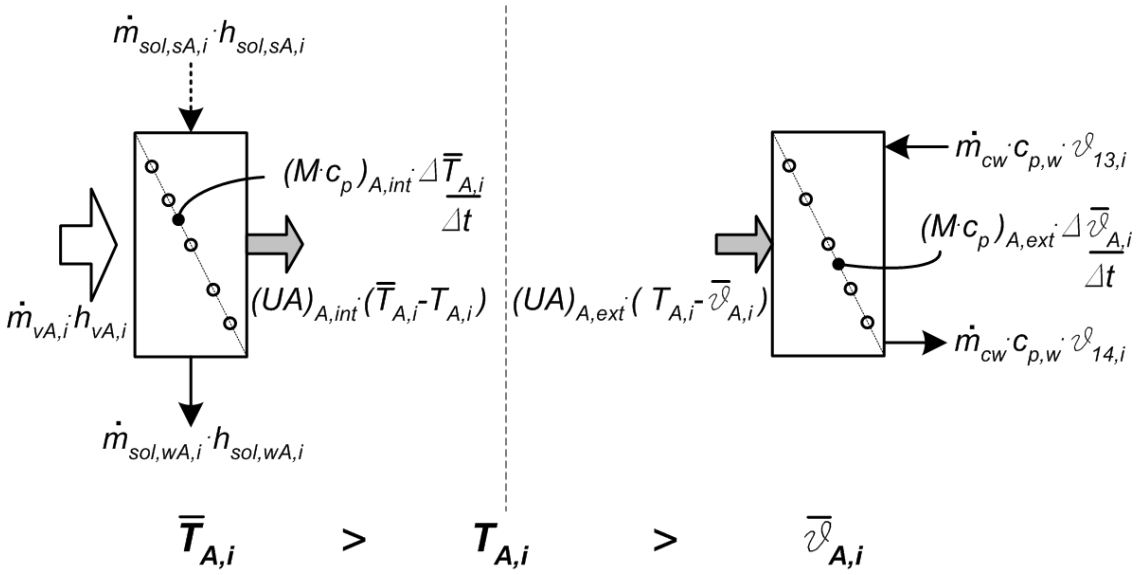

Figure 4. Enthalpy balance for absorber vessel. Grey arrows: heat flow, white arrow: vapour flow, black arrows: fluid flow. Left side: internal, right side: external

Externally, all four chiller vessels incorporate water headers for the distribution of hot, chilled and cooling water through the tube bundles. It is assumed that the headers and the water mass enclosed in those contribute completely to the external heat storage. The tube bundles are assumed to contribute by 50% of their mass to the external heat storage and by 50% to the internal heat storage. This is reasonable because the falling film heat exchanger tubes have flow on both sides, internally by LiBr/water solution and externally by water. The vessel wall is assumed to contribute by 10% of its total weight to the external thermal mass due to the conduction heat transfer from the headers.

Internally, in addition to the tube bundles, the solution contributes by 50% of its mass in generator and absorber. In analogy, the refrigerant is assumed to have a 50% internal contribution in both evaporator and condenser. The mass of solution heat exchanger and solution pump has an internal effect on both generator and absorber heat transfer and is assumed to contribute by 50% of its weight on both. The vessel wall now contributes internally by 50% of its weight due to the larger surface area involved in heat transfer mainly in the sumps.

Enthalpy balances

Taking internal and external thermal storage as in Figures 3 and 4 into account, equations (6) to (9) can be refined and the external and internal enthalpy balances for the vessels can now be expressed. The external enthalpy balance of the vessels describes that the heat which is given off (generator) or taken on (absorber) by the heat carrier (left-hand side of equation (25) or (26)) partly crosses the heat exchanger (first term on the right-hand side, grey arrows in Figures 3 and 4) and reaches the mean vessel temperature, partly is used to heat up parts of the vessel which are more or less at external temperature (second term on right-hand side). For generator and evaporator, the external enthalpy balance reads

$$\dot{m}_{X,w} \cdot c_{p,w} \cdot \left(\vartheta_{X,in} - \vartheta_{X,out}\right) = (UA)_{ext,X} \cdot \left(\overline{\vartheta}_{X,i} - T_{X,i}\right) + \left(M \cdot c_p\right)_{ext,X} \cdot \frac{\overline{\vartheta}_{X,i} - \overline{\vartheta}_{X,i-1}}{\Delta t} \qquad (25)$$

In equation (25), index *X* denotes the different vessels of generator and evaporator (*X = G, E*). For absorber and condenser the external enthalpy balance reads

$$\dot{m}_{X,w} \cdot c_{p,w} \cdot \left(\vartheta_{X,in} - \vartheta_{X,out}\right) = -(UA)_{ext,X} \cdot \left(\overline{\vartheta}_{X,i} - T_{X,i}\right) - \left(M \cdot c_p\right)_{ext,X} \cdot \frac{\overline{\vartheta}_{X,i} - \overline{\vartheta}_{X,i-1}}{\Delta t} \qquad (26)$$

Index *X* in equation (26) denotes absorber and condenser (*X = A, C*).

The internal enthalpy balances for all vessels read as follows.

$$\dot{m}_{v,A,i} \cdot \left(r_{(pc)} - c_{p,v} \cdot \left(\overline{T}_{C,i} - \overline{T}_{E,i}\right)\right) + \left(M \cdot c_p\right)_{E,\mathrm{int}} \cdot \frac{\overline{T}_{E,i} - \overline{T}_{E,i-1}}{\Delta t} = (UA)_{E,\mathrm{int}} \cdot \left(T_{E,i} - \overline{T}_{E,i}\right) \qquad (27)$$

$$\dot{m}_{v,G,i} \cdot \left(r_{(pc)} + l_{(pc)} + c_{p,w,i} \cdot \left(\overline{T}_{G,i} - \overline{T}_{A,i}\right)\right) + \dot{Q}_{SHX,i} + \left(M \cdot c_p\right)_{G,\mathrm{int}} \cdot \frac{\overline{T}_{G,i} - \overline{T}_{G,i-1}}{\Delta t} = (UA)_{G,\mathrm{int}} \cdot \left(T_{G,i} - \overline{T}_{G,i}\right) \qquad (28)$$

$$\dot{m}_{v,G,i} \cdot \left(r_{(pc)} + c_{p,v} \cdot \left(\overline{T}_{G,i} - \overline{T}_{C,i}\right)\right) + \left(M \cdot c_p\right)_{C,\mathrm{int}} \cdot \frac{\overline{T}_{C,i} - \overline{T}_{C,i-1}}{\Delta t} = \left(UA\right)_{C,\mathrm{int}} \cdot \left(T_{C,i} - \overline{T}_{C,i}\right) \qquad (29)$$

$$\dot{m}_{v,A,i} \cdot \left(r_{(pc)} + l_{(pc)} - c_{p,v} \cdot \left(\overline{T}_{G,i} - \overline{T}_{E,i}\right) + c_{p,w} \cdot \left(\overline{T}_{G,i} - \overline{T}_{A,i}\right)\right) + \dot{Q}_{SHX,i} + \left(M \cdot c_p\right)_{A,\mathrm{int}} \cdot \frac{\overline{T}_{A,i} - \overline{T}_{A,i-1}}{\Delta t} = \left(UA\right)_{A,\mathrm{int}} \cdot \left(T_{A,i} - \overline{T}_{A,i}\right) \qquad (30)$$

Equations (27) and (28) describe the internal heat transfer in evaporator and generator, respectively. There, the heat which is given off by the heat exchanger (right-hand side) partly heats up the internal parts of the vessel (second term on left-hand side) and partly is used for the heating of solution and refrigerant (first term on left-hand side). In analogy, equations (29) and (30) describe condenser and absorber, respectively. There, the heat which is given off by the solution and refrigerant (first term on left-hand side) is used partly to heat the internal parts of the heat exchanger (second term on left-hand side) and partly to heat the cooling water (right-hand side).

The equation system is being solved in MATLAB using a Newton-Raphson procedure with finite-difference Jacobian approximation [6].

Experimental Verification

The agreement between simulated and experimental data has been tested using an experimentally measured hot water input step from 75 to 85 ℃. The results of the simulation using these input data are shown in Figure 5. The hot water inlet and outlet temperatures in Figure 5 are taken from experimental measurements of the Phoenix absorption chiller. They show the transient behaviour of the chiller for a 10K step in hot water inlet temperature. Cooling and chilled water inlet temperatures as well as all external mass flow rates were kept constant during the step. It can be seen that it takes approx. 600s or 10 minutes to achieve a new steady-state in hot water inlet temperature after the step. This is shorter than the 15 minutes it takes for all parameters to achieve steady-state again. The simulation was performed using the measured data as inputs in the model and comparing simulated and measured hot water outlet temperatures.

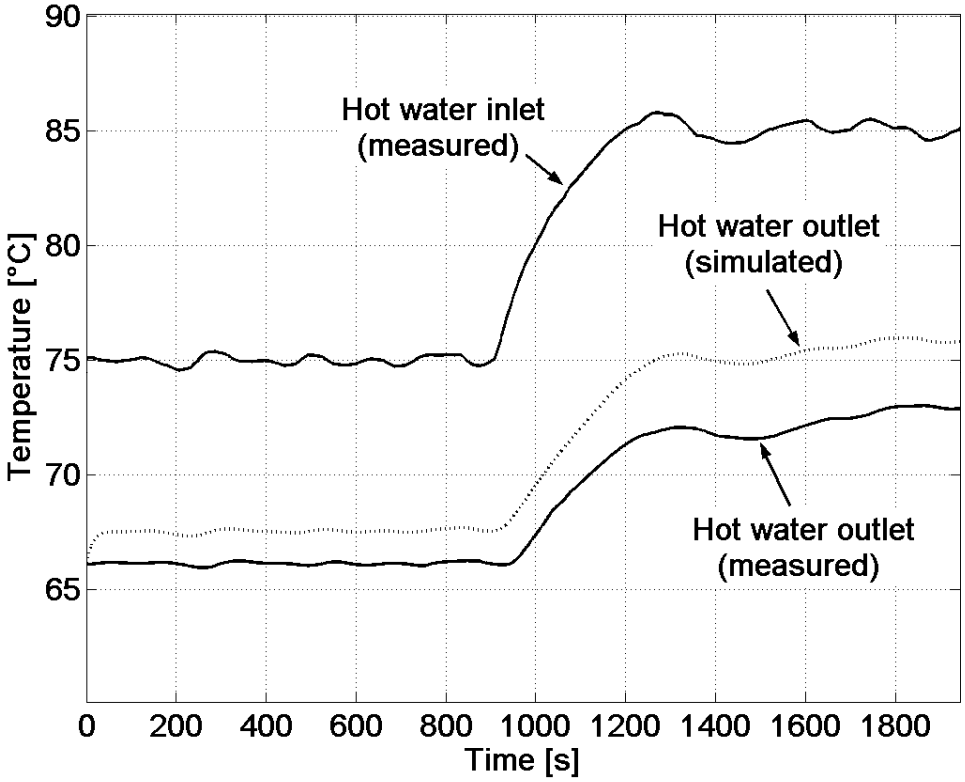

Figure 5. Comparison of simulated and measured generator outlet temperatures.

Figure 5 shows that the steady-state agreement between measured and simulated values is reasonably well despite the fact that steady-state accuracy has been incorporated coarsely only. At simulation start, the simulated temperatures diverge slightly from the initial measured state towards a different steady-state. In general, the temperature difference between experiment and simulation is larger after the step which shows that there is a dependency of the model output on the hot water temperature. This can be related to temperature-dependent parameters which have been assumed constant for the simulation, such as evaporation and solution enthalpy, density and specific heat capacity. As steady-state accuracy is not the focus in this paper this deviation shall not be discussed further.
Much more important is the fact that the dynamic agreement between measured and simulated output data is very good. Figure 5 shows that the fluctuations of simulated and measured hot water outlet temperature are well synchronized, although there is a slight delay of approximately 10 seconds of measured to simulated values. This has to be put into relation to the 600 seconds or 10 minutes that it takes to reach a steady state in the generator temperatures again.
The delay between simulation and experiment can – at least to some extent - be explained with the assumptions of thermal mass for the individual vessels in Table 1 which have not been verified yet. Another reason for the disagreement is the fact that some time delays

existing in reality have not been incorporated into the model. These include the forced circulation of refrigerant in the evaporator by means of a second internal pump. Also, the condensed refrigerant flowing from condenser to evaporator has a time delay which has been neglected. There is no vapour storage in the vessels assumed. The transport delay c_1 has been assumed constant although it changes in proportion to the strong solution mass flow. The transport delay in the cooling water between absorber outlet and condenser inlet due to piping length has also been neglected as well as the change in solution storage on the tube bundles. These time delays have not been included in order to keep the model as simple as possible.
The results in Figure 5 are shown here just in order to demonstrate the basic functionality of the model. A sensitivity analysis along with more experimental data is presented in the second part of this paper [7].

Conclusions

In this paper a dynamic model for absorption chillers has been presented. It is based on internal energy balances as well as mass balances. Dynamic behaviour is implemented via eight thermal and two mass storage terms as well as by two delay times. The heat transfer has been divided into two parts: one which transfers heat from the external heat carrier to the exchanger material and the second from there on to the refrigerant or solution side, or vice versa. In this way the thermal mass of the vessel could be introduced easily. The agreement between experiment and simulation is very good with deviations of 10s for the generator. The total time to achieve a new steady-state after an input temperature step amounts to approximately 15 minutes. Compared to this, the present dynamic deviations are in the magnitude of approximately 1%.
More information about the simulation results, comparison with experiments and sensitivity checks will be presented in the second part of this paper [7].

Appendix

Inputs and outputs of the dynamic model

Table 2. Input parameter of the dynamic model.

No.	Inputs	Unit	Description
1	$\vartheta_{11,i}$	℃	Generator hot water inlet temperature at time
2	$\vartheta_{17,i}$	℃	Evaporator chilled water inlet temperature at
3	$\vartheta_{13,i}$	℃	Absorber cooling water inlet temperature at time
4	$\vartheta_{18,i-1}$	℃	Evaporator chilled water outlet temperature at
5	$\vartheta_{16,i-1}$	℃	Condenser cooling water outlet temperature at
6	$\vartheta_{12,i-1}$	℃	Generator hot water outlet temperature at time
7	$\vartheta_{14,i-1}$	℃	Absorber cooling water outlet temperature at
8	$\overline{T}_{E,i-1}$	℃	Internal mean temperature of evaporator at time
9	$\overline{T}_{C,i-1}$	℃	Internal mean temperature of condenser at time
10	$\overline{T}_{G,i-1}$	℃	Internal mean temperature of generator at time
11	$\overline{T}_{A,i-1}$	℃	Internal mean temperature of absorber at time
12	$x_{sol,w,G,i-c2}$	$kg_{Salt}kg_{Sol}^{-}$	Solution concentration of absorber sump at time
13	$x_{sol,s,A,i-c1}$	$kg_{Salt}kg_{Sol}^{-}$	Solution concentration of generator sump at time
14	$\dot{m}_{sol,s,i-c1}$	kgs^{-1}	Strong solution mass flow at time interval i-c1
15	$x_{s,G,i-1}$	$kg_{Salt}kg_{Sol}^{-}$	Equilibrium concentration in generator at time
16	$x_{s,A,i-1}$	$kg_{Salt}kg_{Sol}^{-}$	Solution concentration of generator sump at time
17	$x_{w,G,i-1}$	$kg_{Salt}kg_{Sol}^{-}$	Solution concentration of absorber sump at time
18	$x_{w,A,i-1}$	$kg_{Salt}kg_{Sol}^{-}$	Equilibrium concentration in absorber at time
19	$M_{st,sol,G,i-1}$	kg	Total mass in generator sump at time interval i-1
20	$M_{st,sol,A,i-1}$	kg	Total mass in absorber sump at time interval i-1
21	Δt	s	Time period between time intervals i and i-1

Table 3. Output parameter of the dynamic model.

No.	Outputs	Unit	Description
1	$\vartheta_{18,i}$	℃	Evaporator chilled water outlet temperature at t ime
2	$\vartheta_{16,i}$	℃	Condenser cooling water outlet temperature at ti me
3	$\vartheta_{12,i}$	℃	Generator hot water outlet temperature at time
4	$\vartheta_{14,i}$	℃	Absorber cooling water outlet temperature at tim e
5	$\overline{T}_{E,i}$	℃	Internal mean temperature of evaporator at time
6	$\overline{T}_{C,i}$	℃	Internal mean temperature of condenser at time
7	$\overline{T}_{G,i}$	℃	Internal mean temperature of generator at time
8	$\overline{T}_{A,i}$	℃	Internal mean temperature of absorber at time
9	$\dot{m}_{v,G,i}$	kgs^{-1}	Vapour mass flow from generator to condenser at
10	$\dot{m}_{v,A,i}$	kgs^{-1}	Vapour mass flow from evaporator to absorber at
11	$x_{s,G,i}$	$kg_{Salt}kg_{Sol}^{-}$	Equilibrium concentration in generator at time
12	$x_{s,A,i}$	$kg_{Salt}kg_{Sol}^{-}$	Solution concentration of generator sump at time
13	$x_{w,A,i}$	$kg_{Salt}kg_{Sol}^{-}$	Equilibrium concentration in absorber at time interval
14	$x_{w,G,i}$	$kg_{Salt}kg_{Sol}^{-}$	Solution concentration of absorber sump at time
15	$\dot{m}_{sol,tb,G,i}$	kgs^{-1}	Solution mass flow after tube bundle in generator
16	$\dot{m}_{sol,tb,A,i}$	kgs^{-1}	Solution mass flow after tube bundle in absorber
17	$m_{st,sol,G,i}$	kg	Stored solution in generator sump at time interval i
18	$m_{st,sol,A,i}$	kg	Stored solution in absorber sump at time interval i
19	z_i	m	Height of solution level in generator sump at time
20	$\dot{m}_{sol,s,i}$	kgs^{-1}	Strong solution mass flow at time interval i
21	$p_{G,i}$	Pa	Generator/condenser pressure at time interval i
22	$p_{A,i}$	Pa	Evaporator/absorber pressure at time interval i
23	$M_{st,sol,G,i}$	kg	Total solution mass in generator at time interval i
24	$M_{st,sol,A,i}$	kg	Total solution mass in absorber at time interval i

References

[1] Bian J, Radermacher R, Moran D. Transient simulation of an absorption chiller in a CHP system. In Proceedings of the International Sorption Heat Pump Conference, June 22-24, *2005*, Denver, CO, USA.

[2] Jeong S, Kang BH, Karng SW. Dynamic simulation of an absorption heat pump for recovering low grade waste heat. *Applied Thermal Engineering 1998*; 18 (1-2); 1-12

[3] Kohlenbach P. Solar cooling systems with absorption chillers: Control strategies and transient chiller performance. 2006; PhD Thesis; Technical University of Berlin, Forschungsberichte des Deutschen Kälte- und Klimatechnischen Vereins; Nr. 74, Erding, Germany

[4] Ziegler F. Sorptionswärmepumpen. 1997; Habilitation Thesis; Forschungsberichte des Deutschen Kälte- und Klimatechnischen Vereins; Nr. 57, Erding, Germany.

[5] Feuerecker G. Entropieanalyse für Wärmepumpensysteme: Methoden und Stoffdaten. 1994; PhD thesis; Faculty of Physics; Technical University of Munich; Germany.

[6] Urroz GE. Solution of non-linear equations. 2004; Lecture handout; Utah State University; U.S.A.

[7] Kohlenbach P, Ziegler F. A dynamic simulation model for transient absorption chiller performance. Part II: Numerical results and experimental verification. 2007; *Int J Refrigeration*, this issue.

2. A dynamic simulation model for transient absorption chiller performance: Numerical results and experimental verification

This section describes the performance and experimental verification of a dynamic absorption chiller model. In [1] the model itself was described with regard to dynamic effects, such as transport delays in the solution circuit, thermal storage and mass storage. In detail, the size of the solution sumps in absorber and generator, the time for the solution to flow from absorber to generator and vice-versa and the thermal mass of the main components has been accounted for. As a special feature, the thermal mass of the components has been split into two parts, one which responds to the temperature of the external fluids, and the other which responds to the temperature of the solution and the refrigerant (internal fluids). These are the main parameters which determine the dynamic behaviour of the chiller.
This second section is looking at internal consistency, sensitivity and accuracy of the model. Results of a performance analysis using ideal conditions to prove correct model behaviour are shown. A sensitivity analysis on thermal storage and solution transport delay has been performed to investigate the influence of the dynamic parameters on the chiller performance. Finally, a model verification using experimental results is also given in this paper.

Nomenclature

Symbols

A	area, (m^2)
A	Duehring factor (deg C)
B	Duehring factor (-)
c	specific heat capacity ($kJkg^{-1}K^{-1}$)
c	number of simulation steps representing time constants for transport delay (-)
D	dew point temperature (deg C)
g	gravity constant (Nm^2kg^{-2})
h	height difference between generator outlet and absorber inlet (m)
h	enthalpy ($kJkg^{-1)}$
l	specific heat of solution ($kJkg^{-1}$)
$m, \dot{m}$	mass flow rate (kgs^{-1})
M	mass (kg)
p	pressure (Pa)
$\dot{Q}, Q$	heat flux (kW)
r	evaporation enthalpy ($kJkg^{-1}$)
R	gas constant for water vapour (Jkg^{-1})
T	temperature (deg C)
t	time (s)
UA	heat transfer coefficient (kWK^{-1})
x	Solution mass fraction ($kg_{Salt}kg_{Sol}^{-1}$)
X	mole ratio (-)
z	solution level in generator sump (m)

Greek letters

η	effectiveness (-)
ρ	density (kgm^{-3})
Δ	difference (-)
ϑ	temperature (deg C)

Subscripts

A	Absorber
Acc	Cooling water inlet
Ach	Cooling water outlet
C	Condenser
d	Duehring
E	Evaporator
Eh	Chilled water inlet
Ec	Chilled water outlet
ext	external
G	Generator
Gc	Hot water outlet
i	simulation time interval
in	inlet
int	internal
meas	measured
p	pump
p, pc	at constant pressure
s	strong
sim	simulated
sol	solution
st	storage
SHX	solution heat exchanger
sG	strong solution leaving the generator tube bundle
sA	strong solution leaving the generator sump and entering the absorber
t	tube
tb	tube bundle
out	outlet
v	vapour
w	water, weak
wA	weak solution leaving the absorber tube bundle
wG	weak solution leaving the absorber sump and entering the generator
X	general index for vessels (X=A, C, E, G)

Performance analysis

The internal consistency of the model can be analysed by applying a step change to one of the external parameters in the model. A step from 75℃ to 85℃ in the hot water inlet temperature has been used for this purpose. Cooling and chilled water inlet temperatures

have been kept constant at 27°C and 18°C, respectiv ely. The simulation interval was 1s. The temperature step was set at 200s after simulation start. This time period is necessary because the preset steady-state is not exactly met by the model: after starting the simulation first the steady state with the given input values has to be reached. 200s are enough in order to equalize the differences between initial and steady-state values.
For the consistency analysis no thermal storage terms were assumed, just solution mass storage and a transport delay of 2 steps or seconds between generator and absorber and 1 step or second the other way. These very short transport delays were chosen to speed up the simulation. Figure 1 shows some internal variables for a short time period before and after the temperature step. Figure 2 shows the external heat flows before and after the temperature step. Each marker symbol in the graph denotes one simulation step.

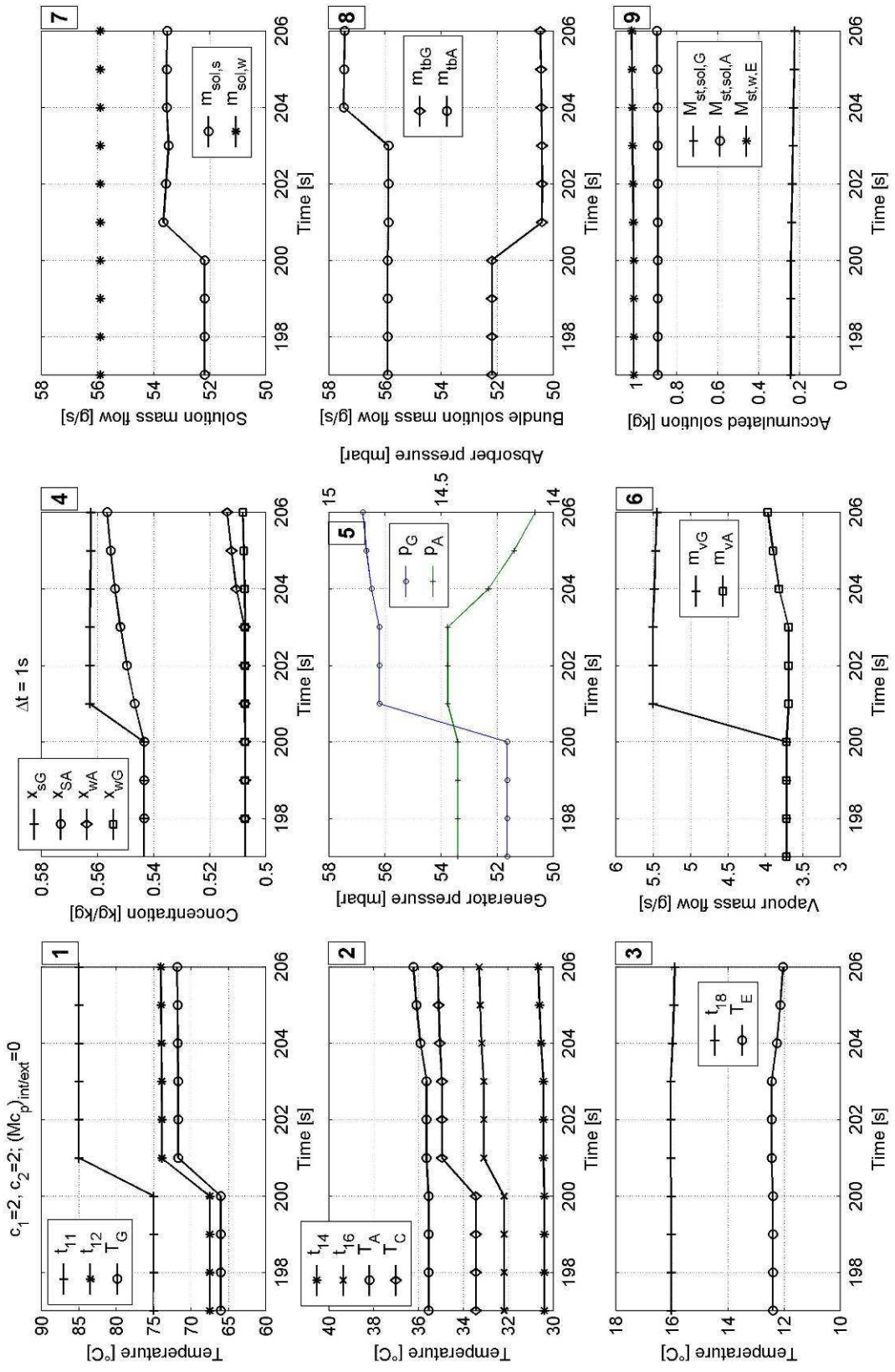

Figure 1. Simulated chiller response on 10K step in generator inlet temperature without thermal mass.

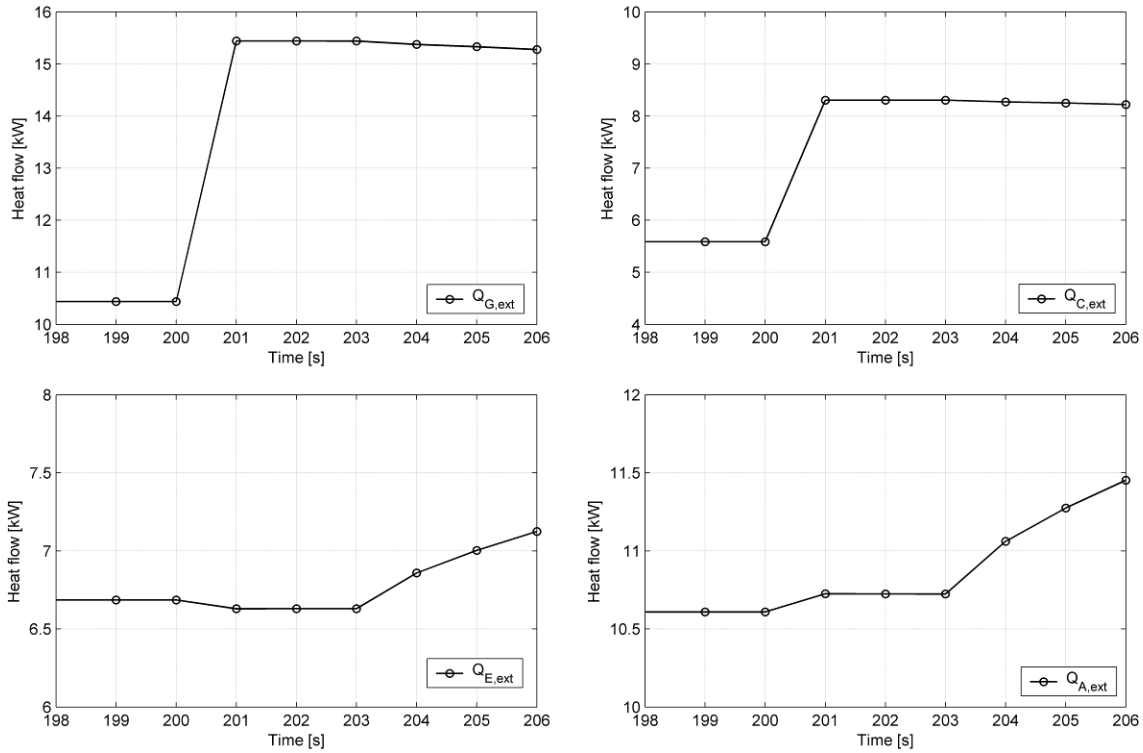

Figure 2. External heat flows of simulated chiller response on 10K step in generator inlet temperature without thermal mass

In Figure 1, graph 1 shows the temperatures in the generator which follow immediately the step of the external inlet temperature, t_{11}, because no thermal storage has been assumed. Accordingly, the heat flow to the generator increases (Figure 2, top left graph). The strong solution leaving the generator bundle follows immediately (x_{sG} in graph 4 of Figure 1). The strong solution leaving the generator sump follows in a damped fashion (x_{sA} in graph 4) because of the mass storage in the sump. The first change in mass fraction of the strong solution reaches the absorber inlet two steps later. Three steps after the initial change the mass fraction of the weak solution leaving the absorber bundle begins to change as well (x_{wA} in graph 4); the solution in the sump follows as well (x_{wG} in graph 4) but this is hardly visible due to the damping effect of the mass which is stored in the sump.

The flow of weak solution is kept constant ($m_{sol,w}$ in graph 7). The flow of strong solution increases immediately ($m_{sol,s}$ in graph 7). This due to the rise in generator pressure (p_G in graph 5), which drives more solution through the expansion valve. The rise in pressure, in turn is a consequence of the rise in the condenser heat flow (Figure 2, top right graph) due to the rise of vapour mass flow to the condenser (m_{vG} in graph 6). The flow of strong solution from the generator bundle to the generator sump (m_{tbG} in graph 8) decreases because the inlet flow is constant and more vapour is being produced. Of course, also the mean generator and condenser temperature (T_G in graph 1 and T_C in graph 2), and the condenser cooling water outlet temperature (t_{16} in graph 2) increases.

When the more concentrated solution reaches the absorber in step 204, the pressure immediately falls (p_A in graph 5). The absorber absorbs more vapour, the vapour flow from evaporator to absorber increases (m_{vA} in graph 6 of Figure 1), the flow from the absorber bundle to the sump increases (m_{tbA} in graph 8), and the absorber heat increases (Figure 2, bottom right graph). Accordingly, the temperature of the cooling water leaving the absorber increases (t_{14} in graph 2). At the same time, the evaporator heat increases (Figure 2, bottom

left graph) and the evaporator temperature as well as the chilled water outlet temperature decreases (T_E in graph 3 of Figure 1 and t_{18} in graph 3).
Summarising Figures 1 and 2, the model predicts the performance of the absorption chiller after an input temperature change with very good consistency and logic. However, there is a small inaccuracy in the model due to the way the solution heat exchanger is being modelled [1]. With the assumed transport delay in the solution circuit, no changes of absorber and evaporator parameters should occur during the first 2s after the temperature step. There is, however, a very small change in the equilibrium mass fraction of the absorber at time interval 201, barely visible in Figure 1 (x_{wA} in graph 4). This also results in small changes of the vapour mass flow from evaporator to absorber (m_{vA} in graph 6), the evaporator equilibrium temperature (T_E in graph 3) and the absorber pressure (p_A in graph 5).
The reason is as follows. In time interval 201, the increase of strong solution mass flow and equilibrium temperature in the generator results in an immediate increase of the solution heat exchanger heat flow as well which, in reality, would be dampened due to the thermal mass of the solution heat exchanger. Therefore, more heat has to be dissipated to the cooling water in the absorber, as visible in Figure 2 (bottom right graph). In consequence, the absorber pressure rises and less vapour can be absorbed, resulting in an equilibrium concentration change in the absorber and a temperature rise in the evaporator. The order of magnitude of these deviations is however very small and can be neglected for the overall model performance. The concentration changes by a value of 0.0002 kg/kg, the equilibrium temperature in the evaporator changes by 0.017K. This results in a vapour mass flow change of $2\ 10^{-5}$ kg/s.

Sensitivity analysis

The sensitivity of the model on its dynamic terms is important information for the model user as well as for developers of chillers. In the following, the influence of thermal storage and solution transport delay on the overall model performance will be investigated. Characterising parameters for the thermal storage are the values of internal and external heat capacity, $\left(Mc_p\right)_{X,\mathrm{int}}$ and $\left(Mc_p\right)_{X,ext}$. The transport delay is characterised by the transport delay constants c_1 and c_2.

Thermal storage variations

To investigate the influence of thermal storage variations, three different cases have been simulated. In the first case, the actual thermal capacity of the absorption chiller on which the model is based is used. See Table 1 for details. The second case assumes 50% of the actual thermal capacity and in the third case no thermal capacity is assumed. In all cases, the external capacity equals the internal capacity and the actual solution transport delays are utilized, i.e. 67s and 61s for c_1 and c_2, respectively. Again a hot water temperature step from 75℃ to 85℃ at 200 s after simulation start has be en used as the model input for all cases. Figure 3 shows the results, expressed by the heat flow from the external heat transfer fluid (the water to be chilled) into the evaporator.

Table 1. Assumed heat capacities for the model.

	Heat capacities, $(Mc_p)_{X,\text{int}}$ and $(Mc_p)_{X,ext}$							
	E,ext	**A,ext**	**G,ext**	**C,ext**	**E,int**	**A,int**	**G,int**	**C,int**
	kJ/K	kJ/K	kJ/K	kJ/K	kJ/K	kJ/K	kJ/K	kJ/K
100%	42	59	62	38	42	59	62	42
50%	21	30	31	19	21	30	31	21
0%	0	0	0	0	0	0	0	0

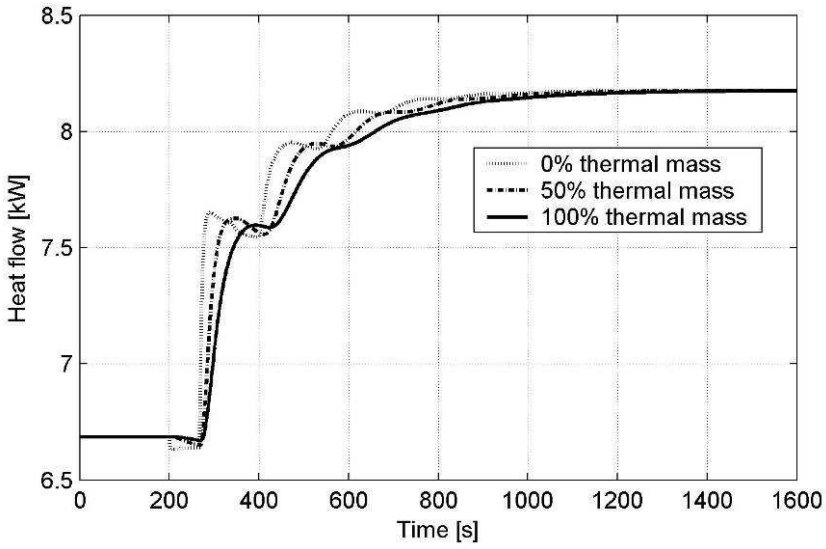

Figure 3. Evolution of evaporator heat flow for different thermal masses.

It can be seen in Figure 3 that the influence of the heat capacity is twofold. A lower capacity value results in a faster time until steady-state but also in bigger variations during the transient period. The first effect, the faster response, is rather obvious, as less thermal mass has to be heated or cooled in order to reach the new steady-state. This can be seen in more detail in Figure 4, where the time period around the step of Figure 3 is shown in enlargement.

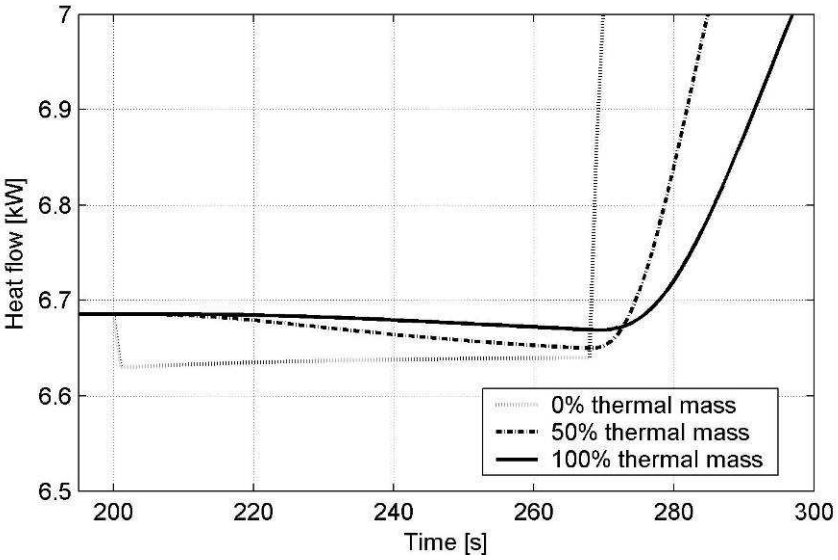

Figure 4. Detail of Figure 3: Time period around step only.

It is clearly visible in Figure 4 that an increase in thermal mass results in a slower response to the step change. Without thermal mass, the heat flow decreases abruptly after the step. This is equivalent to Figure 2 (bottom left graph) where the evaporator heat flow decreases for the time period between the step and the elapsing of time constant c_1. The lower evaporator heat flow is due to the increased heat flow in the solution heat exchanger just after the step which in turn results in increased absorber pressure, an equilibrium concentration change in the absorber, less absorbed vapour and hence a temperature rise in the evaporator. The evaporator heat flow increases sharply again after time constant c_1 has elapsed at time interval 267, i.e. after the change in solution mass fraction reaches the absorber. For the other two cases with higher thermal mass the changes are much less abrupt and the transients are not as steep.
The second effect visible in Figure 3 is bigger variations during the transient period for less thermal mass. This is related to the transport delay in the solution circuit. There, less mass results in more abrupt variations of the heat flow, induced by sharp changes of the solution parameters after either c_1 or c_2 have elapsed. An increase in both internal and external thermal mass provides a damping effect on the heat flow oscillations in the chiller. Regardless of the assumed thermal mass, the model still converges into the same steady-state value after the step.

For Figures 3 and 4, it has been assumed that the external capacity equals the internal capacity. This does not give any information on the influence of either of those capacities by itself and whether the assumption of equal capacities is reasonable. Therefore, another simulation has been performed assuming 100% capacity either only on the external or on the internal side. Figures 5 and 6 show the results for external and internal heat capacity only. As before, a hot water temperature step from 75℃ to 8 5℃ at 200s after simulation start has been used as the model input.

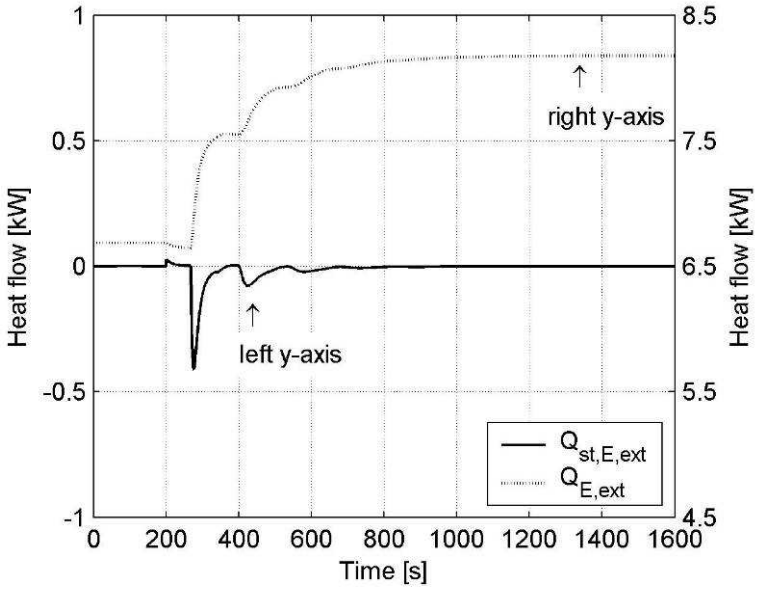

Figure 5. Evolution of evaporator heat flow for externally coupled thermal mass only.

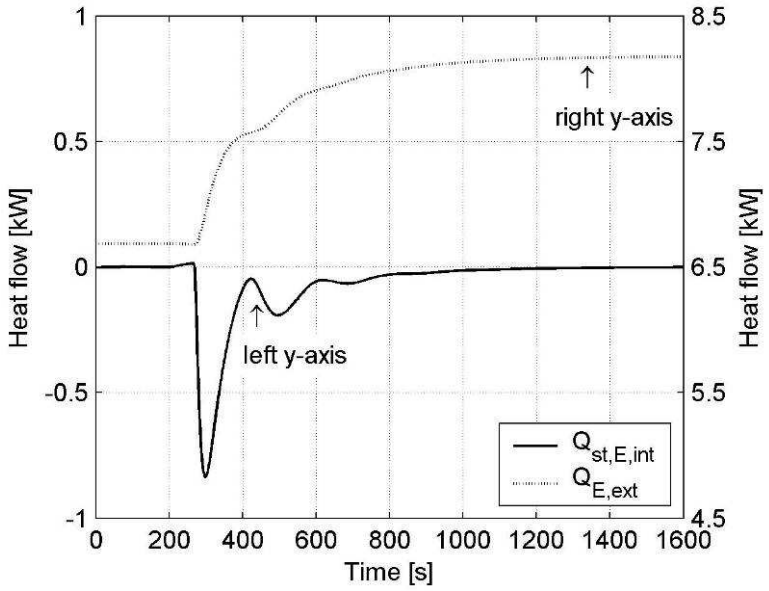

Figure 6. Evolution of evaporator heat flow for internally coupled thermal mass only.

Figure 5 shows the external heat flow from the chilled water, $Q_{E,ext}$, and the heat flow into the external thermal mass, $Q_{st,E,ext}$. The difference between both is the heat flow into the refrigerant. In the first seconds after the step, the temperature of the evaporator rises somewhat due to the increased absorber pressure as previously explained. The external heat flow drops, some heat is stored in the external mass. At 67s after the step (elapsing of c_1) a sharp negative peak can be seen in the heat flow which is stored in the external mass: the evaporator cools down because more absorption takes place as the change in solution mass fraction reaches the absorber. Consequently the external heat flow into the evaporator increases with a steep gradient. In parallel to this process, solution with the initial weak concentration from the absorber reaches the generator at 61s after the step (elapsing of c_2). Therefore the equilibrium concentration in the generator sump decreases due to the mixing. This slightly weaker solution leaves the generator sump and reaches the absorber with a time difference of 6s (Δc_{1-2}). It increases the absorber pressure and decreases the evaporator heat flow, visible in Figure 5 at 128s after the step where the evaporator heat flow plateaus at constant level. At approx. 200s after the step new stronger solution reaches the absorber from the generator, the absorber pressure decreases and the evaporator heat flow increases again. The gradient is, however, less steep than the first time due to the increased mixing in both generator and absorber sump and the corresponding equalisation of solution mass fraction. After this second increase another plateau can be observed in the evaporator heat flow at approx. 260s after the step. This process of alternating solution concentration changes is repeated a few more times with less and less intensity until at 500 seconds after the initial step the heat flow out of the thermal mass has stopped almost completely. A new steady-state is reached at 1200s after the initial step.

Figure 6 shows a similar evolution but with allocation of the thermal mass to the internal evaporator temperature. The behaviour is very similar, but there is an influence on the time to reach a new steady-state and also on the course of the heat flow after the step. Figure 6 shows that allocating the thermal mass to the internal parts results in a slower response with approx. 1400s to reach the new steady-state. Even the cooling down of the evaporator takes about 1000 seconds. The influence of the solution transport delay is much stronger, as the internal mass now includes the solution, the solution heat exchanger, and the solution pump

[1]. Thus the heat flow transient is less steep than in Figure 5 and the plateaus are less distinct.
Comparing Figures 5 and 6 it can be observed that allocating the thermal mass to the external parts as in Figure 5 yields a faster response with regard to achieving a new steady-state. The dynamic course of Figure 5 clearly shows obvious plateaus created by the transport delay in the solution circuit. As no internal thermal mass has been allocated, the solution changes occur quite rapidly after the step and then become weaker and are dampened with time. The course in Figure 6 is much less pronounced and the gradients of heat flows are less steep. The model behaviour shown in Figures 5 and 6 demonstrates that in order to attain a short response time the absorption chiller should be designed with possibly small internal thermal mass, however this will result in stronger variations during the transient period. Internally coupled thermal mass is more important than externally coupled thermal mass.

Transport delay variations

A second analysis has been performed to determine the sensitivity of the model results on time constants c_1 and c_2 which represent the transport time of the solution from generator to absorber and vice versa. The time constants have been set to 0, 50 and 100% of their original values which have been estimated from the design of the experimental plant. Table 2 shows the time constants used. For these simulations, the same hot water inlet step from 75℃ to 85℃ as before has been applied. Also, no t hermal mass has been assumed. Figure 7 shows the results, again expressed using the external heat flow to the evaporator.

Table 2. Assumed transport delays for the model.

	Transport delay	
	c_1	**c_2**
100%	67	61
50%	33	30
0%	2	1

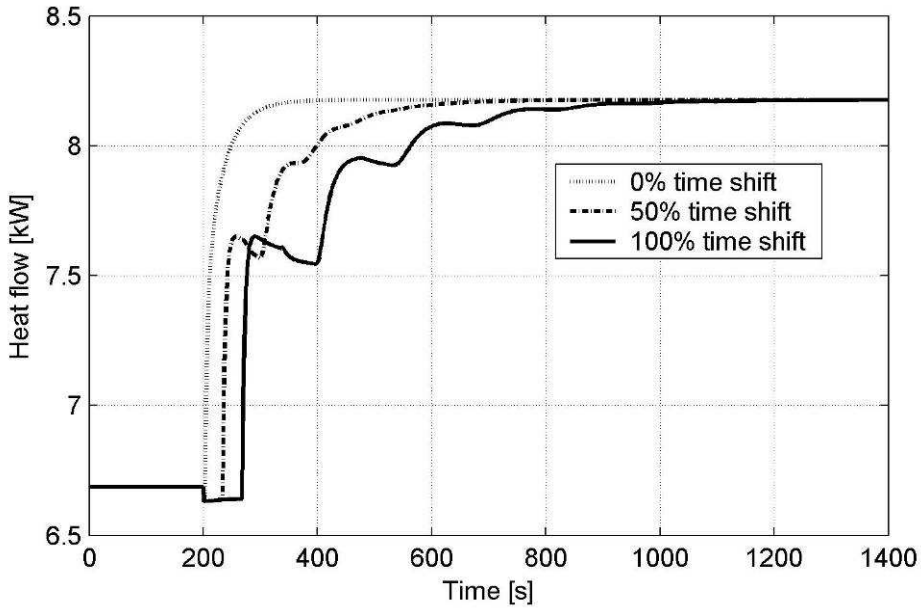

Figure 7. Evolution of evaporator heat flow for different transport delay times.

It is visible that the transport delay has a significant influence on the model performance. Without a transport delay, the new steady-state is reached at approx. 200s after the step. With a transport delay of 50% (which corresponds to about half a minute) it takes approx. 500s, e.g. more than double the time to reach it. For the assumed 100% of transport delay (around 1 minute) it takes approx. 900s or more than four times as long.

Also, with 100% transport delay, the transient period is not only longer but also quite different in its course. After the elapsing of each transport delay constant, a change in heat flow can be observed in a repeated pattern. The pattern consists of a small change and a larger change following each other which is due to the repetitive change in solution mass fraction as previously explained. The changes become less intensive with time and after approx. 12 delay times the new steady-state is reached. In a real absorption chiller the transport delay is determined by the flow rate of the solution. The model results in Figure 7 show that a significantly faster return to steady-state can be achieved if the flow rate of the solution is high and the transport delays are small.

Experimental verification

In Part 1 of this paper, we showed a first comparison of the simulated generator outlet temperature using experimentally measured inlet and outlet temperatures to measured data [1]. In this second part the comparison is also done similarly for the evaporator and absorber. Flow rates and inlet temperatures of the external flows are taken as input data to the simulation model. All internal parameters, the heat flows, and the outlet temperatures of the external flows are simulated. Figure 8 shows measured inlet and outlet temperatures of the chilled water together with the simulated outlet temperature; Figure 9 shows the same for the cooling water through absorber/condenser. The constant simulation parameters for the experimental verification can be found in the Appendix.

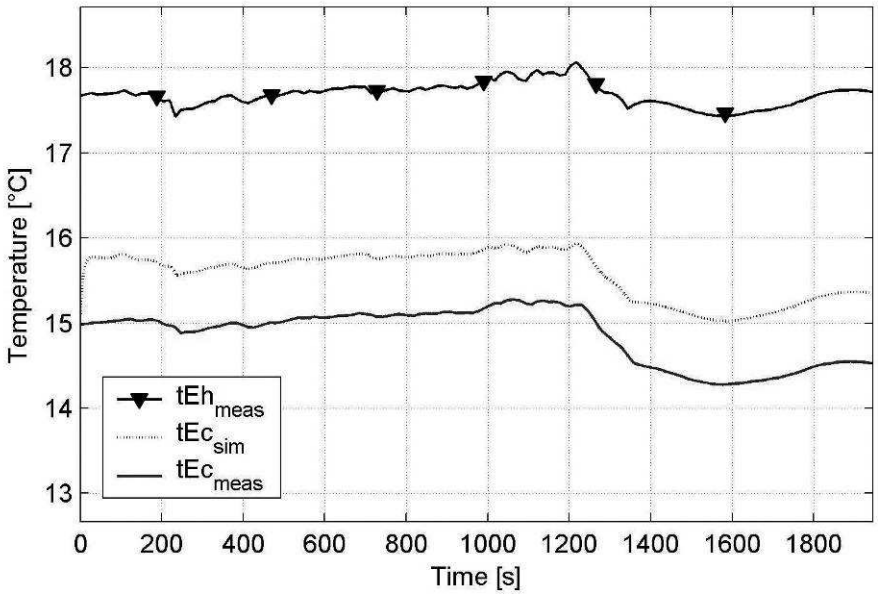

Figure 8. Simulated external evaporator temperatures using experimentally measured input data.

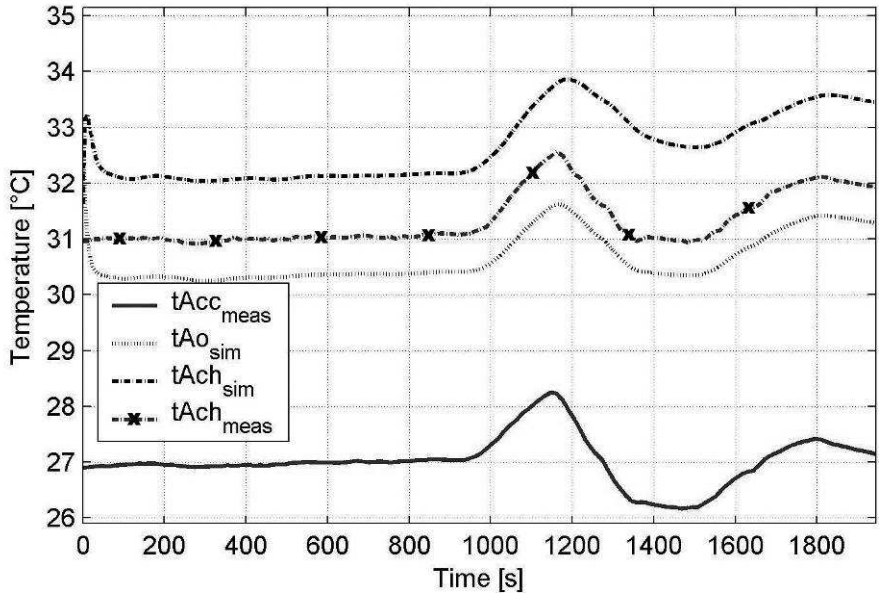

Figure 9. Simulated external absorber temperatures using experimentally measured input data.

Both figures show that the dynamic behaviour including small oscillations is in very good agreement. As discussed in part I, the temperature levels are not reproduced satisfactorily because the thermodynamic steady state model is a very coarse one only. This is tolerated because the focus is laid on the dynamics. In Figure 8, the dynamics are being reproduced very well with only a slight delay of 10s between course of the two temperatures. Figure 9 shows a slightly worse agreement for the cooling water temperatures, with simulated values being approx. 25s ahead of measured ones. Also shown in Figure 9 is the simulated outlet temperature of the absorber, $t_{Ao,sim}$, for which no measured data was available. We want to emphasize that no tuning of the dynamic parameters has been performed up to now: the dynamic response seems to be very robust according to the sensitivity analysis which has been shown before.

Conclusions

In this paper, the performance of a dynamic model for absorption chillers has been investigated. General model functionality is demonstrated and the thermodynamics have been found to be consistent with reality. A sensitivity analysis has been performed on external and internal heat exchange related thermal mass. The analysis shows that an increase in both external and internal thermal mass results in a slower response to the step change but also in smaller heat flow oscillations during the transient period. Also, the thermal mass has been found to influence the heat flow transients more significantly if allocated internally. A time difference of 200s for reaching the steady state (response time) was observed between a complete internal and external allocation of thermal mass.

The transport delay in the solution cycle has been found to influence both the response time and the transients of the heat flow. A smaller transport delay leads to significantly faster response. Assuming half the value of the real transport delay in the absorption chiller leads to a 33% reduction of response time.

The comparison with experimental data shows that the dynamic agreement between experiment and simulation is very good with dynamic temperature deviations between 10 and 25s. The total time to achieve a new steady-state after a 10K input temperature step amounts to approximately 15 minutes for the experimental chiller. Compared to this, the present dynamic deviations of the model are in the magnitude of approximately 1 to 3%. Steady-state results are being reproduced with temperature deviations between 0.7 and 3.5K in the model. Accuracy in this respect, however, was not the aim of the present study.

The dynamic simulation model presented in this paper is a useful tool in the overall design process of absorption chillers. Technical changes in the construction of an existing absorption chiller model can be tested quickly and easily by incorporating the design changes in the model. Also, new chiller designs can be tested on their performance without the need to build a prototype. The model also allows the identification of transfer functions and control parameters of absorption chillers without the need to perform experiments. The model has been designed for the Phoenix 10kW chiller but can easily be adapted to other LiBr/water absorption chillers if the required design data of these chillers are available.

Appendix

Table 3. Constant parameters of the dynamic model.

No.	Constants	Unit	Value	Description
1	$r_{(pc)}$	kJkg^{-1}	2450	Evaporation enthalpy of water
2	$l_{(pc)}$	kJkg^{-1}	272	Solution enthalpy of LiBr/water solution
3	$(UA)_{E,ext}$	kWK^{-1}	2.9	External heat transfer coefficient value of evaporator
4	$(UA)_{C,ext}$	kWK^{-1}	5.2	External heat transfer coefficient value of condenser
5	$(UA)_{G,ext}$	kWK^{-1}	4.0	External heat transfer coefficient value of generator
6	$(UA)_{A,ext}$	kWK^{-1}	3.2	External heat transfer coefficient value of absorber
7	$(UA)_{E,\mathrm{int}}$	kWK^{-1}	3.9	Internal heat transfer coefficient value of evaporator
8	$(UA)_{C,\mathrm{int}}$	kWK^{-1}	8.7	Internal heat transfer coefficient value of condenser
9	$(UA)_{G,\mathrm{int}}$	kWK^{-1}	4.3	Internal heat transfer coefficient value of generator
10	$(UA)_{A,\mathrm{int}}$	kWK^{-1}	3.2	Internal heat transfer coefficient value of absorber
11	$\dot{m}_{sol,w}$	kgs^{-1}	0.0559	Mass flow of weak solution
12	$\dot{m}_{hw}$	kgs^{-1}	0.3322	Mass flow of hot water
13	$\dot{m}_{cw}$	kgs^{-1}	0.7462	Mass flow of cooling water
14	$\dot{m}_{chw}$	kgs^{-1}	0.808	Mass flow of chilled water
15	A_t	m²	4.9*10^{-4}	Cross area of solution tube
16	h	m	0.1	height between solution outlet at generator and inlet at absorber
17	$M_{st,sol,G,start}$	kg	0.24	Initial condition of accumulated solution in generator sump
18	$M_{st,sol,A,start}$	kg	0.19	Initial condition of accumulated solution in absorber sump
19	ς	-	2100	Resistance coefficient of solution heat exchanger and piping
20	c_1	-	67, 2	time constant for solution flow from generator to absorber
21	c_2	-	61, 1	time constant for solution flow from absorber to generator
22	$(Mc_p)_{E,ext}$	kJK^{-1}	6.8	Cumulated heat capacity of evaporator, external
23	$(Mc_p)_{C,ext}$	kJK^{-1}	6.4	Cumulated heat capacity of condenser, external
24	$(Mc_p)_{G,ext}$	kJK^{-1}	9.0	Cumulated heat capacity of generator, external
25	$(Mc_p)_{A,ext}$	kJK^{-1}	9.0	Cumulated heat capacity of absorber, external
26	$(Mc_p)_{E,\mathrm{int}}$	kJK^{-1}	38.4	Cumulated heat capacity of evaporator, internal
27	$(Mc_p)_{C,\mathrm{int}}$	kJK^{-1}	38.2	Cumulated heat capacity of condenser , internal

28	$\left(Mc_p\right)_{G,\mathrm{int}}$	kJK^{-1}	82.2	Cumulated heat capacity of generator , internal
29	$\left(Mc_p\right)_{A,\mathrm{int}}$	kJK^{-1}	81.9	Cumulated heat capacity of absorber , internal
30	η_{SHX}	-	0.9	Efficiency of solution heat exchanger
31	cp_w	$kJkg^{-1}K^{-1}$	4.19	Specific heat capacity of liquid water
32	cp_v	$kJkg^{-1}K^{-1}$	1.86	Specific heat capacity of water vapour
33	$cp_{sol,s}$	$kJkg^{-1}K^{-1}$	3.8	Specific heat capacity of strong solution
34	$\rho_{sol,s}$	kgm^{3-1}	1600	Density of strong solution
35	Δt	s	1	Time increment of simulation

References

[1] Kohlenbach P, Ziegler F. A dynamic simulation model for transient absorption chiller performance. Part I: The model. *Int J Refrigeration 2007*,

Conclusion

In this report the new development concerning simulation tools for solar cooling are presented. First are presented the most commonly used simulation tools in the domain of solar air conditioning. It was shown that most of simulation tools requires high knowledge of the simulated process as well as internal development for each project, except some simple simulation tools with predefined configurations and fixed boundaries. Most of simulation environment used in each research group in the solar cooling domain are internally developed and used. In the commercially available detailed softwares; the models of the solar installation are widely used as in found in the libraries, however the model of the cooling process itself are usually re-developed by the users.

New development of solar cooling models and their validation are then presented. A detailed desiccant air handling unit powered by heat pipe vacuum tube collectors is developed and implemented in SPARK. The model of the unit showed good accuracy on a component level and on a system level under different operating conditions. The supply conditions of the air handling unit are estimated with good accuracy as well as the potential of solar energy in the desiccant cooling process. The transient behaviour of the collector is very well predicted by the model. A transient model of the desiccant wheel is also developed and experimentally validated. The model calculates the evolution of the temperature and humidity ratio of the air across the wheel and at its outlet. It gives also a good estimation of the mean air outlet conditions of the desiccant wheel.

A transient detailed model of a Li/Br absorption chiller is developed. The model is experimentally validated and is capable to predict the transient behaviour of the chiller. The comparison with experimental data shows that the dynamic agreement between experiment and simulation is very good with dynamic temperature deviations between 10 and 25 s The dynamic simulation model presented is a useful tool in the overall design process of absorption chillers. Technical changes in the construction of an existing absorption chiller model can be tested quickly and easily by incorporating the design changes in the model.